Characterization of Atrial Repolarization Alternans and Activation Time Kinetics based on Intracardiac Electrograms

ÉCOLE POLYTECHNIQUE
FÉDÉRALE DE LAUSANNE

Suisse
2011

« Dans les sciences, le chemin est plus important que le but. Les sciences n'ont pas de fin. »

Erwin Chargaff

Abstract

Interdisciplinary collaboration between physicians and engineers is now widespread in fundamental and clinical studies, due to the increasing complexity of the physiological problems tackled, and the development of novel measurement devices and data analysis techniques. The present work is a clear illustration of this fact. In the study that triggered it, elaborate experiments on an animal model yielded large amounts of data perturbed by unavoidable interferences, and the phenomenon of interest had an elusive nature. This thesis describes the physiological motivation for this study, introduces the signal processing techniques developed to remove interferences and extract the parameters of interest, and proposes an interpretation of the results obtained. The present thesis is aimed at providing new insights into the mechanisms promoting atrial fibrillation during rapid pacing.

Atrial fibrillation is the most common arrhythmia in the developed world, affecting millions of individuals. Atrial fibrillation initiates when triggers such as pulmonary vein tachycardias interact with substrates. However, the exact nature of the electrophysiological substrates that favor transition from runs of pulmonary veins tachycardia to persistent atrial fibrillation remains unclear. Interestingly, repolarization alternans, a beat-to-beat alternation in action potential duration or amplitude, has been mechanistically implicated in transitions from rapid pacing to atrial fibrillation by facilitating dispersion of atrial refractory periods. During rapid pacing, however, transitions from 1:1 to 2:1 atrial capture may supposedly antagonized the dispersion of repolarization driven by repolarization alternans.

The ability of atrial unipolar depolarization and repolarization parameters (i.e. activation time and repolarization alternans) to predict the imminence of atrial fibrillation initiation by rapid pacing was evaluated at baseline (i.e. before any burst-pacing induced remodeling occurred). A chronic free-behaving ovine pacing model was developed to study the interplay between atrial repolarization alternans that may facilitate atrial fibrillation initiation during rapid pacing, and the onset of reduced excitability that may cause atrial capture failure and prevent atrial fibrillation initiation.

We observed in human atria using monophasic action potential recordings transient decrease in excitability (as exemplified by activation time prolongation) and capture failure that appeared to quench repolarization alternans driven by rapid pacing. Using our ovine model of rapid pacing, human observations were successfully reproduced, which allowed us to analyze repolarization alternans and activation time kinetics until the first beat of capture failure. Prolongation of activation time suggestive of decreased excitability and repolarization alternans preceded 90% of the transitions from 1:1 to 2:1 atrial capture during rapid pacing. Notably, 2:1 atrial capture was imminent at pacing cycle lengths <40 ms above effective refractory period. In the rare cases where capture fail-

i

ure did not occur, repolarization alternans preceded most episodes of non sustained atrial fibrillation, suggesting that intermittent capture plays a protective role against repolarization alternans-induced reentrant arrhythmias. Moreover, the dynamics of atrial repolarization alternans as a function of pacing rate were studied in details. Repolarization alternans amplitude increased as a function of pacing rates, but appeared intermittently without periodicity. This latter finding was suggestive of the presence of nodes (i.e. sites separating islands in opposite phase) spanning the atrial surface.

In summary, since rapid atrial tachycardias may also slow propagation velocity, known to be proarrhythmic, transitions to 2:1 atrial capture may protect against dispersion of repolarization and atrial fibrillation. A better understanding of the mechanisms causing intermittent atrial capture may allow treatments to be tailored for preventing atrial fibrillation induction at lower rates.

Resumé

De nos jours, la complexité des problèmes physiologiques, le développement de nouveaux outils de mesure ainsi que les techniques d'analyse de données amènent à des collaborations interdisciplinaires entre médecins et ingénieurs. Ce travail de thèse, effectué à la fois dans le cadre d'une étude fondamentale et clinique, s'inscrit dans cette optique. Les expériences menées sur un modèle animal ont conduit à de nombreuses données perturbées par des interférences inévitables, le phénomène d'intérêt présentait un comportement difficile à observer. Cette thèse décrit les motivations physiologiques de cette étude, introduit les techniques de traitement de signaux développées pour supprimer ces interférences et extraire les paramètres d'intérêt et propose une interprétation des résultats obtenus. Le but de cette thèse est de fournir de nouvelles pistes concernant les mécanismes favorisant la fibrillation auriculaire durant une stimulation rapide.

La fibrillation auriculaire est l'arythmie cardiaque soutenue la plus commune dans le monde, affectant des millions de personnes. La fibrillation auriculaire est initiée lorsque certains déclencheurs, tels que des décharges électriques provenant des veines pulmonaires, interagissent avec le substrat. Néanmoins, la nature électrophysiologique exacte de ce substrat favorisant l'initiation de la fibrillation auriculaire reste floue. Il est intéressant de souligner que le phénomène d'alternance de la repolarisation, représenté par des changements dans la durée ou l'amplitude des potentiels d'actions de battement à battement, a été systématiquement observé lors de transitions d'une stimulation rapide vers une fibrillation auriculaire en favorisant la dispersion des périodes réfractaires auriculaires. Cependant, pendant une stimulation rapide, les transitions d'une capture auriculaire 1 :1 à une capture auriculaire 2 :1 seraient opposées au phénomène de dispersion induite par l'alternance de la repolarisation.

Certains paramètres de dépolarisation et de repolarisation, tels que le temps d'activation et l'alternance de la repolarisation, ont été extraits d'électrogrammes unipolaires. La capacité de ces marqueurs à prédire l'initiation de la fibrillation auriculaire par stimulation rapide a été évaluée à l'état basal (c'est-à-dire avant tout remodelage induit par stimulation). Un modèle ovin de stimulation rapide a été conçu pour étudier le lien entre, d'une part le phénomène d'alternance de la repolarisation qui peut faciliter l'initiation de la fibrillation auriculaire pendant une stimulation rapide, et d'autre part une réduction de l'excitabilité qui peut causer un défaut de capture auriculaire et ainsi empêcher l'initiation de la fibrillation auriculaire.

A l'aide d'enregistrements de potentiels d'action monophasiques, nous avons observé chez l'homme une diminution transitoire de l'excitabilité (illustrée par la prolongation du temps d'activation), puis un défaut de capture qui a pour conséquence de supprimer l'alternance de la repolarisation induite par la stimulation rapide. Les observations faites chez l'humain ont été reproduites

avec succès dans notre modèle ovin, ce qui nous a permis d'analyser l'alternance de la repolarisation et les dynamiques des temps d'activation jusqu'au premier défaut de capture. La prolongation du temps d'activation et l'alternance de la repolarisation ont précédé 90% des transitions d'une capture auriculaire 1 :1 à une capture auriculaire 2 :1. En particulier, en réponse à des périodes de stimulation proches de la période réfractaire effective, le nombre de captures auriculaires 2 :1 augmente rapidement. Dans les rares cas où il n'y a pas de défaut de capture, l'alternance de la repolarisation a précédé la plupart des épisodes de fibrillation auriculaire non-soutenue, suggérant que la capture intermittente joue un rôle protecteur contre les réentrées dues à l'alternance de la repolarisation. D'autre part, les dynamiques de l'alternance de la repolarisation auriculaire en fonction de la fréquence de stimulation ont été étudiées en détail. L'amplitude de cette alternance augmente avec la fréquence de stimulation mais apparaît de façon intermittente sans périodicité. Cette dernière observation suggère la présence de nœuds, c'est-à-dire des sites séparant des zones d'alternance de phase opposée, balayant la surface auriculaire.

Les tachycardies auriculaires, connues pour être proarythmiques, peuvent également ralentir la vitesse de propagation. Dans ce cas, les transitions vers une capture auriculaire 2 :1 peuvent prémunir contre une dispersion de la repolarisation, et donc contre la fibrillation auriculaire. Une meilleure compréhension des mécanismes sous-jacents aux captures auriculaires intermittentes pourrait permettre l'amélioration des traitements prévenant l'induction de la fibrillation auriculaire à des rythmes moins soutenus.

Mots clés : fibrillation auriculaire, électrogrammes intracavitaires unipolaires, suppression de l'activité ventriculaire, capture auriculaire intermittente, réduction de l'excitabilité, alternance de la repolarisation auriculaire.

Remerciements

Ce travail de thèse est le résultat d'une collaboration étroite entre le CHUV et l'EPFL. Je souhaite donc remercier toutes les personnes grâce auxquelles ce projet a été possible :

– Je tiens tout d'abord à remercier mon directeur de thèse à l'EPFL, le Dr Jean-Marc Vesin, pour son inestimable soutien technique et moral. J'ai eu la chance de pouvoir apprécier l'étendue de ses connaissances en traitement des signaux mais également son sens de l'humour inégalable ! Jean-Marc, tu rends vraiment le travail au sein de ton groupe agréable.

– Cette recherche a été initiée et guidée par le Docteur Etienne Pruvot, mon co-directeur au CHUV. Je le remercie pour sa disponibilité, sa motivation et les discussions durant les nombreuses heures passées dans les sous-sols du CHUV avec nos amis ovins.

– L'acquisition des données a été possible grâce à la collaboration du centre opératoire protégé au CHUV. Merci Marco pour les préparatifs lors des lundi-acquisition et « Bon week-end ! ».

– Plus récemment, Joanna a rejoint notre projet de recherche au CHUV. J'ai pu apprécier ses questions pertinentes, son regard neuf sur le projet et également profiter de sa maîtrise de la langue de Shakespeare.

– Un grand merci au président du jury, Prof. Vandergheynst, ainsi qu'aux rapporteurs : Prof. Atienza, Dr Kucera et Dr Jacquemet.

– Je souhaite bien sûr remercier les « *Jean-Marc Boys* » de ces dernières années : Cédric Duchêne, Laurent Uldry, Jérôme Van Zaen, Yann Prudat, Mathieu Lemay, Aline Cabasson et Andrea Buttu. Un merci particulier à Aline, Andrea, Jérôme et Yann pour le travail de traduction. Les pages iii et iv doivent vous sembler familières ! Une mention spéciale à mes collègues de bureau, Cédric et Vincent pour l'ambiance de travail et les pauses café-baby. Merci à Vincent de marcher de plus en plus en téléphonant (cette technique de communication mobile provient initialement de Michel).

– Je remercie également Anna qui a accepté de m'accueillir durant les dernières semaines d'écriture, m'éloignant des pauses café précitées et m'offrant un cadre beaucoup plus propice à la rédaction.

– Merci à l'ensemble des membres des SPLABS grâce à qui ces laboratoires sont agréables durant le travail et également après ! Merci au staff pour la résolution de problèmes techniques et administratifs : Gilles Auric, Marianne Marion, Rosie de Pietro et Christine Gabriel.

– Un grand merci à ma famille pour leur soutien tout au long de cette thèse ; mes parents Alain et Maria, mon frère Eric, ma belle-sœur Céline et ma nièce Ophélie.

– Finalement, je voudrais remercier ma fiancée Marie-Laure qui a su me motiver et surtout me supporter durant ces derniers mois de rédaction !

Contents

List of Acronyms

AA	Atrial activity
AF	Atrial fibrillation
AP	Action potential
APD	Action potential duration
ARI	Activation recovery interval
AT	Activation time
AV	Atrioventricular
CHF	Congestive heart failure
CL	Cycle length
ECG	Electrocardiogram
EGM	Electrogram
EP	Electrophysiology
ERP	Effective refractory period
MAP	Monophasic action potential
PC	Principal component
PCA	Principal component analysis
PCL	Pacing cycle length
RA	Right atrium
Re-ALT	Repolarization alternans
SA	Sinoatrial
SR	Sarcoplasmic reticulum
T_a	Atrial T wave apex
TWA	T wave alternans (ECG)
VA	Ventricular activity

List of Figures

List of Tables

1

Introduction

1.1 Problem statement

Atrial fibrillation (AF) is the most common arrhythmia in the developed world, affecting millions of individuals [1]. Paroxysmal AF, a common manifestation of the disease, naturally evolves at unpredictable speed toward persistent AF [2]. AF initiates when triggers such as pulmonary vein (PV) tachycardias interact with substrates [3–5]. However, the exact nature of the electrophysiological substrates that favor transition from runs of PV tachycardia to persistent AF remains unclear.

Over the last years, several studies have associated ventricular arrhythmias risks to electrocardiographic markers, such as T wave alternans (TWA). TWA, a beat-to-beat variation in the shape, amplitude or timing of the T waves on the electrocardiogram has been linked with inducible and spontaneous ventricular arrhythmias and with basic mechanisms leading to their initiation [6, 7]. TWA is felt to reflect a combination of spatial and temporal dispersion of repolarization.

Although most efforts have focused on the role played by alternans in reentrant ventricular arrhythmias, clinical, experimental and modeling studies suggest that atrial repolarization alternans (Re-ALT) may play a role in promoting atrial arrhythmias [8–11]. Re-ALT appears involved in the transition to AF during rapid pacing or following atrial flutter by facilitating spatial dispersion of refractory periods.

1.2 Objectives

The present thesis intends to investigate the ability of original electrophysiological parameters extracted from intracardiac unipolar EGMs, such as repolarization alternans and activation time kinetics, to predict AF susceptibility in a pacing-induced model of AF.

In this study, a chronic free-behaving ovine model of pacing-induced atrial tachycardia has been developed. This experimental model makes possible the acquisition of intracardiac unipolar atrial electrograms (EGMs) during rapid pacing protocols and allows us to study the dynamics of atrial Re-ALT *in vivo* during rapid pacing mimicking firing from pulmonary veins, as seen in humans suffering from AF.

We hypothesized that decreased excitability during rapid pacing plays a protective role against Re-ALT induced wavebreaks and AF. A chronic free-behaving ovine pacing model was developed to study the interplay between atrial Re-ALT that may facilitate AF initiation during rapid pacing, and the onset of decreased excitability that may cause 2:1 capture and prevent AF initiation.

Intracardiac EGMs can provide local informations that cannot be extracted from the surface ECG. However, they include activities related to both local atrial activity and far-field ventricular depolarization and repolarization waves.

To provide a useful tool which permits the practical observation and exportation of signals, we have developed a standalone application which enables to:

– cancel the ventricular far-field activity from unipolar atrial electrograms,
– characterize atrial repolarization alternans,
– analyze specific patterns in activation times or activation recovery intervals.

1.3 Organization

This dissertation is divided in three parts:

1. **Introduction to cardiac electrophysiology, atrial fibrillation and repolarization alternans.** After introducing the cardiovascular system and the normal propagation of electrical impulses throughout the heart, electrocardiographic measurements and principles of electrophysiology study are presented in chapter 2. The mechanisms underlying AF and alternans are detailed in chapter 3 and 4, respectively.

2. **Presentation of the experimental model.** The second part introduces the ovine model and the pacing protocols used (chapter 5).

3. **Signal processing of the unipolar atrial electrograms.** The final part explores the processing techniques applied to detect fiducial points, denoise the signal and cancel the ventricular activity (chapter 6). The detection of transient repolarization alternans is addressed in chapter 7. Finally, the results from the analysis of experimental data are presented and compared to clinical observations in chapter 8.

1.4 Original contributions

The main contributions of this work are:

- *In vivo* experimental model
    - The development of an ovine model of pacing-induced AF.
    - The acquisition of intracardiac unipolar EGMs displaying atrial repolarization during pacing protocols.

- Signal processing
    - The development of a synthetic model of intracardiac unipolar EGMs.
    - The adaptation of preprocessing and denoising techniques applied to EGMs.
    - The refinement of ventricular cancellation techniques to single lead atrial EGMs.
    - The detection of transient short duration repolarization sequences.

- Electrophysiological results
    - The assessment of the rate dependence of atrial repolarization alternans.
    - The evaluation of the intermittency of atrial repolarization alternans.
    - The prevalence of repolarization and activation time prolongation preceding transitions from 1:1 to 2:1 atrial capture.
    - The distribution of 2:1 atrial capture duration in function of the paced effective refractory period.

Part I

Introduction to electrophysiology, electrography, atrial fibrillation and alternans

Cardiac electrophysiology and electrography

<div style="text-align: right; font-size: 3em;">2</div>

As an introduction, this chapter reviews the anatomy of the cardiovascular system and describes how electrical impulses are normally generated and propagated throughout the heart. Then, the different electrocardiographic measures are explained in section 2.2 and the principles of electrophysiology study introduced in section 2.3.

2.1 Cardiac electrophysiology

The heart spontaneously generates electrical impulses, which are vital to all cardiac functions. On a basic level, by controlling the flux of ions across the cardiac cell membrane, electrical impulses trigger cardiac muscle contraction. On a higher level, electrical impulses organize the sequence of muscle contractions during each heartbeat, and optimize the stroke volume. Finally, the pattern and timing of these impulses determine the heart rhythm. Derangements in this rhythm often impair the ability of the heart to pump enough blood to meet the natural body demand.

2.1.1 The cardiovascular system

The cardiovascular system is composed of two primary components: the heart and the blood vessels. The main function of the cardiovascular system is to facilitate exchange of gases, fluid, large molecules and heat between cells and the outside environment. The heart and vasculature ensure that adequate blood flow is delivered to organs so that this exchange can take place [12].

The heart can be viewed functionally as two pumps with the pulmonary and systemic circulations situated between the two pumps (fig. 2.1.1). The pulmonary circulation is the blood flow within the lungs that is involved in the exchange of gases between the blood and the alveoli. The systemic circulation is comprised of all the blood vessels within and outside of the organs, excluding
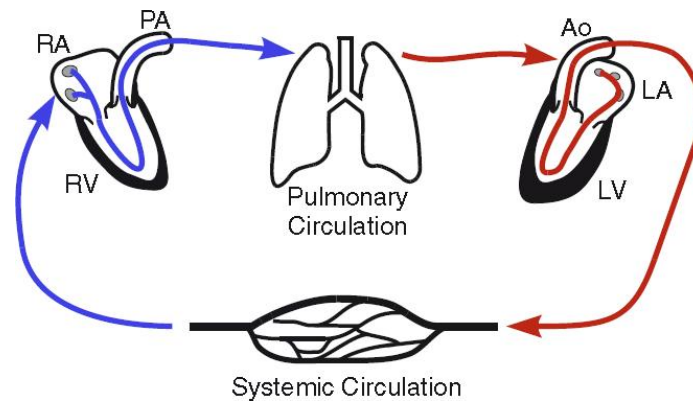
Figure 2.1: *Overview of the cardiovascular system. The right side of the heart, pulmonary circulation, left side of the heart and systemic circulation are arranged in series. Red indicates oxygenated blood, blue indicates deoxygenated. RA, right atrium; RV, right ventricle; PA, pulmonary artery; Ao, aorta; LA, left atrium; LV, left ventricle. Image adapted from Klabunde [12].*

the lungs.

The right side of the heart is composed of the right atrium and the right ventricle. The right atrium receives venous blood from the systemic circulation and the right ventricle pumps it into the pulmonary circulation where oxygen and carbon dioxide are exchanged between the blood and alveolar gases.

The left side of the heart comprises the left atrium and the left ventricle. The blood leaving the lungs enters the left atrium by way of the pulmonary veins. Blood then flows from the left atrium into the left ventricle. The left ventricle ejects the blood into the aorta, which then distributes the blood to all the organs via the arterial system. Within the organs, the vasculature divides into smaller and smaller vessels, eventually forming capillaries, which are the primary site of exchange. Blood from the capillaries enters veins, which return blood to the right atrium via large systemic veins, the superior and inferior vena cava.

2.1.2 Cardiac cycle

The successive mechanical events characterizing the pump function of the heart during the cardiac cycle can be divided into two general categories: diastole (filling) and systole (ejection). The **diastole** refers to the period of time when the ventricles are undergoing relaxation and filling with blood from the atria (fig. 2.2a). Ventricular filling is primarily passive, although atrial contraction has a variable effect on the final extent of ventricular filling (end-diastolic volume). The **systole** is associated with the ventricular contraction and ejection and is initiated by electrical depolarization of the ventricles (fig. 2.2b). Ventricular ejection begins when ventricular pressure exceed the pressure within the outflow tract (aorta or pulmonary artery) and continues until ventricular relaxation causes the ventricular pressure to fall sufficiently below the aortic and pulmonary artery pressures leading to the aortic and pulmonic valves closing. The volume of blood remaining in the ventricle at the end of ejection is the end-systolic volume. The cardiac cycle can be further divided into seven phases: atrial systole, isovolumetric contraction, rapid ejection, reduced ejection, isovolumetric relaxation, rapid filling and reduced filling [12].
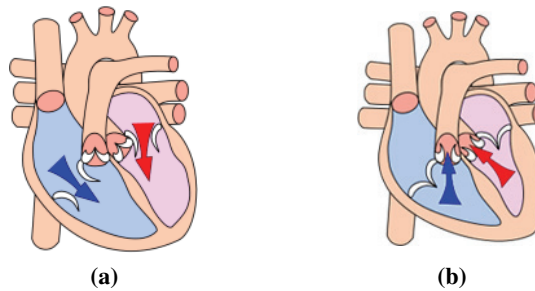
Figure 2.2: *Atrial 2.2a and ventricular 2.2b systoles. Image from wikipedia (cc by-sa).*

2.1.3 Cardiac electrical activity

Cardiac mechanical function is the consequence of an organized electrical activation of the myocardium. In order to properly accomplish this pumping role, the myocardium is mainly made up of two types of tissues: *contractile* and *conducting* tissue [13]. Contractile cells are the cells of the working myocardium and constitute the bulk of the muscle cells that make up the atria and the ventricles. An action potential in any one of these cells leads to vigorous force development and/or mechanical shortening. Conducting cells are specialized muscle cells that are involved in the initiation or propagation of action potentials rather than direct generation of force. The conducting cells are principally concentrated in the structures indicated in figure 2.4.

The primary function of cardiac myocytes is to contract. Electrical changes within the myocytes initiate this contraction. This section examines:

1. the electrical activity of individual myocytes, including resting membrane potentials and action potentials;

2. the way action potentials are conducted throughout the heart to initiate coordinated contraction of the entire heart.

The cardiac action potential

The inside of the cardiac cells have a negative electrical charge compared to the outside of the cells. The resulting voltage difference across the cell membrane is called the *transmembrane potential* . The resting transmembrane potential is around -80 to -90 mV in cardiac muscle [13].

When the cardiac cells are stimulated appropriately, channels in the cell membrane open and close sequentially. Channels opening allows ions to travel back and forth across the cell membrane, leading to patterned changes in the transmembrane potential. When these voltage changes are graphed against time, the result is the cardiac action potential (AP), illustrated in fig. 2.3. The cardiac AP is the reflection of the electrical activity of a single cardiac cell.

By convention, the AP is classically divided into five phases. The following description introduces them and indicates the current involved during each phase:
  – **Phase 0.** Phase 0 is the rapid depolarization phase, caused by a rapid influx of Na$^+$ ions into the cell (I_{Na}).
  – **Phase 1.** Phase 1 represents the initial fast repolarization caused by the inactivation of the

fast Na^+ channels and the opening of a special type of K^+ channels (transient outward, I_{to1}).

- **Phase 2.** This plateau phase is sustained by a balance between inward movement of Ca^{2+} (I_{Ca}, through L-type calcium channels) and outward movement of K^+ (I_{Ks}, through the slow delayed rectifier potassium channels).

- **Phase 3.** During this phase of rapid repolarization, the L-type calcium channels close while the slow delayed rectifier potassium channels (I_{Ks}) are still open. This ensures a net outward current, corresponding to negative change in membrane potential, thus allowing more types of potassium channels to open (I_{Kr} and I_{K1}). This net outward current causes the cell to repolarize.

  The delayed rectifier K^+ channels close when the membrane potential is restored to about -80 to -85 mV, while the inward rectifier K^+ channels (I_{K1}) remains conducting throughout phase 4, contributing to set the resting membrane potential.

- **Phase 4.** Phase 4 is the resting membrane potential. This is the period that the cell remains in until it is stimulated by an external electrical stimulus (typically an adjacent cell).

During the phases 0, 1, 2 and part of phase 3, the cell is refractory to the initiation of a new AP (*absolute refractory period*). This period is followed by the *relative refractory period* during which high intensity stimuli are required to elicit APs. Because not all the sodium channels have fully recovered at this time, the APs generated during this phase have a decreased phase 0 slope and lower amplitude.
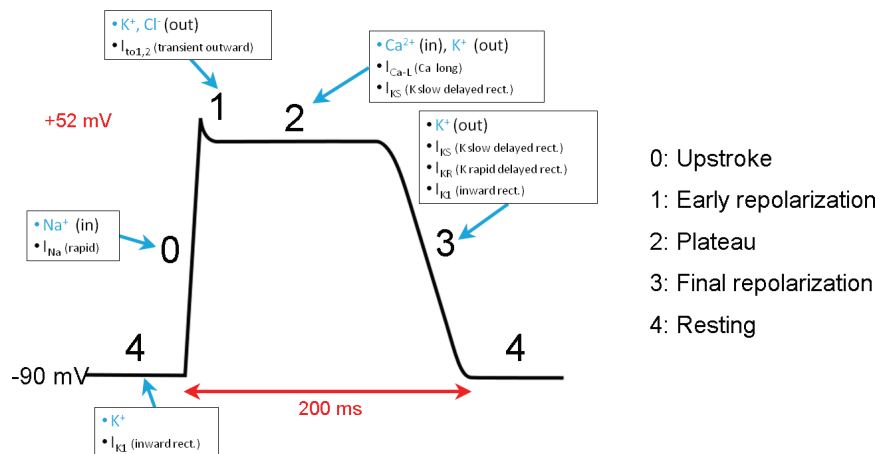
Figure 2.3: *Phases of the cardiac action potential. The types of ion channels (blue) and the currents (black) are indicated in the text boxes. The sharp rise in voltage (phase 0) corresponds to the influx of sodium ions, whereas the two decays (phase 1 and 3) corresponds to the sodium channel inactivation and the repolarizing efflux of potassium ions. The characteristic plateau (phase 2) results from the opening of voltage-sensitive calcium channels. Image adapted from wikipedia (cc by-sa).*

Excitability property

Cardiac muscle differs from skeletal or smooth muscles in three important aspects. First, the cardiac action potential is not initiated by neural activity. Instead, specialized muscle tissue in the heart itself spontaneously initiates the action potential (i.e. automaticity), making the heart contraction originating within the muscle (*myogenic*). Because of *gap junctions* between adjacent cardiac muscle cells, electrical activation spreads directly from cell-to-cell. Second, the duration
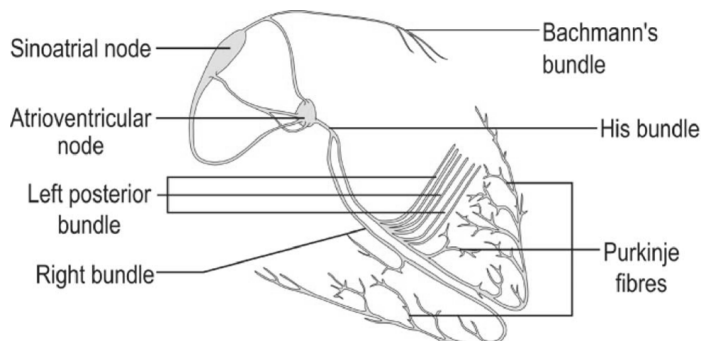
Figure 2.4: *The conduction system of the heart. Image from wikipedia (cc by-sa).*

of the cardiac action potential is much longer than that in skeletal muscle and lasts for almost a third of a second. As a result, a single action potential maintains tension development throughout systole. Neural and humoral influences have only a modulatory effect on heart rate. The third difference is that the contraction is not an all-or-none phenomenon. Skeletal muscle grades the strength of contraction through temporal and spatial summation. Because the heart contraction responses to a single action potential transmitted to all fibers, the cardiac muscle cells have evolved in a sophisticated system by which the force of contraction can be modulated from beat to beat (fig. 2.4) [13].

Of critical importance, is the *sinoatrial (SA) node*. The SA node lies in the right atrium near the entrance of the superior vena cava. SA nodal cells generate spontaneous action potentials and act as the normal pacemaker of the heart. An action potential in a cardiac muscle cell will, through its gap junctions, stimulate neighboring cells to generate an action potential such that each action potential in the SA node will be propagated over the whole heart. Because the SA node is located within the atria, action potentials will first be propagated over the atria.

Action potentials spreading across the atria eventually reach another conduction structure known as the *atrioventricular (AV) node*. The AV node is located at the junction between the interatrial septum and the ventricular one, between the origin of the coronary sinus and the septal leaflet of the tricuspid valve. The AV node serves two important functions. The first is to relay the wave of depolarization from the atria to the ventricles. A skeleton of connective tissue associated with the valves separates the atria from the ventricles, and the AV node is normally the only conductive link between the atria and the ventricles. The second function of the AV node is to delay the spread of excitation from the atria to the ventricles. AV node cells are specialized to conduct very slowly from cell to cell. This delay permits the atrial contraction (i.e. atrial systole, section 2.1.2), to fill the ventricles before the next contraction.

Fibers of the AV node give rise to fibers of the AV bundle (common bundle or *bundle of His*), which in turn divides into the *left bundle branch* and the *right bundle branch* (fig. 2.4). These branches then divides into an extensive network of *Purkinje fibers*. Purkinje fibers are conductile cells that conduct action potentials very rapidly. They are interconnected among the contractile cells of the ventricles and serve to quickly spread the wave of excitation throughout the ventricles. If conduction over the ventricles were slow, the heart would contract in a wave from base to apex, which would be very inefficient at ejecting blood out of the ventricles. The rapidly conducting Purkinje fibers, however, cause the ventricular cardiomyocytes to contract almost simultaneously.

Regional differences in action potentials

It is important to emphasize that all of these conducting structures (i.e. SA node, AV node, Purkinje network) are made of specialized cardiac muscle cells. Action potentials differ from region to region, reflecting the roles played by the different cell types.

Atrial cells have action potentials similar in many aspects to the ventricular action potentials described earlier. Thus, the resting potential (*phase 4*) is approximately -85 mV, and there is a fast upstroke (*phase 0*) generated by I_{Na}. The most distinguishing feature of the atrial action potential is that it has a more triangular appearance than the ventricular one [13]. This feature seems to be due to a prominent phase 1. Thus, in atrial cells, phases 1, 2 and 3 tend to run together, producing a triangular shape, with a distinct plateau not always apparent. This is likely due to a large I_{to} in atrial cells (cf. fig. 2.3) [13]. Figure 2.5 shows simulated atrial action potentials obtained with a modified Luo-Rudy membrane kinetics model at different pacing cycle lengths [14, 15]. This figure shows the rate-dependence of the action potential duration [16].
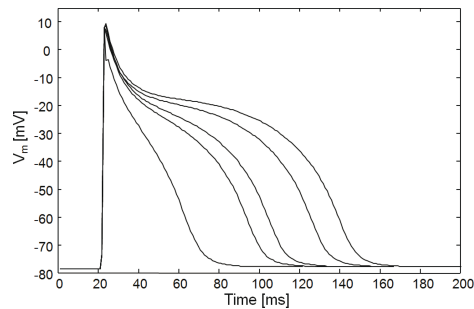
Figure 2.5: *Atrial action potentials at different pacing cycle length, from left to right: 80 ms, 100 ms, 120 ms, 150 ms and 200 ms. Image from Uldry et al. [16].*

2.2 Electrocardiography

2.2.1 Electrocardiogram

As cardiac cells depolarize and repolarize, electrical currents spread throughout the body and potential differences are established on the surface of the skin. The recording of body surface potentials as a function of time is called an electrocardiogram (ECG). The goal of electrocardiography is to utilize body surface potentials, available noninvasively, to evaluate the state of the heart.

The very first ECG recordings in man were made by Augustus Waller in the 1880s [17]. The Dutch physiologist Willem Einthoven further developed the recording device in the beginning of the 20th century by making use of a string galvanometer to record electrical potentials on the body surface [18]. He also defined sites for electrode placement on the arms and legs (first row of fig. 2.6), which remain in use today. Einthoven was rewarded with the Nobel Prize in medicine in 1924. Since then, the ECG has been widely developed, becoming an indispensable clinical tool in different contexts.

ECG recording

The electrical activity of the heart is measured on the body surface by attaching a set of electrodes to the skin. The electrodes are positioned so that the spatiotemporal variations of the cardiac electrical fields are sufficiently well reflected. For an ECG recording, the difference in voltage between a pair of electrodes is referred to as a *lead*. The ECG is typically recorded in a multiple-lead configuration, including unipolar and/or bipolar leads. An *unipolar lead* reflects the voltage variation of a single electrode and is measured in relation to a reference electrode whose voltage remains almost constant throughout the cardiac cycle. A *bipolar lead* reflects the voltage difference between two electrodes, e.g. between the left and right arm.
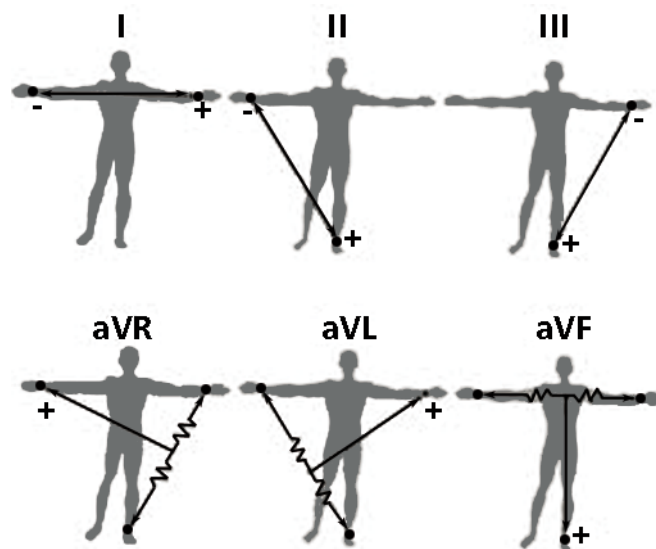
Figure 2.6: *Bipolar derivations forming Einthoven's triangle (upper row) and augmented unipolar derivations (lower row).*

A number of lead systems exist today with standardized electrode positions, including the standard 12-lead ECG and the orthogonal lead system producing a vectocardiogram (VCG). In practice, the preferred lead system is not necessarily chosen on the basis of maximized information content, but more often by clinical issues and practical considerations.

Standard 12-lead ECG

The standard 12-lead ECG is the most widely used lead system in clinical routine and is defined by a combination of three different lead configurations: the bipolar limb leads, the augmented unipolar limb leads (fig. 2.6) and the unipolar precordial leads. The 12-lead ECG is recorded by placing 10 electrodes at standardized positions on the body surface.

The three bipolar limb leads are denoted *I*, *II* and *III*, and are obtained by measuring the voltage difference between the left arm (V_{LA}), right arm (V_{RA}) and left leg (V_{LL}).

The augmented unipolar limb leads (aVF, aVL and aVR) use the same electrodes as the bipolar limb leads, but are defined as voltage differences between one corner of the triangle and the average of the remaining two corners. The augmented limb leads are considered to be unipolar because one electrode is exploring while the average of the other two serves as the reference electrode. The electrodes for the precordial leads (V_1, V_2, V_3, V_4, V_5 and V_6) are directly on the chest (fig. 2.7) and are considered to be unipolar.
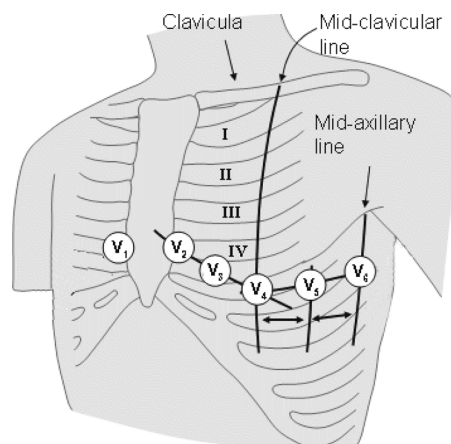
Figure 2.7: *Position of the precordial electrodes. Image adapted from Malmivuo and Plonsey [19].*

ECG waves and time intervals

We will now introduce the wave-naming convention and the relations between the different ECG complexes and the heart activation.

Each cycle of depolarization/repolarization of the heart (fig. 2.8) corresponds to the electrical activation of the atria and then the ventricles. On an electrocardiographic view, it becomes a sequences of waves named: P, Q, R, S and T.
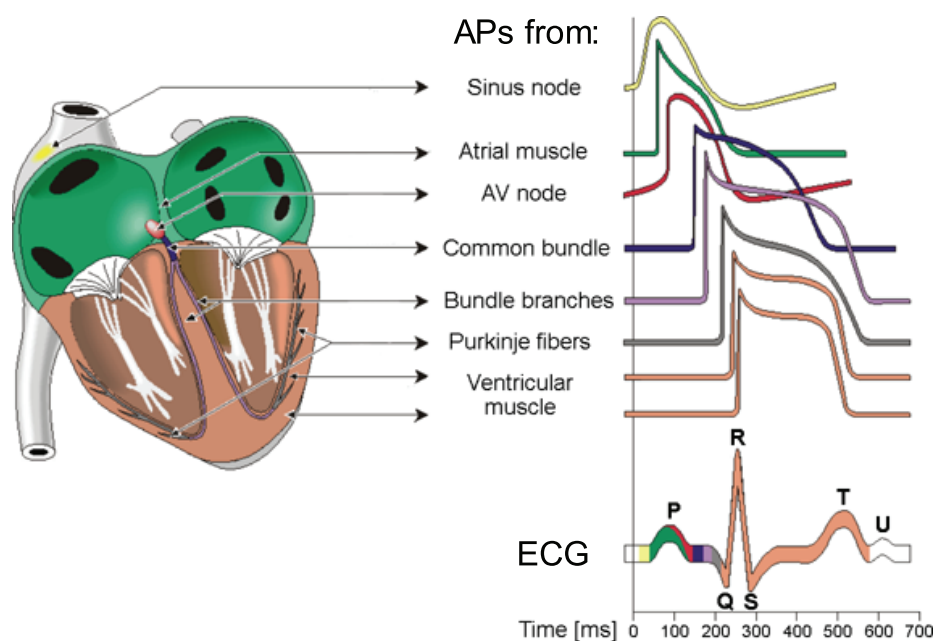
Figure 2.8: *APs and corresponding surface ECG. Image adapted from Malmivuo and Plonsey [19].*

The **P wave** represents the wave of depolarization that spread from the SA node throughout the atria. Its duration ranges usually usually from 80 to 110 msec. The brief isoelectric period after the P wave represents the time during which the atrial cells are depolarized and the impulse is traveling within the AV node. The **QRS complex** represents the depolarization of the ventricles. Its duration ranges from 60 to 110 ms, indicating that ventricular depolarization occurs rapidly. The **T wave** represents ventricular repolarization. The ST segment following the QRS is the period during which the ventricle is fully depolarized, and roughly corresponds to the plateau phase of the ventricular AP (fig. 2.8). The QT interval roughly estimates the duration of the ventricular AP.

2.2.2 Electrograms

The recording made of the cardiac electrical activity from an electrode placed inside the heart is called an *intracardiac electrogram* (EGM). The EGM is essentially an ECG recorded from within the heart. The major difference between a body surface ECG and an EGM is that the surface ECG gives a summation of the electrical activity of the entire heart, whereas the intracardiac EGM records the electrical activity of a localized area of the heart only, that is, the cardiac tissue surrounding the electrode.

The electrode is an electrical conductor used to make contact with the heart and convert ionic currents into electric currents that can be detected by electronic devices. The measured electrical potentials are actually measuring difference in potentials between two points. *Unipolar EGMs* represent the potential difference between the electrode in contact with the heart and a reference indifferent electrode, distant from the heart. Ideally, this reference electrode is placed at infinite distance, in practice, the pacemaker can is used (fig. 2.10a). *Bipolar EGMs* represent the potential difference between two closely spaced electrodes, the tip electrode and the ring electrode, proximal to the lead tip (fig. 2.10b). This setting is only possible with bipolar leads (fig. 2.9).
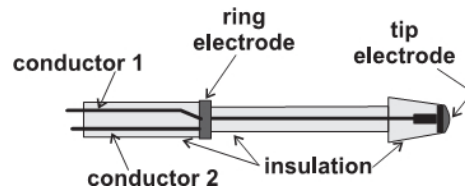
Figure 2.9: *Example of bipolar lead. Image from Barold et al. [20].*

The location of the electrode will define the type of EGM, i.e. atrial EGM (AEGM) or ventricular EGM (VEGM). An EGM may also record an electrical component originating away from the lead tip which is called the "far-field" signal, while the signal originating at the lead is called the "near-field" signal. For example, an AEGM may have a ventricular component, as illustrated in figure 2.11, where a far-field ventricular R wave (R_V) can be observed following the atrial near-field wave. Far-field signals are typically less sharp. Unipolar atrial EGM is thus typically composed of atrial and ventricular activities.

(a) *Unipolar system*   **(b)** *Bipolar system*
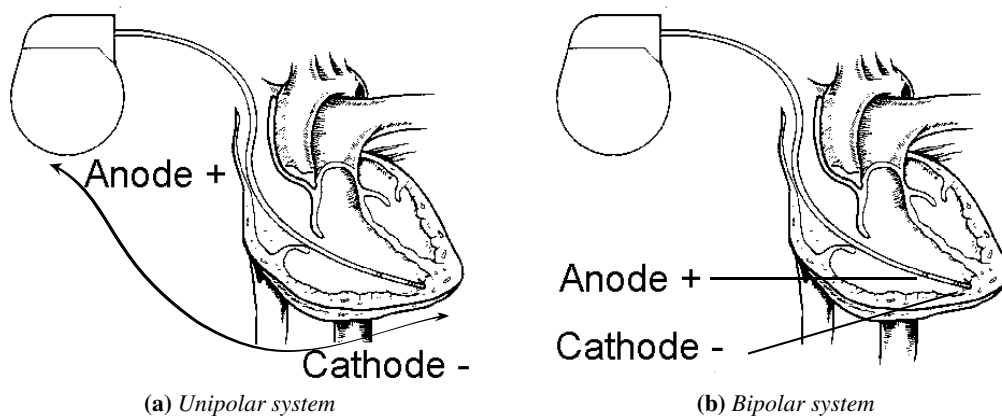
Figure 2.10: *Unipolar and bipolar configurations in a single chamber example.*
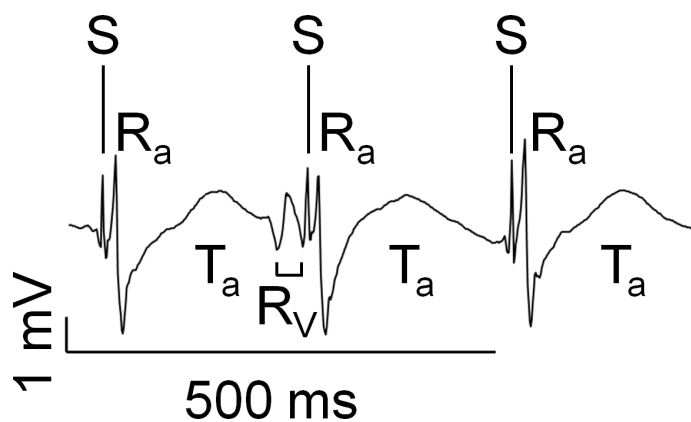
Figure 2.11: *Example of an unipolar atrial EGM. S: pacemaker stimulus; R_a: atrial depolarization wave; T_a: atrial repolarization wave; R_V: ventricular far-field depolarization wave.*

The potential being recorded is extracellular, but is a direct result of the transmembrane currents generated during the action potential of excited myocardial cells in a volume conductor (represented by the myocardial extracellular space, intracardiac blood and surrounding tissues) [21].

2.2.3 Monophasic action potentials

The monophasic action potential (MAP) is a reflection of local transmembrane action potentials [22], as illustrated in figure 2.12. MAP recordings are used to explore local myocardial activation and repolarization kinetics.

The sharp upstroke of the MAP waveform denotes cellular activation of surrounding tissue. The crest of the MAP plateau phase defines the peak positive amplitude (zero repolarization, denoted by an arrow in fig. 2.12), while the diastolic MAP level is determined as the 100% repolarization potential.

The action potential duration (APD) is commonly measured from the most rapid upstroke to the point on the repolarization phase that has returned to 90% of the amplitude towards baseline (APD_{90}) [23]. Other APD corresponding to different percentages of repolarization can be defined, as shown by the dashed lines (APD_{60}, APD_{30}). The most rapid upstroke is labeled "intrinsic deflection" (i.d.) in figure 2.12.
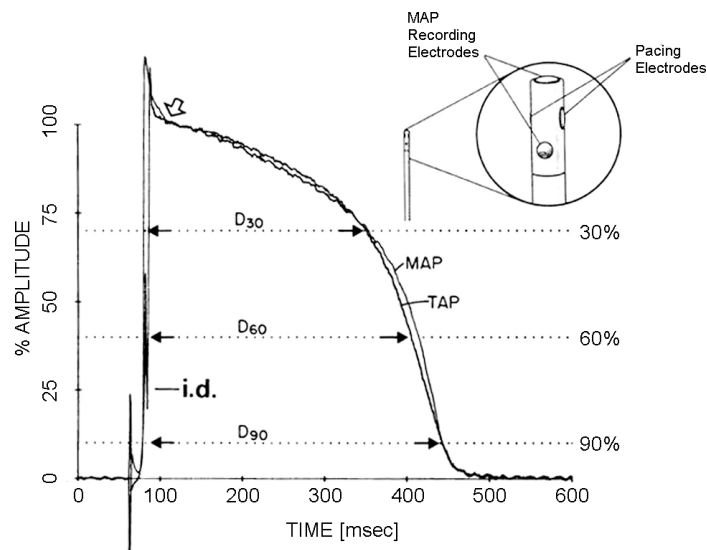
Figure 2.12: *Simultaneous recordings of intracellular transmembrane action potential and extracellular monophasic action potential (MAP). The white arrow denotes the 0% repolarization and the dashed lines the 30%, 60% and 90% of the return from plateau to resting potential. Image adapted from Moore et al. [22].*

2.3   Principles of electrophysiology study

In this section, we introduce the principles used in performing an electrophysiology (EP) study.

2.3.1   Recording and pacing

To discuss intracardiac recording and pacing, we need to introduce two terms related to time measurements: the *cycle length* and the *coupling interval*. When physicians talk about heart rate, they typically speak in terms of cycle length defined as the time interval between heartbeats. Thus, the faster the heart rate, the shorter the cycle length. The time interval between pacemaker stimuli is called pacing cycle length (PCL). When using a pacemaker to introduce a premature impulse, the time interval between the last normal impulse and the premature impulse is called coupling interval.

2.3.2   The leads

An EP study is performed by inserting conducting wires (electrodes) in strategic locations within the heart. Once in position, electrodes are used to perform the two essential tasks: recording and pacing.

Leads are made of 2 to 10 poles used for the simultaneous recording of cardiac EGM. They consist of insulated wires; each wire is attached to an electrode, which is exposed to the intracardiac surface. At the proximal end, wires are attached to a pin, connected to an external or internal device (such as a recording device or a pacemaker).

2.3.3   Pacing

To pace, a pulse of electrical current is delivered by an electrode to the cardiac muscle, where it causes cardiac cells near the electrode to depolarize, which is then propagated across the heart. By careful positioning of an electrode, one can initiate electrical impulses from almost any desired intracardiac location.

During EP study, *programmed stimulation* designates the delivery of stimuli at given PCL. There are several reasons for performing programmed stimulation. Precisely timed premature impulses (S2) allow one to measure the refractory periods of cardiac tissues. By introducing premature impulses in one location and recording EGMs in other locations, one can also assess the conduction properties of cardiac tissue.

Programmed stimulation consists of two general types of pacing: incremental pacing and delivery of extrastimulus.

Incremental pacing consists of delivering trains of impulses whose coupling interval decreases gradually (increased rate). The train may last for a few beats or for several minutes.

The *extrastimulus* technique consists in introducing one or more premature extrastimuli, each at its own specific coupling interval. The first extrastimulus is introduced at a coupling interval timed from the last of a short train of incrementally paced impulses. The term S1 (stimulus 1) is used for

(a) *APD$_{90}$ and preceding DI*

(b) *Restitution curve*
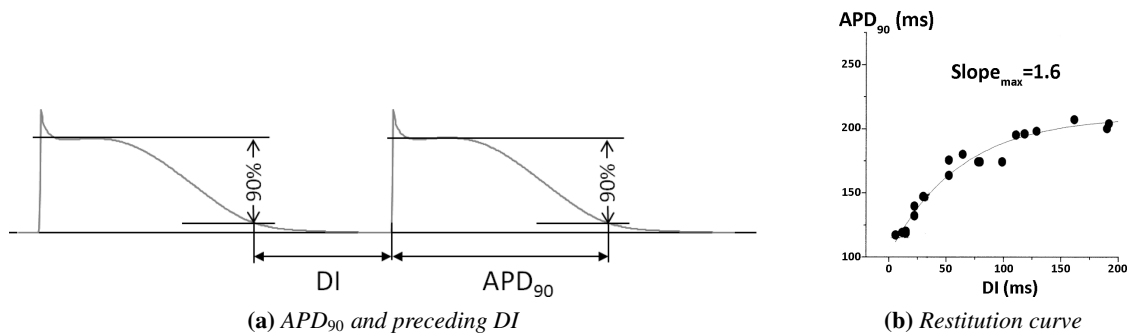
Figure 2.13: *(a) Example of MAP with the corresponding APD and DI. (b) Example of a restitution curve with slope >1.*

the incrementally paced impulses; S2 is used for the first programmed extrastimulus; S3 stands for the second programmed extrastimulus and so on.

2.3.4 Restitution curves

Restitution curve describes the relationship between the duration of an AP and its preceding diastolic interval (DI, fig. 2.13). This relationship describes the gradual decrease in APD with shorter DIs. The decrease in APD at faster rates decreases systolic (contraction) time which, in turn, maintains diastolic time and adequate cardiac filling for the next contraction.

Two restitution protocols are commonly used: the *standard* and the *dynamic* restitution protocols.

In the *standard* S1S2 restitution protocol, the preparation is paced at a fixed CL (S1S1) until steady-state is reached and is then perturbed by the delivery of an extrastimulus (S2) of varying coupling. Couples of DI and APDs are then used to build the APD restitution curve.

In the *dynamic* restitution protocol [24], the preparation is paced at a given CL until steady-state is reached. APD and DI couples acquired at multiple PCLs are used to construct the APD restitution curve.

2.3.5 Evaluation of the electrophysiologic properties of the heart

By recording and pacing from electrode leads, one can evaluate the fundamental EP properties of the heart, namely: conduction velocity and refractory periods.

Conduction velocity

Conduction velocity refers to the speed of conduction of an electrical impulse across the heart and is related both to the rate of rise (i.e., the slope) of the depolarization phase (phase 0) of the action potential and to the intercellular coupling (i.e. connexins). By measuring the time it takes for an electrical impulse to travel from one intracardiac location to another (referred to as a conduction

interval), one can use electrode catheters to assess the conduction velocities of a given portion of the cardiac tissue.

Refractory periods

The effective refractory period (ERP) is the period after depolarization during which a cell cannot be depolarized again and the relative refractory period (RRP) as the time period during which an incomplete AP is generated. Typically, the ERP extends to the end of the second third of the APD and the RRP from the ERP to the end of the APD at a time point where the first full blown AP is generated.

The refractory periods are assessed by the extrastimulus technique. The ERP is associated to the longest premature coupling interval (S1S2) at a designated stimulus amplitude that fails to propagate. The RRP is associated to the longest premature coupling interval that results in capture, generally at a prolonged conduction time.

Atrial Fibrillation

<div style="text-align: right; font-size: large;">**3**</div>

Atrial fibrillation (AF) is characterized by rapid and irregular activation of the atrium, at a rate between 300-600 bpm [25], as exemplified in figure 3.1. AF is the most common and troublesome arrhythmia in clinical practice and is a significant contributor to cardiovascular morbidity and mortality. Although AF can clearly occur in patients without evident heart disease (so-called lone AF), organic heart diseases, such as congestive heart failure (CHF), mitral valve disease and coronary artery disease, are major co-existing conditions contributing to the occurrence and persistence of AF. Understanding the mechanisms by which cardiac conditions favor the occurrence of AF may help designing more effective therapeutic interventions.
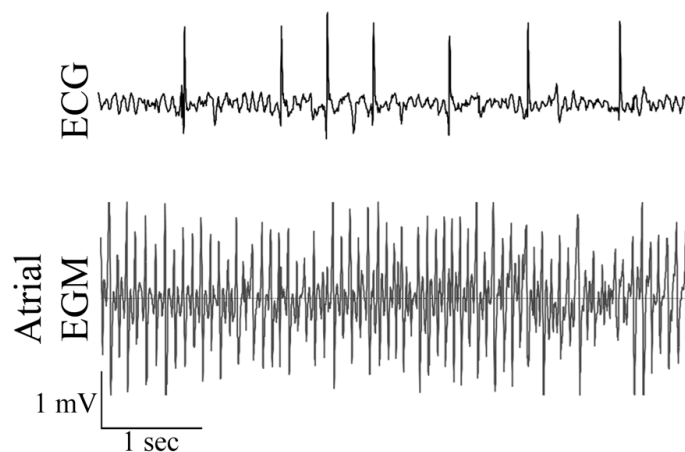
Figure 3.1: *Example of sustained AF. The upper row shows an ECG during AF. Note the absence of P waves, replaced by disorganized atrial depolarization and irregular R-R intervals due to irregular AV conduction. The bottom row shows the corresponding intracardiac atrial EGM.*

3.1   Mechanisms of atrial fibrillation

The underlying mechanisms of AF can be divided in two main components: the factors that trigger the arrhythmia and the factors that perpetuate the arrhythmia [26]. In general, patients with frequent, self-terminating episodes of AF are likely to have a predominance of triggering factors, whereas patients with persistent AF display some atrial remodeling perpetuating the arrhythmia.

The onset and maintenance of reentrant arrhythmias usually require the simultaneous presence of triggers and substrates. In human AF, foci from the pulmonary veins or other cardiac veins (i.e coronary sinus, superior and inferior vena cava) have been identified as common sources of rapid tachycardia, promoting fibrillatory conduction and reentry [26].

3.1.1   Mechanisms of atrial fibrillation initiation

The mechanisms favoring the emergence of foci from great cardiac vein have not been fully characterized and are likely to be multifactorial. Atrial triggers may initiate multiple reentrant wavelets and AF. In some patients with paroxysmal AF [1] impulses initiated by ectopic foci propagate across the left atrium and encounter tissue with variable recovery states that may in turn promote wavebreaks and reentry. If reentry is assumed to be the mechanism of AF, initiation would require an area of conduction block and a wavelength of activation short enough to maintain reentry.

AF triggering factors include sympathetic or parasympathetic stimulation, bradycardia, premature atrial complexes, atrial flutter, supraventricular tachycardias and acute atrial stretch.

3.1.2   Mechanism of maintenance of atrial fibrillation

Multiple factors may perpetuate and maintain AF [26]. For instance, AF can be maintained by sustained rapid firings from pulmonary veins, whose isolation helps to restore sinus rhythm. However, most AF episodes, once triggered, last without sustained focal firing, which is suggestive of additional factors such as electrical and structural remodeling. Importantly, atrial remodeling is associated with reduced atrial ERP, slowing of conduction velocity and decreased wavelength, all favoring emergence of multiple reentrant wavelets.

3.2   Role of regional factors

3.2.1   Pulmonary veins

Since the first description of spontaneous, independent firings of the pulmonary veins (PVs) by Brunton and Fayrer in 1876 [27], it has been known that PVs may exhibit electrical activity. More recently, PVs have been identified as potential source of AF triggers as reported for the first time by Haissaguerre et al. in 1998 [3]. However, the mechanism of focal activity within the PVs and what makes the PVs such fertile ground for focal activity remain unclear.

---

1. characterized by self-terminating episodes that generally last less than seven days.

3.2.2 Other vein triggers

Although over 90% of triggers that are mapped during EP studies occur in the PVs in paroxysmal AF, foci within the superior vena cava, the ligament of Marshall and the musculature of the coronary sinus have been identified [3]. Although these latter locations of triggering foci are uncommon, they helped to develop the concept that great cardiac veins harboring striated muscles are potentiel sources of triggers.

3.3 Atrial remodeling and atrial fibrillation

The term *remodeling* refers to the adaptation of the atria to sustained rapid rhythm such as during tachycardia or chronically elevated pressure such as during hypertension. More specifically, changes primarily affecting excitability and AP characteristics of atrial myocytes have been termed *electrical remodeling* , and the changes in chamber size, collagen deposition, and gross tissue structure have been termed *structural remodeling* [28]. This section focuses on recent studies that characterized the electrophysiologic remodeling taking place in human AF and in experimental models and on some of the molecular mechanisms underlying these changes. Historical aspects of electrical remodeling in human AF have been recently reviewed by Allessie et al. [29].

From experimental and clinical studies, it appears that electrical and structural remodeling play a significant role in the genesis and maintenance of AF. In figure 3.2, the different types of remodeling and their interactions are depicted.
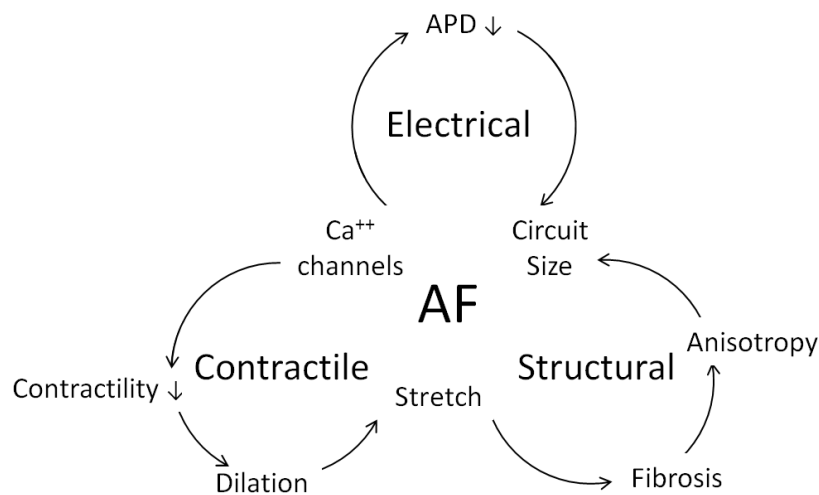
Figure 3.2: *Three proposed positive feedback-loops of atrial remodeling on AF. Figure adapted from Allessie et al. [30].*

3.3.1 Atrial electrical remodeling

Two independent experimental studies published in 1995 renewed the interest for the remodeling process taking place during AF [31, 32]. In a dog model of prolonged rapid atrial pacing (400 bpm), Morillo et al. found that the atrial ERP was reduced by about 15%. In a goat model, Wijffels et al. induced and maintained AF by automatically delivering bursts of stimuli (1 s, 50 Hz) as soon

as sinus rhythm occurred. This study showed that, in the presence of maintained fibrillation, the atrial ERP was reproducibly and rapidly attenuated, with much of the effect being evident within 24 hours of AF. Changes in the ERP were complete within one week of high-rate activity and after 2-3 weeks AF was persistent in 90% of the goats. This observation of tachycardia-induced electrical remodeling creating a substrate for persistent AF, led to the concept that "AF begets AF" [32].

The ionic mechanisms related to tachycardia-induced electrical remodeling have been explored in experimental [33] and clinical studies [34, 35]. AP recordings and patch clamp experiments in isolated atrial cells from animal models and patients in chronic AF showed a consistent pattern. AF affected the ion channels and mostly reduced the L-type Ca^{2+} current, explaining the shortening of the atrial AP and the loss of the physiological rate adaptation of the APD [33].

It has been shown that this process can be repeated several times without accumulation of ERP changes. Clinical studies showed that even very brief periods (minutes) of high-rate pacing were associated with reversible abbreviation of the atrial ERP [36].

The lack of accumulation in ERP changes, together with the clinical observation that the time course for development of persistent AF is somewhat slower than that for the atrial electrical remodeling, suggests that a second factor (structural remodeling) is important in the development of sustained AF.

3.3.2 Atrial structural remodeling

Structural change have been described in atrial myocytes after long-term lone AF and AF in combination with other etiologies. The first study to show that AF causes alterations in the structure of atrial myocytes was published by Morillo et al., in 1995 [31]. Rapid atrial pacing was applied to dogs over prolonged periods (6 weeks). Light microscopy and electron microscopy revealed changes in the atria. This observation was confirmed later in experimental study involving dogs and goats [5, 37–41].

The remodeling produced by atrial tachycardia and AF has been termed "tachycardia remodeling" to differentiate it from other forms of atrial remodeling [25]. The AF-induced structural changes in atrial myocytes include [30]:
   – increase in cell size,
   – perinuclear accumulation of glycogen,
   – central loss of sarcomeres,
   – alterations in the proteins involved in cell-to-cell propagation (connexins),
   – changes in mitochondrial shape,
   – fragmentation of sarcoplasmic reticulum,
   – changes in quantity and localization of cellular and nuclear proteins.

To summarize, it appears from clinical and experimental studies that electrical and structural remodeling play an important role in the genesis and maintenance of AF. Uncomplicated AF induces mainly electrical remodeling as represented by shortening of ERP.

4

Alternans

Congestive heart failure (CHF) is a major public health problem. It affects nearly 5 million people in the United States, with about half a million new cases each year [42].

T wave alternans (TWA) is a promising ECG index that indicates risk for sudden cardiac arrest from beat-to-beat alternations in the shape, amplitude or timing of ventricular T waves on the ECG [43]. This pattern was first described by Herring in 1909 and was initially thought to be of little significance [44]. TWA was subsequently observed in a surprisingly wide variety of clinical and experimental conditions associated with ventricular arrhythmias [45, 46].

As will be shown in this chapter, TWA is felt to reflect a combination of spatial and temporal dispersion of repolarization (fig. 4.1). Furthermore, TWA has been linked with inducible [6, 47] and spontaneous [7, 48, 49] ventricular arrhythmias and with basic mechanisms leading to their initiation [50, 51].

4.1   Microvolt T wave alternans

In the 80's Cohen and co-workers measured visually undetectable microvolt T wave alternans (MTWA) using signal processing tools based on a power spectrum analysis of T wave indices [47, 53]. They established for the first time a quantitative relationship between MTWA and susceptibility to ventricular fibrillation (VF). A clear relationship emerged from these studies: faster pacing rates were associated with a decrease in the minimum electrical current able to trigger VF (VF threshold) and an increase in TWA amplitude. Importantly, this peculiar pattern was generally not detectable by visual inspection of the ECG. In 1994, MTWA was established as a marker of susceptibility to sudden cardiac death (SCD) in patients with structural heart disease including CHF [6], a finding which was subsequently reaffirmed by a number of clinical trials [49, 54–64].

Recently, some advances have been made regarding the mechanisms of repolarization alternans
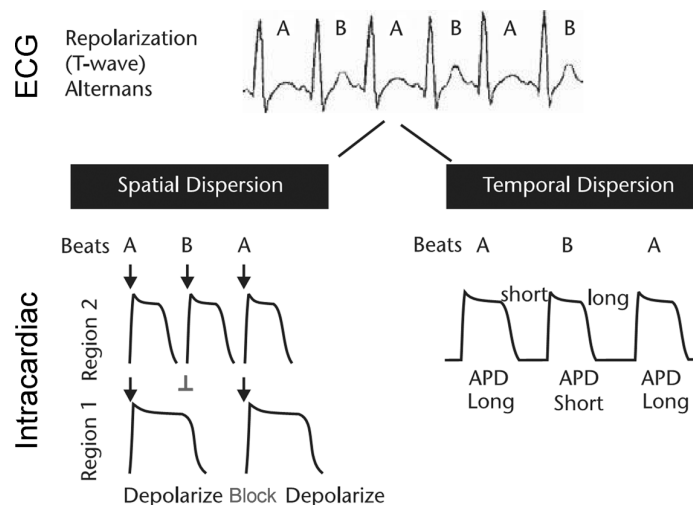
Figure 4.1: *Mechanisms underlying TWA. Left: spatial dispersion of repolarization. Compared to region 2, region 1 has longer APD and depolarizes every other cycle (beats 1 and 3). Right: temporal dispersion of repolarization. APD alternates between cycles. Figure adapted from Narayan [52].*

in patients suffering from CHF. Starting from the hypothesis that action potential duration (APD) restitution kinetics drives repolarization alternans, Koller et al. [65] compared dynamic (i.e. constant pacing) and standard (S1S2) APD restitution kinetics in patients with moderately reduced and normal left ventricular (LV) function. They found that in patients with LV dysfunction, alternans of APD occurred at lower heart rates, but both APD restitution kinetics showed similar steepness compared to the control group. The authors did show, however, that the dynamic restitution kinetics predicted APD alternans during induced ventricular tachycardia (VT) or rapid pacing, where VTs showing APD alternans had a diastolic interval (DI) that fell below the slope >1.

Narayan et al. [66] later on showed that MTWA results but not the steepness of the standard APD restitution separated patients with and without an adverse outcome during follow-up, and that DIs during which APD alternans was observed fell largely above the slope >1. Moreover, kinetics of standard APD restitution were similar between the right ventricle with normal function and the left ventricle with depressed function. More recently, Narayan et al. [67] observed that MTWA test correlated better with alternans of phase 2 (i.e. plateau) of the AP than with phase 3 (i.e. APD). They also showed that propagation velocity was not involved in the onset of APD alternans and that AP alternans was intermittent and of longer duration in CHF patients than in control ones. In a companion modeling study, the authors reported that decreasing I_{up} lowered the CL at which APD alternans appears (alternans threshold), increased phase 2 AP alternans and the number of alternating beats (i.e. decreased intermittency). Neither the clamping of $I_{Ca,L}$ nor that of cytosolic Ca^{2+} prevented alternans, but AP alternans was prevented by clamping sarcoplasmic reticulum Ca^{2+}.

Recently, Selvaraj et al. [68] studied spatiotemporal distribution of intracardiac alternans based on unipolar signals recorded from the endocardium and epicardium, and its relationship with MTWA. They found that intracardiac alternans was more prevalent at the epicardium than at the endocardium, that the amount of alternating electrodes increased as function of pacing rate, and that spatially discordant alternans displayed a base to apex distribution with non-alternating patterns (nodes) preferentially located at the mid myocardium. Moreover, LV apex (see Figure 4.2)

preferentially displayed alternans of the early ST segment (suggestive of phase 2 AP alternans), while the LV base preferentially showed alternans of the late ST segment (suggestive of phase 3 AP alternans). Similarly to the findings of Narayan et al. [67], repolarization alternans also appeared intermittent. Figure 4.2 shows an example of alternans intermittency at which apical early-ST alternans was present at the beginning of the recording, while basal late-ST alternans appeared at the end of the recording. Of note is the observation that a critical amount of intracardiac unipolar signals ought to alternate before being visible with MTWA testing.
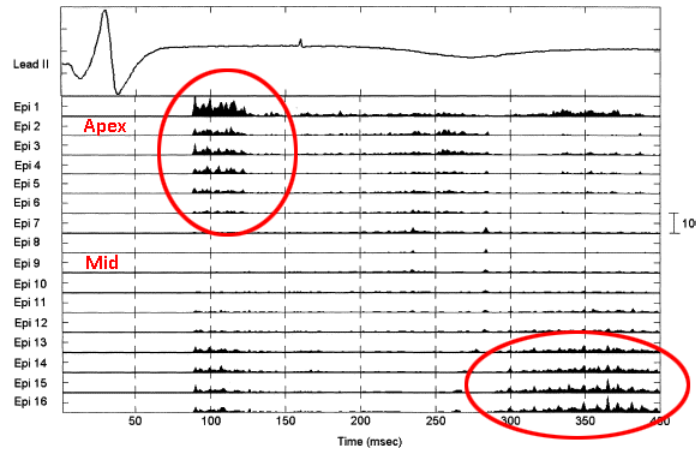
Figure 4.2: *Temporal heterogeneity of alternans. The top line shows a surface QRS complex and JT segment from lead II. The other lines show a measure of alternans based on power spectrum analysis, as a function of the JT interval for 16 epicardial electrodes (epi) along the anteroseptal ventricle. Figure adapted from Selvaraj et al. [68].*

4.2 Mechanism of repolarization alternans

TWA results from alternation of cardiac repolarization (i.e. APD and amplitude) at the cellular level [50, 51, 69]; however, the underlying mechanisms are not fully understood. One hypothesis states that repolarization alternans arises when the heart rate exceeds the capacity of myocytes to cycle intracellular Ca^{2+} [69, 70]. When one or more of the Ca^{2+} cycling proteins are impaired, the amount of released Ca^{2+} can only be fully reclaimed on an alternating beat basis, giving rise to alternation of free cytosolic Ca^{2+} levels. This, in turn, can cause alternans of membrane voltage (i.e. AP) via several electrogenic Ca^{2+} sensitive sarcolemmal currents ($I_{Ca^{2+}}$, I_{to2} and I_{Ks} for instance). A second hypothesis states that alternans of APD occurs when the slope of the APD restitution curve is >1 as determined by the kinetics of membrane currents [71–74]. The slope of the APD restitution curve appears to play a critical role in APD alternans and wavebreak [71, 74–76]. A number of experimental [75, 76] and theoretical studies [71, 77] have shown that a slope >1 promotes alternans, while a slope <1 prevents it. The APD restitution curve depicts the relationship between APD and its DI (see fig. 2.13). This relationship is typically monotone and concave. Theoretical studies have shown that below a critical value, which corresponds to the APD-DI coordinates of slope =1, stable alternans occurs in response to an increase in heart rate. Above this critical value, repolarization alternans will subside progressively (i.e. transient alternans) until a new steady state APD value is reached (i.e. APD accommodation).

Theoretically, it is believed that stable APD alternans occurs when the new pacing rate is above

the recovery kinetics of some sarcolemmal currents [78]. Some recent experimental works, however, seem to contradict this hypothesis, while pointing toward intracellular Ca^{2+} handling proteins as potential candidates for the pathogenesis of TWA [70, 79–84]. In the early nineties, it was shown that intracellular Ca^{2+} could alternate while keeping the membrane voltage clamped, suggesting that alternation of intracellular Ca^{2+} is the mechanism for AP alternans [85, 86].

Alternans of cytosolic Ca^{2+} [87, 88] may underlie APD alternans at an ionic level [82]. Normally, Ca^{2+} ions enter the myocyte via voltage-gated L-type Ca^{2+} channels and activate ryanodine receptors to trigger Ca^{2+} release, from the sarcoplasmic reticulum (SR), and cell contraction. A recirculating fraction of this Ca^{2+} is sequestered by Ca^{2+}-ATPase, and the remainder is extruded by the Na^+-Ca^{2+} exchanger (NCX). Rapid heart rates may overload this homeostatic capacity to cause alternans of Ca^{2+} cycling [86, 87] and AP, via effects on membrane currents [82, 89]. Ca^{2+} accumulation appears to underlie the hysteresis in repolarization alternans [90] and TWA threshold [91], such that alternans is larger in magnitude following deceleration from a rapid heart rate. Impaired Ca^{2+} cycling may facilitate APD alternans in heart failure [92]. Ca^{2+} cycling also links electrical with mechanical alternans [88, 93], giving a reasonable explanation for mechanical alternans preceding electrical alternans in some preparations [86]. Finally, APD alternans during ischemia may also follow transmural differences in potassium channel (I_{KATP}) activity [94], reduced ATP availability [70], or cellular uncoupling [95].

As discussed in the preceding section, the "restitution" hypothesis as the driving mechanism for AP alternans in humans can be reasonably discarded. Single cell studies, either based on experimental preparation or on computer models, have also recently reported the lack of relationship between standard and dynamic restitutions and AP alternans. The elegant study by Goldhaber et al. [84] showed that the DI at which AP alternans appeared was largely above the value of slope >1 for both restitution protocols. Inhibiting SR Ca^{2+} cycling function or buffering cytosolic Ca^{2+} both suppressed APD alternans, but did not affect the slope of the standard APD restitution, which is mostly dependent on the recovery kinetics from inactivation of the $I_{Ca,L}$. On the contrary, because rapid pacing increases diastolic and systolic Ca^{2+}, preventing Ca^{2+} build-up at the tubular SR space with SR Ca^{2+} cycling blockers flattened dynamic APD restitution and prevented APD alternans.

In a modeling study, Livshitz et al. recently attempted to determine the respective role of key SR Ca^{2+} cycling proteins in the promotion of AP and Ca^{2+} alternans [96]. Fitting experimental data, they observed that the releasable pool of SR Ca^{2+} (junctional SR) after reaching a maximum during incremental pacing slightly decreased with a further increase in pacing rate; then, due to the long time constant of SR Ca^{2+} release from the junctional SR compartment, Ca^{2+} release started to alternate. Both I_{up}, the SR Ca^{2+} uptake and I_{tr}, the refractoriness of Ca^{2+} release by Ryanodine receptor and Ca^{2+} diffusion across the SR, were involved. Importantly, inhibition of CaMKII suppressed Ca^{2+} build-up during rapid pacing (i.e. force-frequency relationship) and AP alternans. CaMKII is an SR regulatory enzyme that is overexpressed in CHF and cardiac hypertrophy. Its overexpression, as an attempt to compensate for the reduced cardiac function, may therefore facilitate Ca^{2+} and AP alternans, and predispose patients to tachyarrhythmias.

4.3   From spatially concordant to spatially discordant alternans

Experimentally, two types of repolarization alternans have been reported, i.e. *spatially concordant alternans* (SCA) and *spatially discordant alternans* (SDA). When alternans occurs in a tissue,

different spatial patterns can develop. In the simplest case, the entire tissue experiences collectively a long or short AP. However, a number of factors can promote the formation of more complex spatial dynamics, when different regions of the tissue respond inhomogeneously. The APD may vary spatially, but as long as the entire tissue still alternates "long-short" uniformly, the tissue is said to exhibit SCA. When the tissue begins to alternate "long-short" in some areas but "short-long" in other areas, SDA is present [50].

It is possible to determine whether alternans is concordant or discordant by plotting two successive APDs at all points in the tissue. In a one-dimensional cable, for instance, such a plot will show two non-intersecting lines of APD if the alternans is concordant, but will have one or more intersections during discordant alternans. The points of intersection are called nodes (or nodal lines or surfaces in two or three dimensions) and represent locations where the APD is constant from beat to beat. Nodes may be stationary or may travel, generally toward the site of stimulation [97].

During SCA, dispersion of repolarization was not different from values measured at slower rates without AP alternans [50]. SDA is usually triggered by faster rates than SCA [50]. Dispersion of refractoriness increased substantially during SDA, which greatly enhanced the susceptibility to reentrant arrhythmias [50, 51]. The delivery of a single premature beat resulted in a unidirectional block of conduction in the region of most delayed repolarization, which was retrogradely activated, forming the first spontaneous beat of a reentrant arrhythmia [50, 51]. Importantly, initiation of reentrant arrhythmias requires a certain amount of repolarization dispersion to favor unidirectional block of conduction, retrograde invasion of the refractory tissue and reentry [50, 98]. However, all arrhythmogenic diseases do not necessarily display the required amount of APD dispersion. SDA is a mechanism for amplifying physiological heterogeneity of repolarization to pathophysiological level which serves as a substrate for reentrant excitation. SDA might be one of the candidates, because it appears only above a given heart rate threshold.

Despite considerable progress in the understanding of the pathophysiological process leading to alternans, the mechanisms promoting SDA remain elusive. Interestingly, some clues have been recently provided by theoretical studies using computer models [71, 72, 77]. These studies are pointing towards conduction velocity (CV) as a possible candidate for the promotion of phase reversal between islands of alternating tissue. CV depends on many cellular and extracellular factors among which membrane excitability and cell-to-cell coupling play a major role. Interestingly, both abnormal membrane excitability and cellular uncoupling have been shown to be arrhythmogenic. Restitution of CV assesses the ability of an excitation front to propagate across a tissue as a function of the pacing or DI. Under normal conditions, CV is maintained over a broader range of DI (i.e. CV is engaged for shorter DI) than APD. The earlier the premature beat, the slower its propagation and the longer its activation time (AT). Theoretical studies suggest that CV restitution opposes APD restitution. The increase in AT over space at short coupling interval (i.e. rapid rates) tends to oppose the reduction in DI as a result of the APD-DI relationship. Figure 4.3 shows two consecutive APD and their AT values in a fiber paced at the left end [72]. The plain line represents the even beat and the dashed line the odd beat. At an intermediate pacing rate (CL 230 ms), APD alternans appears maximal at the pacing site, but decreases over space because of the small engagement of CV as shown by the small alternation in AT values. At a faster pacing rate, CV is much more engaged as shown by the increase in AT. For the even beat for instance, the prolongation of the AT at a given point may overcome the reduction in DI, allowing the DI and therefore its APD to increase again. This, in turn, results in a phase reversal of APD value, also called SDA because islands of APD are spatially in opposite phase [72]. Importantly, theoretical studies have clearly established that the
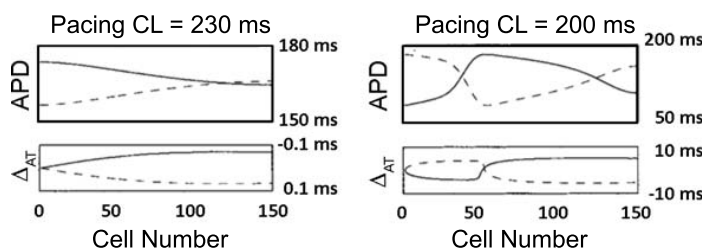
Figure 4.3: *APD and AT dynamics of even (plain) and odd (dashed) beats at two different pacing CL. Image from Fox et al. [72].*

engagement of CV at low heart rate (i.e. CV restitution curve with a long time constant) promotes phase reversal and therefore SDA and dispersion of refractory periods.

Over the last years, two hypotheses prevail for the formation of SDA:

1. pre-existing tissue heterogeneities result in variation in alternans amplitude, upon which an appropriately timed premature beat or an increase in pacing rate reverses alternans phase in one part of the tissue [50, 99, 100]. SDA thus appears around locations of heterogeneity immediately as pacing rate increases [101];

2. modeling and experimental studies also suggested that steep CV restitution underlies SDA formation [72, 77, 102–104].

Finally, others [71, 73] have suggested that both tissue heterogeneities and steep CV restitution may be involved in SDA.

Recently, Hayashi et al. [101] in a modeling study reported that these two mechanisms may be distinguished by behavior of nodal lines. If SDA develops according to the 1st mechanism: nodal lines would form at locations dictated by underlying tissue heterogeneity with two different scenarios: 1A) in presence of APD heterogeneity, nodal lines form and drift away from the pacing site on a beat-to-beat basis without reaching steady state; 1B) in presence of intracellular Ca^{2+} heterogeneity, nodal line may reach steady state and remain pinned despite an increase in pacing rate. If SDA develops according to the 2nd mechanism: nodal lines may reach steady state and move towards pacing site as pacing rate increases.

In 2008, in an elegant optical mapping study based on langendorff-perfused rabbit hearts, Mirinov et al. [105] reproducibly reported two patterns of nodal lines behavior. The first and most prevalent one was a pattern of stable SDA, where nodal lines drifted towards the stimulus site as pacing rate increased. This pattern showed a tight spatial correlation between CV alternans and APD alternans (top row of Figure 4.4) suggesting that CV restitution kinetics may be the mechanism for stable SDA formation. The second and less prevalent behavior was a pattern of unstable SDA, where nodal lines continuously drifted across the recording field. Importantly, both the stable and the unstable behaviors did not correlate with APD heterogeneity. Bottom row of Figure 4.4 shows the lack of spatial correlation between CV and APD alternans for the unstable behavior as opposed to the stable one (top row). Most importantly, sites showing unstable nodal line behavior displayed slower APD accommodation to changes in pacing rate than sites with stable behavior, suggesting that short-term memory, i.e. the dependence of APD on the entire pacing history and not only on the preceding DI, plays a significant role in preventing the spatial pining of SDA. It can be speculated that because APD continuously change over time but also depend on the overall pacing history, APD values may never reach steady state. The cellular mechanisms underlying the
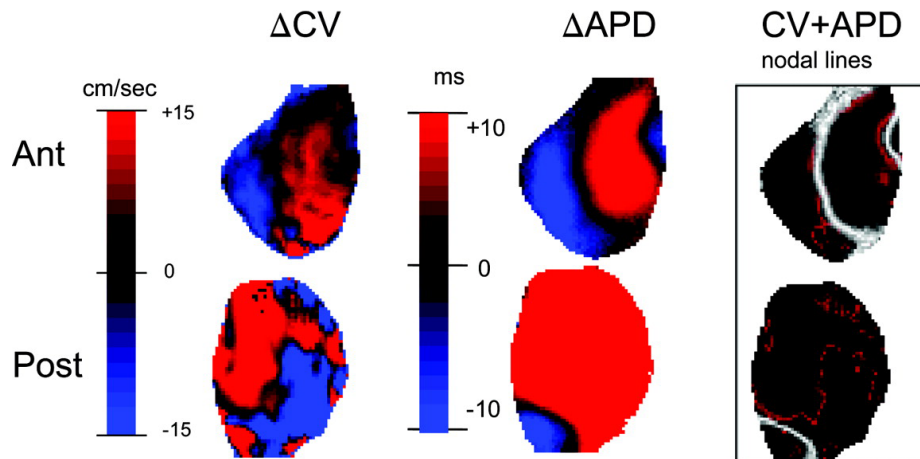
Figure 4.4: *CV and APD alternans. Steady-state alternans maps for posterior and anterior surfaces at a basic cycle length of 135 ms showing alternans in CV (left), alternans in APD (middle), and superposition of their nodal lines (right). The APD and CV nodal lines are shown in white and red, respectively. Image from Mironov et al. [105].*

slow APD accommodation remains, however, undetermined yet.

4.4   Repolarization alternans and susceptibility to arrhythmias

Although most efforts have focused on the role played by APD alternans in reentrant ventricular arrhythmias, clinical, experimental and modeling studies suggest that repolarization alternans may also play a role in promoting atrial arrhythmias [8–11].

Kim et al. [10] were among the first to report APD restitution kinetics and AP alternans from the right atrium of patients with persistent and paroxysmal AF. Patients with persistent AF displayed shorter APD and ERP, allowing steeper APD restitution slopes as compared to controls. Patients with paroxysmal AF laid in between. Interestingly, patients with persistent AF showed an increased dispersion of APD slopes as measured at five right atrium sites. The increased dispersion produced an increase in APD dispersion near ERP but not at slow pacing rate. The same year, Narayan et al. [8] showed that in patients with typical atrial flutter (i.e. isthmus dependent) who developed AF during overdrive pacing, a progressive increase in pacing rate caused alternans of APD from the cavo-tricuspid isthmus, followed by AF. Conversely, in patient with typical atrial flutter who did not develop AF, APD alternans was less common and occurred only at faster pacing rates. Cavo-tricuspid isthmus of inducible patients displayed longer APD, rate-maladaptation and lower APD alternans threshold than non inducible patients. SDA was also observed in the right atrium of inducible cases. Importantly, APD alternans and conduction block also preceded episodes of spontaneous disorganization of atrial flutter into AF.

In a canine experiment with autonomic blockade, Watanabe et al. [9] showed that 60 min of rapid atrial pacing decreased APD alternans threshold as compared to baseline values. APD alternans was also observed before episodes of rapid-pacing induced AF. Interestingly, the right atrium ERP measured at short pacing CL that induced APD alternans showed double values, with long ERP following long APD and short ERP following short APD. This substantiates the concept

that APD alternans increases dynamically the dispersion of ERP, and may explain the paradoxical increase in atrial ERP observed in several atrial experiments at rapid pacing [32]. Recently, Narayan et al. [106] compared right and left atrium APD and AT kinetics in patients with paroxysmal and persistent AF. Major differences in both kinetics were reported. Patients with paroxysmal AF displayed steep APD and AT kinetics as compared to persistent AF patients whose APD restitution was flat because of an early prolongation of AT at long coupling intervals. Only patients with paroxysmal AF developed AF following the delivery of a single premature beat. Interestingly, the oscillations of APD of the first beats at AF onset followed tightly the APD restitution curve. This finding suggests that APD restitution governs APD values for this mode of AF onset triggered by single premature beat, but not by rapid pacing. In patients with persistent AF, striking differences in APD and AT kinetics were observed between the left and the right atrium. In contrast to the left atrium, right atrium APD and AT kinetics were steep and comparable to the values of patients with paroxysmal AF, confirming the findings of Kim et al. [10]. The underlying mechanisms for right and left atrium differences as well as for the early prolongation of AT in the left atrium of persistent AF remained undetermined yet. One can speculate, nevertheless, that if the driving source of persistent AF is indeed in the left atrium, as suggested by recent clinical papers [107], the right atrium is partly protected from electrical and/or structural remodeling by left-to-right fibrillatory conduction.

TWA is dependent on the heart rate but is independent of any sympathetic activity as shown by experimental [50, 51] and clinical studies [64]. TWA amplitude, however, increased more during exercise than during atrial pacing [108]. Furthermore, beta-blockers reduced the amplitude of TWA but did not change the threshold at which alternans occurred [64], suggesting that the sympathetic nervous system may play a substantial role. Experimentally, the autonomic nervous system (ANS) plays a role in the initiation and maintenance of AF. Stimulation of the parasympathetic system alters substantially the electrophysiology of the atria. Vagal stimulation decreases APD, increases dispersion of refractoriness, promotes triggered beats, all of which favors AF during rapid pacing [109–113]. Although sympathetic stimulation also decreases APD and increases triggered beats, it does not promote dispersion of refractoriness and thus AF during fast pacing [110]. The precise role of the ANS for AF in humans remains elusive. Coumel and colleagues were the first to report vagal and adrenergic AF [114, 115]. These cases typically concerned young adults, in their 30's to 40's. Vagal AF was preceded by some slowing of the sinus rhythm, which favored the emergence of ectopic beats (presumably early afterdepolarization from the pulmonary veins) and AF. In contrast adrenergic AF was preceded by some critical increase in heart rate, above which AF was triggered by some ectopic beats. Interestingly, these cases appear to fit the clinical description originally done by Haïssaguerre and colleagues of young adults with focal paroxysmal AF [3].

Is there a link between susceptibility to AF, repolarization alternans and the ANS? The first clue came from the elegant study of Jayachandran and colleagues [116]. The authors showed that weeks of rapid atrial pacing in dogs resulted in some heterogeneous sympathetic hyperinnervation, which, in turn, favored dispersion of repolarization and AF in contrast to unpaced dogs. Then, Miyauchi and colleagues [117] showed that myocardial infarction of limited size in dogs produced sympathetic hyperinnervation but no mechanical remodeling of the atria. Dogs with sympathetic hyperinnervation showed increased susceptibility to AF and dispersion of repolarization, and steeper APD restitution curves. Immediately before the onset of AF, APD alternans was maximal in remodeled dogs, but not in controls. Optical mapping showed multiple wavebreaks at the onset of AF, suggesting that repolarization alternans, by enhancing dynamically dispersion of APD, promoted block of conduction and reentry.

4.5   Concluding remarks

Considerable progress has been made in the understanding of the mechanisms leading to AF. Decreased APD [118], increased dispersion of refractory periods [118] and inhomogeneous atrial conduction [119] due to electro-anatomical remodeling are the hallmark of patients suffering from AF. However, up to 30% of AF episodes occur without cardiopulmonary disease (i.e. lone AF), and experimentally specific interventions such as vagal stimulation or rapid pacing are necessary to reach the critical amount of dispersion of repolarization for wavebreaks and reentry. Repolarization alternans, a beat-to-beat alternation in APD [61], appears to be dependent both on the heart rate and on the ability of Ca^{2+} cycling proteins to recycle intracellular Ca^{2+} [51, 64, 76]. Importantly, repolarization alternans: 1) is promoted by interventions decreasing the function of Ca^{2+} -induced Ca^{2+} release mechanisms [51, 64, 74, 76] (such as seen in electromechanically remodeled atria and ventricles), 2) enhances dynamically dispersion of repolarization (i.e. SDA) when conduction velocity is engaged at long coupling intervals [105] (i.e. slowing of propagation at long DI), 3) has been shown to be theoretically [120, 121] and experimentally [61, 63, 67, 87, 121] involved in reentry and wavebreaks, and 4) appears to be enhanced by sympathetic activation [59, 87].

Part II

Experimental Model

5

Experimental setup

In this study, we have developed a chronic model of pacing-induced atrial tachycardia in sheep. This ovine model makes possible the acquisition of unipolar atrial EGMs during EP (electrophysiological) protocols, from baseline conditions until the development of pacing-induced sustained AF. This chapter explains the implantation procedure, recording setup, pacing protocols and analyses performed. Experiments were carried out in accordance with the European convention for the protection of vertebrate animals used for scientific purposes.

5.1   Implantation procedure

The implantation procedure is organized as follows: sheep are premedicated, sedated and intubated. Under general anesthesia, two pacemakers are implanted. The first one is used for the recording of intracardiac unipolar EGMs and is implanted subcutaneously in the right neck region. The second one is used for stimulating the right atrium and is implanted under the muscles in the right shoulder region. The screw-in leads (fig. 5.1) are inserted via the right jugular vein into the right atrium or the right ventricle as shown in figure 5.2.

Figure 5.1: *Tip of a screw-in lead.*

We developed two different experimental setups, the first one with normal atrioventricular (AV) conduction and the second one with AV block after the ablation of the AV node. In the first setup, two atrial leads are implanted and connected to one of the pacemakers. An impulse initiated in the right atrium will therefore propagate normally to the ventricles via the AV node. In the second setup, two additional ventricular leads are implanted and the AV node is ablated by applying
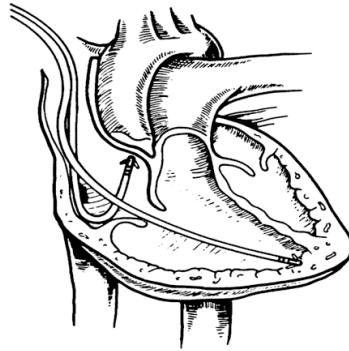
Figure 5.2: *Schematic of dual chamber pacemaker implantation. One lead is implanted in the right atrium, the other one in the right ventricle.*

(a) *Two leads*   **(b)** *Four leads*
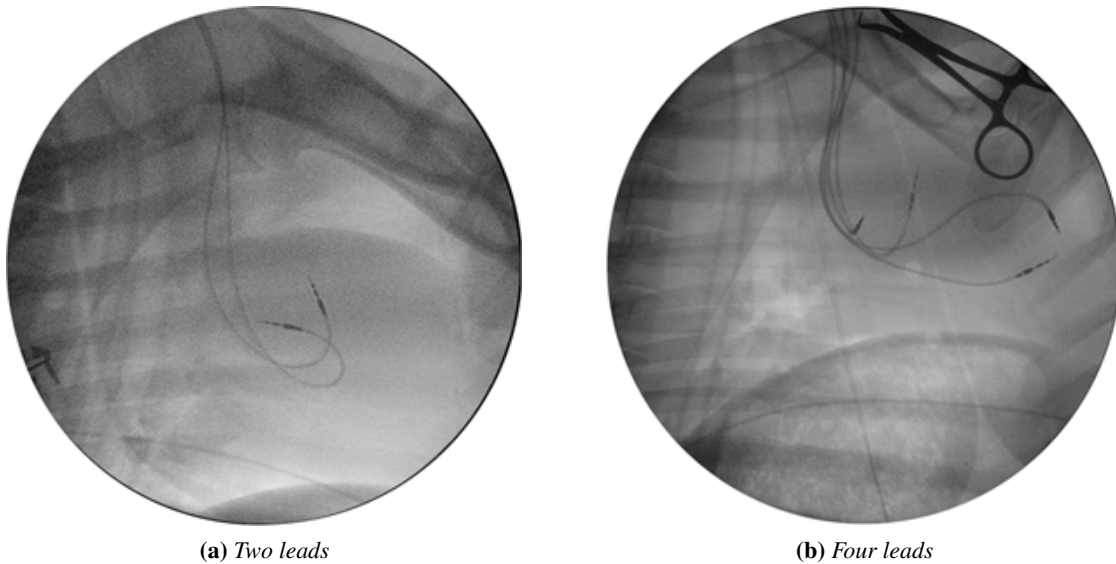
Figure 5.3: *Radiographs (X-ray images) of the electrodes. (a) Two atrial leads with normal AV junction. (b) Two atrial and two ventricular leads following ablation of the AV junction.*

radiofrequency currents. In the latter setup, the ventricular rhythm is maintained by the pacemaker. Importantly, far-field ventricular potentials of variable amplitude altered the recording of atrial EGMs. During rapid pacing with 2:1 AV conduction, far-field ventricular waves impinging on atrial repolarization waves could artificially produce atrial repolarization alternans and prevent quantitative measurement of alternans. Thus, controlling the ventricular rate is useful to avoid 2:1 AV conduction at short pacing cycle lengths.

5.1.1 Atrioventricular node ablation

As introduced before, the AV junction has been ablated in a subgroup of sheep with additional ventricular leads. 8-mm ablation catheters (EPT, Boston Scientific) were successfully used for the ablation of the AV junction. Figure 5.3 shows representative radiographs of a sheep with two right atrial leads and normal AV conduction (5.3a) and of a second sheep with two right atrial and right

(a) *Before AV node ablation*   **(b)** *After AV node ablation*
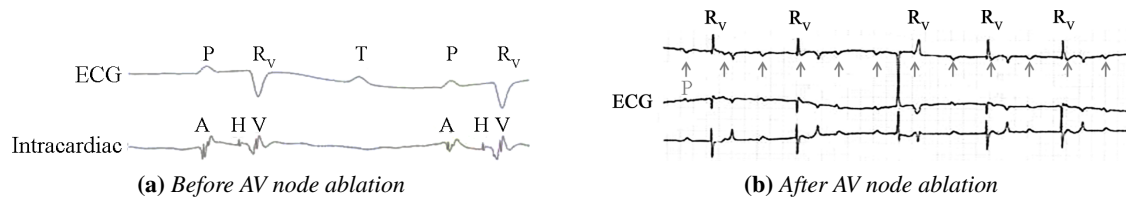
Figure 5.4: *Intracardiac and surface recordings before (a) and after (b) ablation of the atrioventricular node. The intracardiac signal in panel (a) was recorded with the ablation catheter, the labels A, H and V refer to the right atrial, His and right ventricular potentials respectively. The surface ECG in panel (b) shows the dissociation of atrial (arrows) and ventricular contractions.*

ventricular leads following ablation of the AV junction (5.3b). The ventricular rate was programmed at 40 bpm (1500 ms) in the AV block group during the recordings of atrial EGMs at variable PCL, and between 60 and 170 bpm in DDD mode in-between recordings.

Figure 5.4 shows intracardiac EGM and ECG recordings before (5.4a) and after (5.4b) ablation of the AV junction. In panel (a), the labels A, H and V respectively denote right atrium, His and right ventricular potentials as recorded by the ablation catheter. Radiofrequency burns at this location, close to the His bundle, produced sustained AV block as shown in panel (b). Note the lack of relationship between P waves (red arrows) and right ventricular escape rhythm (R_V).

5.2   Pacemakers

5.2.1   Recording pacemaker

Vitatron T70 pacemakers are used as recording pacemakers. As for most pacemaker connectors, the atrial port filters the signal using a 20-80 Hz band-pass filter preventing any recording of slow repolarization components [20]. In contrast, the ventricular port of the T70 Vitatron PM filters the signal using a 0.4 Hz high-pass filter, which allows the recording of smooth repolarization waves. The atrial lead is thus plugged into the ventricular channel in order to record both depolarization and repolarization waves. Figure 5.5 shows a typical unipolar broadband atrial EGM, where the pacemaker stimulus (S) is followed by atrial depolarization (R_a) and repolarization (T_a) waves. A far-field ventricular depolarization (R_V) can also be observed, as discussed before, which may contaminate atrial repolarization waves during 2:1 AV conduction. The EGM are high-pass filtered by the pacemaker at 0.4 Hz and digitized at 800 Hz with 8-bit resolution.

5.2.2   Stimulation pacemaker

The stimulation pacemaker model is a Medtronic Diamond 3, with a special routine for the delivery of customized pacing protocols, including S1S1, S1S2 and burst pacing protocols, developed in collaboration with Vitatron Arnhem, NL [1]. The uploading and the control parameters of the pacing protocols are detailed in appendix B.

---

1. With the collaboration of H. de Bruyn and P. van Dam
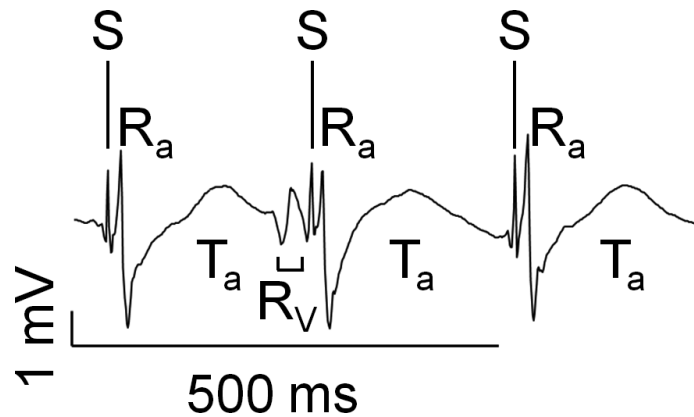
Figure 5.5: *Unipolar atrial EGM. S: pacemaker stimulus; R_a: atrial depolarization wave; T_a: atrial repolarization wave; R_V: ventricular depolarization.*

5.3   Recording setup

Once the pacemakers have been implanted, EGM recordings during EP protocols are performed weekly after light sedation (intramuscular Xylazine 0.2 mg/kg). During the stimulation protocols, three ECG derivations and one intracardiac right atrial EGM are simultaneously recorded. Four needles are used to record the subcutaneous ECGs, placed at locations corresponding to the limb electrodes in a standard 12-lead ECG, i.e. on the right arm (RA), left arm (LA), right leg (RL) and left leg (LL) (fig. 5.6). The needles are connected to a Holter device which stores the three resulting unipolar ECGs: *aVL*, *aVR* and *aVF* (as defined in section 2.2.1).

Pacemakers are interrogated and programmed using a Medtronic programmer (fig. 5.6, right hand side). An antenna connected to the Holter device is placed above the recording pacemaker and receives the RF signal emitted by the pacemaker. The ECG and EGM signals are stored by the Holter on an internal memory and can be monitored during the acquisition on a laptop connected to the Holter by Bluetooth^{TM}.
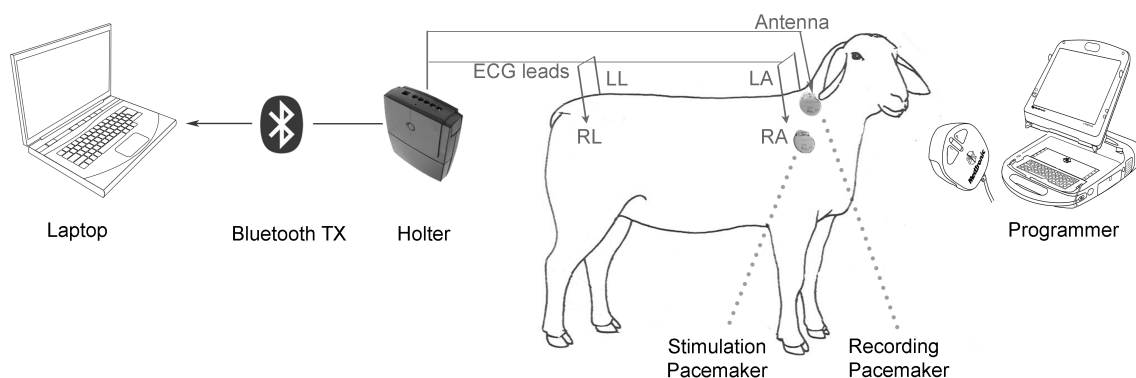
Figure 5.6: *Recording setup. The programmer (right) sets the pacing parameters to the stimulation pacemaker (right shoulder). The recording pacemaker (neck) transmits the atrial EGM (RF signal) via the antenna to the Holter device. Four subcutaneous electrodes (RA, LA, RL and LL) are used to record three ECGs, stored by the Holter device. Subcutaneous ECG and EGM signals are monitored on a laptop, communicating with the Holter device via a Bluetooth transmission.*

5.4   Pacing protocols

The recording sessions typically included three parts: a few minutes in sinus rhythm, one S1S2 protocols and one S1S1 protocol. The burst pacing protocol was used to remodel the atria.

S1S2 protocol

The S1S2 protocol consisted of 20 paced impulses (S1) followed by an extrastimulus (S2), which automatically decreased by steps of 10 ms (fig. 5.7). The pacing CL of the S1 impulses was set at 400 ms. Figure 5.7 shows a representative example during a S1S2 protocol. The extrastimulus is delivered after a train of 20 paced beats to allocate time for reasonable stabilization of refractoriness, which is usually accomplished after the first three or four paced beats [122].The stimuli are rectangular pulses of 0.5 ms duration with a voltage at least twice the diastolic threshold and usually set at 2.5 V at 0.5 ms. The atrial diastolic threshold is defined as the minimal voltage resulting in consistent atrial capture at 120 bpm.

This protocol allows us to measure the kinetics of atrial activation time (AT) and effective refractory period (ERP) during pacing-induced remodeling. AT is measured from the pacing stimulus to the atrial depolarization peak. As shown in figure 5.7, AT gets prolonged for shorter S1S2 intervals, close to ERP. At ERP, the S2 fails to capture the atrium.
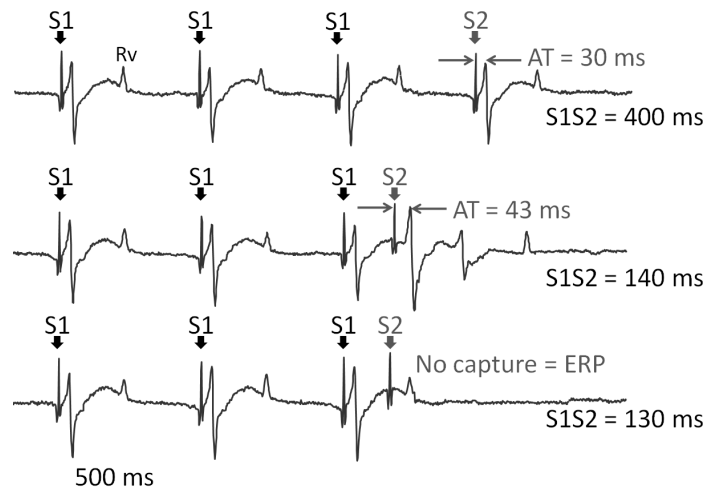
Figure 5.7: *EGM during a S1S2 pacing protocol with a drive train set at 400 ms. The first row shows a 400 ms S1S2 interval. The middle row shows a prolongation of the activation time at a 140 ms S1S2 interval. The last row shows the largest S1S2 interval failing to capture the atrium, which corresponds to the ERP.*

S1S1 protocol

The S1S1 protocol consisted of a sequence of 400 impulses, starting at 400 ms CL down to the atrial ERP, with steps of 50 ms down to 300 ms and followed by steps of 10 ms afterwards. The number and duration of the beats are programmable, but 400 beats have been chosen in order to reach steady state and being able to assess patterns in repolarization alternans.

Burst pacing protocol

The pacing protocol used to remodel the atria consisted of bursts of programmable CL and duration, in intermittence with sinus rhythm of variable duration in order to mimic salvos of pulmonary vein atrial tachycardia. Figure 5.8 shows a representative example consisting of a burst of 5 sec

duration followed by 4 sec of sinus rhythm. The programmable CL ranges from 80 to 200 ms with incremental steps of 10 ms.
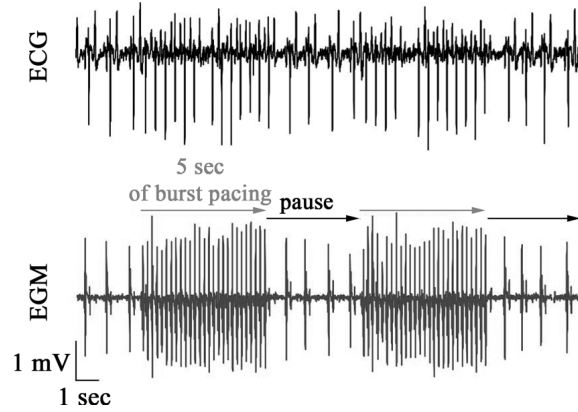
Figure 5.8: *Intermittent atrial burst pacing of 5-second duration with 3 seconds of sinus rhythm in-between.*

Figure 5.9 shows an example of AT as a function of S1S2 coupling interval, before burst pacing activation, after 2 and 4 weeks of burst pacing. Paced ERP decreased from 150 ms at baseline to 100 ms and 90 ms after 2 and 4 weeks of burst pacing.
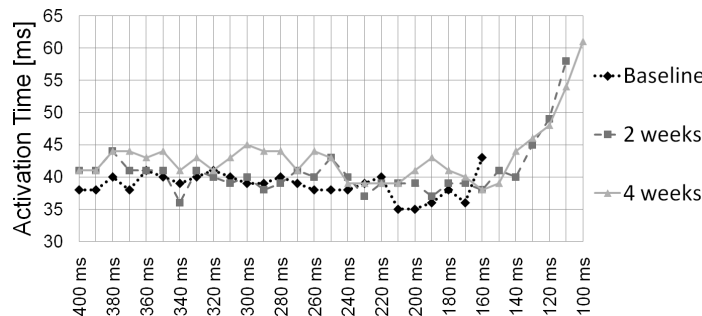
Figure 5.9: *Activation time and ERP as a function of S1S2 coupling interval, throughout remodeling process for one representative sheep with normal AV conduction.*

5.5   Biochemistry and histology

Biochemistry was performed on samples from the right and left atria to determine the expression of proteins involved in intracellular Ca^{2+} cycling and histological analysis to determine any fibrosis or enlarged nuclei. Details and preliminary findings can be found in Annexe A.

5.6   Inter-electrodes distance

In order estimate the linear distance between the stimulating and the recording electrodes, X-rays were taken and inter-electrode distance measured at the end of the implantation, during the

remodeling process and once the sheep were in AF. Sheep were under general anesthesia and intubated (tracheal intubation), with a tube whose diameter was used as a reference (typically 10.2 mm). Once the plane maximizing the inter-electrodes distance has been found, a simple translation of the X-ray device was performed. The distance from the X-ray tube to the electrodes and to the tracheal the tube is considered constant as they lay approximately in the same plane.

Figure 5.10 shows an example of two radiographs of the tracheal tube (left) and the right atrial electrode leads (right). Knowing the distance between the electrodes, one can compute an estimate of the propagation velocity from the stimulation electrode to the recording electrode. Any large atrial stretch would result in an increase of the measured inter-electrode distances.

Figure 5.10: *Inter-electrodes distance. X-ray of the tracheal tube (left) and of the two right atrial leads (right). Using the diameter of the tracheal tube as reference (10.2 mm) gave a distance of 26.7 mm between the two leads.*

5.7 Echocardiography

Echocardiograms were performed following X-ray pictures. We typically measured ventricular and atrial diameters during diastole and systole, and looked for signs of pericardial effusion.

5.8 Sheep database

Our study included two main groups of sheep, the group with normal AV conduction and the group with AV block. Those two groups were further divided in two subsets, remodeled until sustained AF appeared and non remodeled ones. The subsets are listed in table 5.1. Five additional sheep without pacemaker implantation were used for biochemistry and histology as a non operated control group. Data have not been analyzed yet.

	Remodeled	Not remodeled
With normal AV conduction	8	8
With AV block	3	5

Table 5.1: *Sheep database*

5.9 Conclusion

This chapter introduced our chronic free-behaving sheep model of pacing-induced AF. This model has the unique ability to allow the follow-up from a healthy non remodeled state to the initiation of AF. Once the pacemakers are implanted, the setup makes possible the non-invasive recording of *in vivo* intracardiac EGMs, which is of great advantage compared to *ex vivo* experiments where measurements are done in a non physiological environment.

Part III

Signal Processing

EGM and ECG processing

<div style="text-align: right; font-size: xx-large;">**6**</div>

One relevant issue to understand the pathophysiological mechanisms of AF is the analysis and interpretation of atrial EGM. Therapies can be improved through this analysis, such as radio-frequency ablation [123], analysis of antiarrhythmic drug effects [124] or performance improvement of atrial implantable cardioverter defibrillators [125].

The major problem in the analysis of atrial EGM is the presence of ventricular activity (VA). A straightforward approach to solve it consists in performing analysis on EGM segments free of ventricular complexes. However, the information contained in the rejected parts is lost, which is not suitable for analysis requiring continuous atrial segments (as Re-ALT analysis) or when the ventricular rate is too high to produce EGM segments without VA, with most of the atrial complexes superimposed with VA.

To properly study the EGM signals, VA has to be removed from the EGM. In a similar context, various methods to cancel out this activity from the surface ECG during AF have been proposed [126–128]. Because of the spectral overlapping of the AA and VA, linear filter based methods do not permit the extraction of AA. Two approaches are usually used: source separation algorithms and average beat subtraction [129].

The source separation algorithms assume that AA and VA arise from different electrical sources, and that they possess different statistical characteristics. Principal component analysis (PCA) and independent component analysis (ICA) are the main representatives of this approach [127, 130, 131]. However blind source separation algorithms using ICA require at least as many recordings as sources, and are generally applied to 12-lead ECG, eight of them being linearly independent. Application of such algorithms in our study provides poor results, due to the large morphological differences between the ECG and EGM signals and to the limited quality of our ECG recordings. The application of PCA will be detailed in this chapter and illustrated with recordings obtained from sheep with normal AV conduction and with AV block.

The average beat subtraction method applied to the analysis of AA in ECG during AF, relies on the uncoupling between AA and VA during AF. It also assumes small variabilities in the ventricular complexes in the same patient. The main idea is to create an average VA template and to subtract it from the signal; the residual signal should be the AA. This technique has been used in non-invasive AF studies [132].

The purpose of this chapter is to evaluate preprocessing and VA cancellation techniques. First, preprocessing of the signals, fiducial point detection and denoising are introduced in section 6.1. Then, in order to evaluate the denoising procedure and the cancellation techniques, a model of EGM signals, used as ground truth is proposed in section 6.2. The modeled EGM signals contain atrial and ventricular activities displaying characteristics similar to those of experimental EGM signals. Finally, in section 6.3, VA cancellation algorithms adapted to our single-lead configuration are presented: median template subtraction (MTS), PCA applied on atrial beats (PCA_1) and PCA applied on atrial and ventricular beats (PCA_2). These cancellation techniques are illustrated on experimental EGM signals and their performance validated on modeled EGMs.

6.1 Preprocessing

ECGs and EGMs may be corrupted by various kinds of noise and artifacts, including baseline wander, electrode motion artifacts, powerline interference or muscle noise [133].

6.1.1 Baseline wandering

Baseline wander may result from various causes including respiration, body movements and poor electrode contact [133]. The upper row of figure 6.1 provides an example of an ECG showing baseline wander. ECG baseline wandering is suppressed with a fifth-order Butterworth high-pass filter with a 0.5 Hz cutoff frequency (fig. 6.1, bottom row). Signals are first filtered in the forward time direction and then the filter output is filtered again in the backward time direction. The result has precisely zero-phase distortion [133].
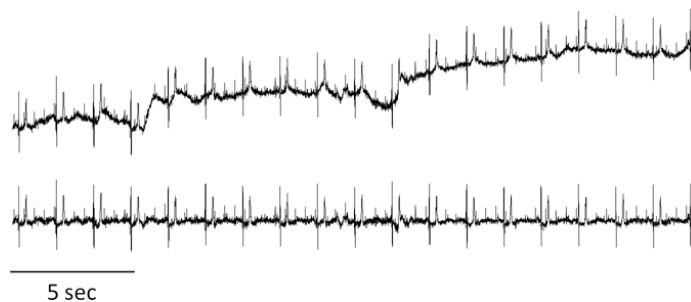
Figure 6.1: *Baseline wander. Example of an ECG before (upper row) and after filtering (bottom row).*

6.1.2 Wavelet denoising

Wavelet transform analysis uses wavelike functions known as *wavelets*. These wavelets are used to transform the signal under investigation into another representation, where the signal information

is in a more useful form [134]. Wavelet transform is the convolution of the basis wavelet function with the signal. The so called *mother wavelet* is manipulated in two ways: it can be translated to various locations on the signal and it can be stretched or squeezed. If the wavelet matches well the shape of the signal at a given scale and location, the transform results in a large value. On the other hand, if the signal and the wavelet do not correlate well, a low transform value is obtained.

Computation of the wavelet coefficients is possible at any scale, but would be too large to handle easily. Selection of a subset of scales and positions based on powers of two results in a more efficient analysis. Mallat introduced repetitive application of *high pass* and *low pass* filters to calculate the wavelet decomposition of a given sequence, as depicted in figure 6.2 [135]. The pairs of filters at each level are defined by the mother wavelet and its scaling function (complementary). Temporal analysis is performed with a contracted, high frequency version of the wavelet, while frequency analysis is performed with a dilated, low-frequency version of the same wavelet. The signal is thus represented in terms of a wavelet expansion, using coefficients in a linear combination of the wavelet function. Data manipulation such as denoising can be performed using just the wavelet coefficients.
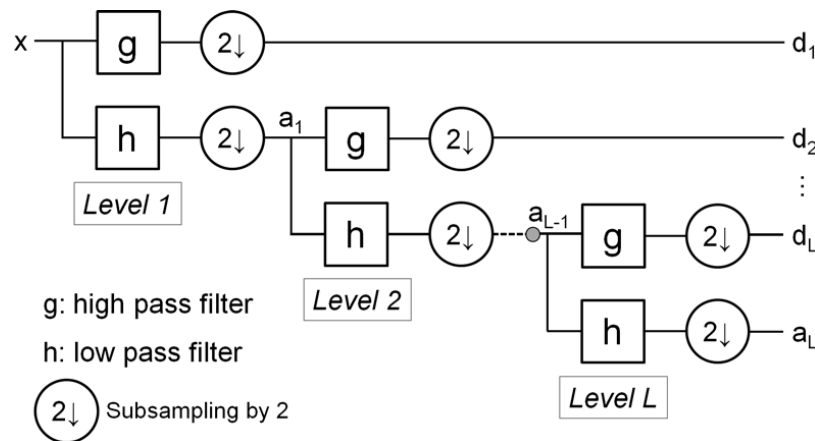
Figure 6.2: *Mallat's cascaded filters. d_i refers to the detail coefficients at level i and a_L to the approximation coefficients at level L.*

Conventional wavelet denoising (WD) is now a common approach for the denoising of biomedical ssignals such as ECGs. Donoho and Johnstone [136] proposed a soft thresholding method for the so-called shrinkage of the noise components in the wavelet domain. Their approach, together with variants, has since been used in many applications. The general denoising procedure involves three steps:

1. Decomposition
   A mother wavelet and a level L are chosen. Wavelet decomposition of the signal at level L is performed.

2. Thresholding of the detail coefficients
   For each level from 1 to L, a suitable threshold is selected and soft thresholding is applied to the detail coefficients.

3. Reconstruction
   Wavelet reconstruction using the original approximation coefficients at level L and the modified detail coefficients at levels from 1 to L is computed.

WD schemes are characterized by various parameters that customize the algorithms for different mixtures of signal and noise sources. The type of the *mother wavelet*, *shrinkage rule*, *rescaling strategies* are the main WD parameters to select [137].

The mother wavelet is usually selected from a wavelet family with a shape close to the shape of the signal to be denoised, and the rescaling approach and shrinkage rules are selected according to the nature and variance of the noise. Four threshold selection rules are available, namely the Stein's Unbiased Risk Estimate (SURE), the fixed threshold form, a mixture of the two (heursure), and the minimax principle [137]. The universal fixed threshold selection rule by Donoho and Johnstone [138] proposes a threshold value $\sigma\sqrt{2\log M}$ proportional to the amount of noise σ and the number of samples M. In practice, the universal threshold tends to over-smooth the signal. The SURE threshold selection rule estimates Stein's unbiased risk for a particular threshold value and minimizes it [139]. The minimax threshold selection presented by Donoho and Johnstone [138] uses an optimal threshold in terms of L^2 risk. This optimal threshold depends on the sample size M and is derived to minimize an upper bound of the risk involved in estimating a function. The SURE and minimax threshold selection rules are more conservative and are thus more convenient to keep small details of signal close to the noise level (like the pacemaker stimuli). Those two selection rules and the hybrid version (heursure) were tested.

A wavelet denoising method was applied on both EGM and ECG signals. The wavelet decompositions (Symmlet 4 level 4 decomposition) were soft-thresholded. The threshold was rescaled based on a level-dependent estimation of the level noise. The choice of the wavelet and threshold selection rule are detailed in section 6.2.4.

6.1.3   Fiducial point detection

Identification of the timing of pacemaker stimuli, atrial depolarization and repolarization waves (fig. 6.4) was performed as follows: atrial depolarization was detected by applying a nonlinear energy operator (NEO) to the EGM and thresholding its output. The NEO is defined by [140] as:

$$x[n] = x^2[n] - x[n+\delta]\,x[n-\delta], \quad 1 \le \delta \le 4 \tag{6.1}$$

This first stage emphasized the spikes and the threshold determined their position. The NEO parameter was typically set to $\delta = 4$ and the threshold to 30% of the maximal value of the processed signal (fig. 6.3). The same procedure can be applied to an ECG derivation in order to get the time location of ventricular depolarization. Thus, any false detection on the EGM of ventricular depolarization can be discarded, based on ECG information. The pacemaker stimuli were defined as the maximum in an interval preceding atrial depolarization.

Following the detection of atrial depolarization waves, repolarization waves were smoothed by a Savitzky-Golay filter of order three [141]. Then, the zeros of the second derivative determined the onset and end of the repolarization wave. For each fitted T wave segment, the local maximum was extracted and defined the amplitude apex (T_a) (fig. 6.4).
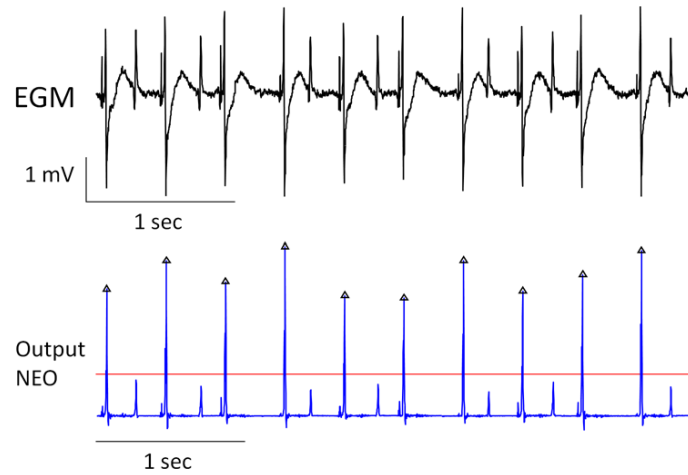
Figure 6.3: *EGM (upper row) and output of the non linear energy operator (bottom row). The threshold is indicated by the red line and the detected atrial R wave by triangles.*
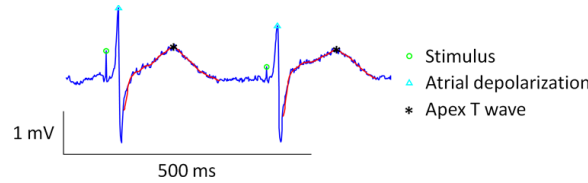
Figure 6.4: *Examples of fiducial points from two consecutive atrial beats. The pacemaker stimuli are denoted by green circles, the atrial depolarizations by cyan triangles and the apex of the T waves by black stars. The T waves smoothed by the Savitzky-Golay filter are shown in red.*

6.2 Modeling of the EGM

In order to evaluate the performance of the denoising procedure and the VA cancellation algorithms, the need for a reference signal arose. This section presents models of AA, VA and noise.

6.2.1 Modeling of the atrial activity

Synthetic EGM were generated using a combination of bi-Gaussian waveforms. A bi-Gaussian function (BGF) is a four-parameter function, composed of two half-Gaussian functions (fig. 6.5) [142]. As defined in eq. 6.2, the parameters of the function are:

μ: location in time
σ_1:   standard deviation of the first Gaussian
σ_2:   standard deviation of the second Gaussian
A: amplitude

$$BGF\left(x, \mu, \sigma_1, \sigma_2, A\right) = \begin{cases} A \cdot exp\left[-\frac{1}{2}\left(\frac{x-\mu}{\sigma_1}\right)^2\right] & \text{if } x \leq \mu \\ A \cdot exp\left[-\frac{1}{2}\left(\frac{x-\mu}{\sigma_2}\right)^2\right] & \text{if } x > \mu \end{cases} \tag{6.2}$$

In order to build a synthetic EGM as close to real ones as possible, an experimental EGM
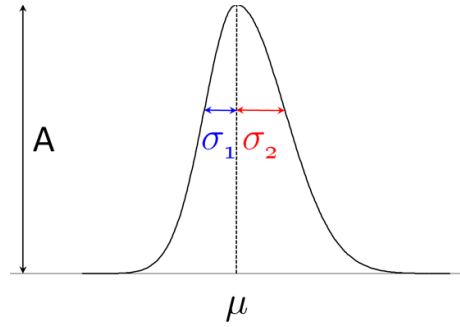
Figure 6.5: *Bi-Gaussian function (BGF). μ represents the position of the function, σ_1 the standard deviation of the first Gaussian function, σ_2 the standard deviation of the second Gaussian function and A the amplitude of the function.*
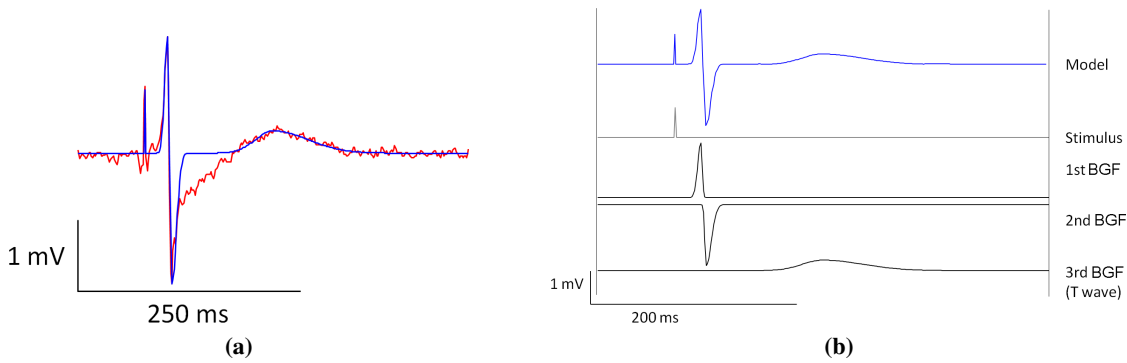
Figure 6.6: *(a) Original EGM (red) and combination of BGF (blue). (b) Decomposition into three BGF and one pacemaker stimulus.*

at a PCL of 400 ms was considered and a combination of three BGF was used to model it (fig. 6.6a). The parameters of each BGF used to model the R, S and T waves were optimized in order to minimize the mean square modeling error MSE defined in equation 6.3, where S_{EGM} was the EGM signal template used as reference and N_s the number of samples. Two optimizations were performed, using the intervals of S_{EGM} corresponding to the QRS complex and the T wave. Note that a constrained optimization was performed since σ_1, σ_2 must be positive. Figure 6.6b shows the decomposition into three BGF of the synthetic EGM shown in figure 6.6a (blue).

$$MSE(\mu, \sigma_1, \sigma_2, A) = \frac{1}{N_s} \sum_{i=1}^{N_s} (S_{\text{EGM}}(i) - BGF(i, \mu, \sigma_1, \sigma_2, A))^2 \tag{6.3}$$

Once the parameters minimizing the modeling error had been determined (tab. 6.1), the resulting model was used as a basic EGM beat. Variations in the parameters of the BGFs (tab. 6.2) allowed the creation of synthetic EGM with various R, S and T waves shapes, close to intracardiac EGMs (fig. 6.7).
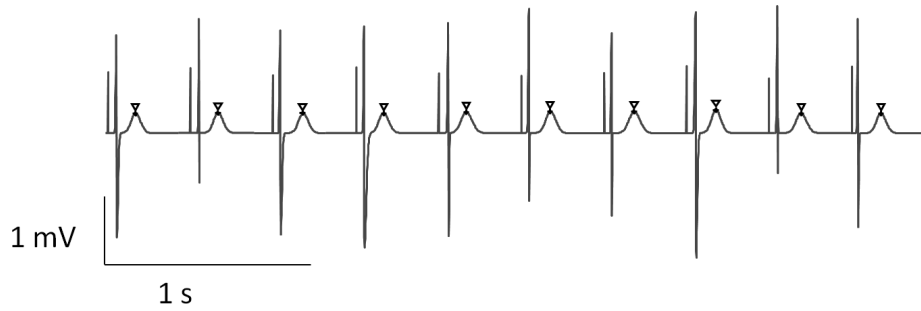
Figure 6.7: *Synthetic EGM at a PCL of 400 ms. The apexes of the T waves are highlighted with triangles.*

		μ	σ_1	σ_2	A
1st BGF	R wave	81	2.5	1	1650
2nd BGF	S wave	82	0.1	19.8	-1789
3rd BGF	T wave	175	21	31.5	317

Table 6.1: *Parameters of the BGF to model a standard EGM.*

6.2.2 Modeling of the ventricular activity

The next step was to add ventricular activity (VA) to this model. The VA was extracted in a sheep with AV block (see section 6.3). Four BGF were used to model the *Q*, *R*, *S* and *T* waves of the VA. The parameters of the QRS part were jointly optimized. Figure 6.8a shows an experimental VA (in red) and the resulting combination of BGF (in blue). The decomposition is shown in figure 6.8b and the values of the parameters are given in table 6.3.

		μ	σ_1	σ_2	A
1st BGF	R wave	81±8	2.5±1	1	1650±250
2nd BGF	S wave	μ_R+1	0.1	19.8±5	-1789±250
3rd BGF	T wave	175±10	21±2	31.5±2	317±30

Table 6.2: *Range of the parameters of the BGF to model a standard EGM. μ_R denotes the time location of the BGF related to the R wave.*

		μ	σ_1	σ_2	A
1st BGF	Q wave	10	1.8	2	-159.6
2nd BGF	R wave	19	2.5	6.1	426.9
3rd BGF	S wave	50	5.9	27.2	-46.3
4th BGF	T wave	223	24.1	13.2	-235.4

Table 6.3: *Parameters of the BGF to model VA.*
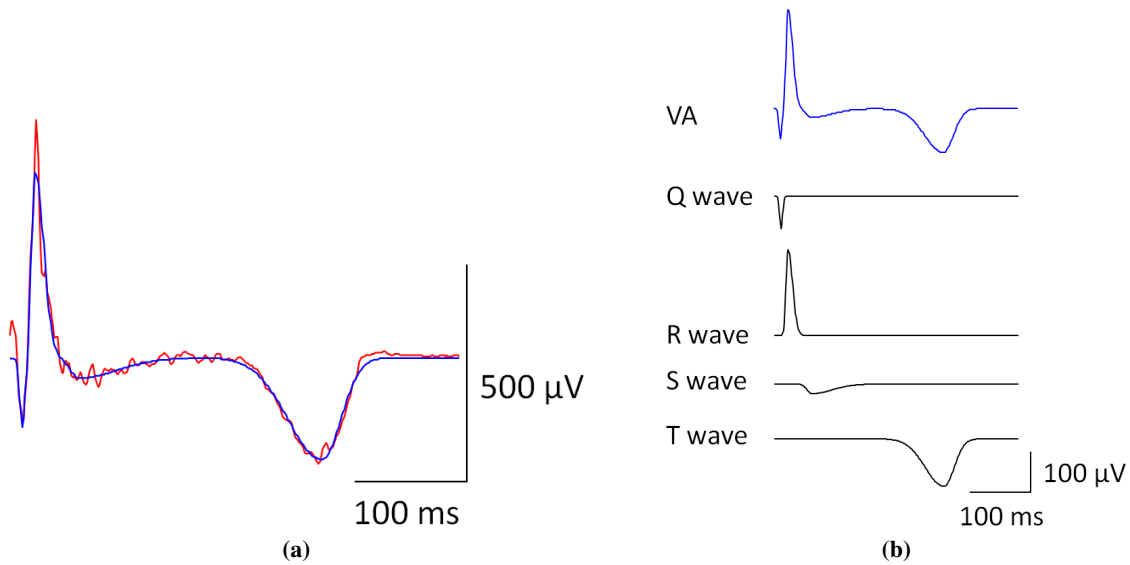
Figure 6.8: *(a) Ventricular activity (red) and combination of BGF (blue). (b) Decomposition into four bi-Gaussian functions.*

Modeling AV conduction

As introduced before, our data is composed of two main groups, the group with normal AV conduction and the group with AV block. During normal AV conduction, the ventricular contraction follows the atrial one, on a N_{AA}:1 basis (N_{AA} atrial beats for one ventricular). During AV block, the VA is programmed at 40 bpm (1500 ms), VA is completely dissociated from AA and the ventricular beats superimpose to different interval of atrial beats.

The length of atrial and ventricular beats can easily be adjusted in order to create these types of AV conductions. Figure 6.9 shows examples of 2:1 AV conduction (left), 3:1 AV conduction (center) and AV block (right).
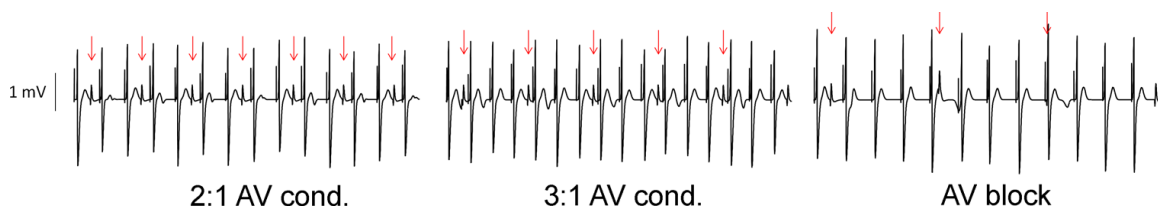
Figure 6.9: *Simulated AV conductions. Red arrows indicate R_V. Left: AA at 350 ms PCL with 2:1 AV conduction. Center: AA at 300 ms PCL with 3:1 AV conduction. Right: AA at 400 ms PCL with AV block.*

6.2.3   Modeling of the noise

In order to quantify the noise in terms of signal-to-noise ratio (SNR) and then create a model of it (subsection 6.2.3), T waves were extracted from an experimental EGM (fig. 6.10). The difference between the T waves and the fitted curves is shown in panel B of figure 6.10.
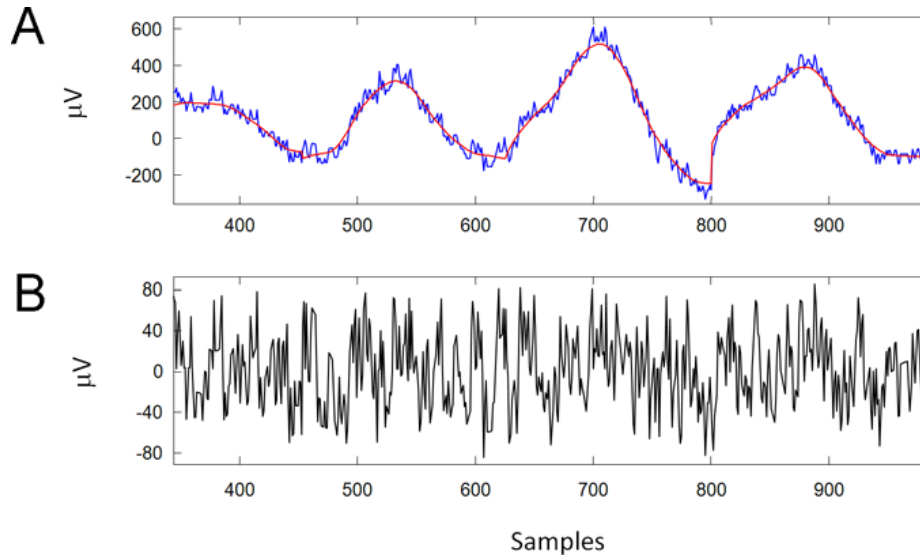
Figure 6.10: *Estimating noise. Panel A shows consecutive T waves from an experimental EGM (blue) and the corresponding fitted curves (red). Panel B shows the difference of the signals from panel A and defines the noise present in the experimental EGM.*

The SNR measured in the different experiments (nine sheep, three recording sessions per sheep), ranged from 10.0 to 19.4 dB (14.5 ± 2.6 dB).

Additive AR noise

The residue after T wave fitting can be considered approximately as the additive noise present in experiments. A Kolmogorov-Smirnov test confirmed that it is indeed Gaussian-distributed, but the classical Ljung-Box test for randomness [143] revealed that this residue is correlated. Hence we modeled this noise using an autoregressive (AR) model instead of using a non-correlated (white) noise as typically done in signal simulations.

An AR model of order p (AR(p)) is defined as:

$$x(n) = -\sum_{i=1}^{p} a_i x(n-i) + \epsilon(n) \tag{6.4}$$

where $a_1, \cdots, a_n$ are the parameters of the model and $\epsilon(n)$ is a white noise. An autoregressive model can thus be viewed as the output of an all-pole filter of the form:

$$H(z) = \frac{1}{1 + \sum_{i=1}^{p} a_i z^{-i}} \tag{6.5}$$

the input of which is a white noise.

$$\epsilon \longrightarrow \boxed{\frac{1}{1 + \sum_{i=1}^{p} a_i z^{-i}}} \longrightarrow x$$

Estimation of the AR parameters. The Yule-Walker equations provide a direct correspondence between the model parameters and the covariance function of the process, and this correspondence can be inverted to determine the parameters $(a_1, \cdots, a_n)$ from the autocorrelation function (r_x):

$$r_x(k) = \sum_{i=1}^{p} a_i r_x(k - i) + \sigma_\epsilon^2 \delta_{k,0} \tag{6.6}$$

where $k = 0, \cdots, p$, yielding $p + 1$ equations. The parameter σ_ϵ is the standard deviation of the input noise process and $\delta_{k,0}$ is the Kronecker delta function [144]. Of course, in practice estimates of the autocorrelation function obtained from the available samples are used.

Selecting the model order. The order of the model has been set using the simplified Rissanen's minimum description length (MDL) criterion:

$$MDL(p) = N \ln \hat{\sigma}_e^2 + (\ln N) p \tag{6.7}$$

where $\hat{\sigma}_e^2$ is the estimated variance of the excitation, N is the number of samples, and p the number of parameters [145]. The MDL contains a penalty term $(\ln N)p$, which increases with the data record length N and the model order p. The idea is to select the model corresponding to the best compromise between model complexity (size) and accurate representation of the data $(\hat{\sigma}_e^2)$.

The order minimizing the MDL was eight as shown in figure 6.11.
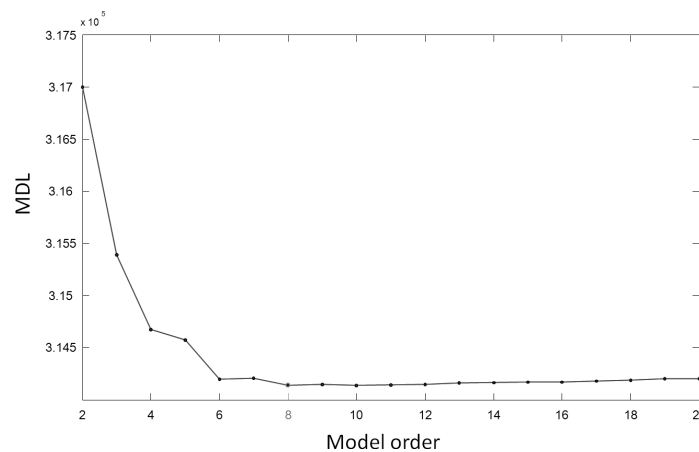
Figure 6.11: *MDL and AR model order. The smallest MDL was found on AR model order of 8.*

Example of synthetic EGM with an AR noise

Figure 6.12 shows an example of a clean synthetic EGM (upper row) to which AR noise has been added (middle row). An experimental EGM is shown for comparison (bottom row).
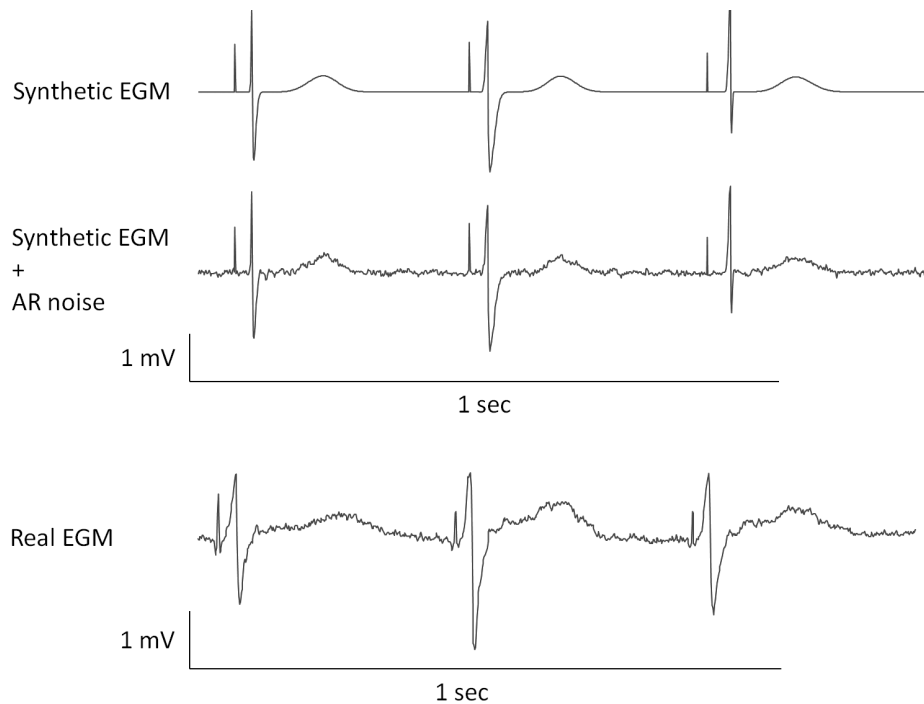
Figure 6.12: *Synthetic EGM with AR noise. The upper row shows a synthetic EGM to which is added the AR noise. The result is shown in the middle row. The bottom row shows an experimental EGM.*

6.2.4   Wavelet denoising results

Synthetic signals (400 beats) with additive AR noise were used to compute the SNR improvement, given by

$$\text{SNR}_{\text{imp}}[\text{dB}] = 10\log\left(\frac{\sum_i |x_n(i) - x(i)|^2}{\sum_i |x_d(i) - x(i)|^2}\right) \tag{6.8}$$

where x denotes the clean EGM, x_n the noisy EGM and x_d the denoised EGM. A mean SNR improvement was computed over 50 noise realizations. Figure 6.13 shows an example of the thresholding procedure, using the *heursure* threshold selection rule.

The parameters investigated were:
– Threshold selection rules
  SURE
  minimax
  heursure
– Types of mother wavelet basis function:
  Daubechies filters of order 1 to 8
  Coiflet filters of order 1 to 5
  Symmlet filters of order 1 to 8
– Decomposition levels, from 3 to 6

The combinations of parameters were ranked based on their mean SNR improvement over the 50 noise realizations. The best improvement was obtained with the Symmlet4 wavelet with four levels of decomposition, using the heuristic SURE shrinkage rule, together with a multi-level rescaling
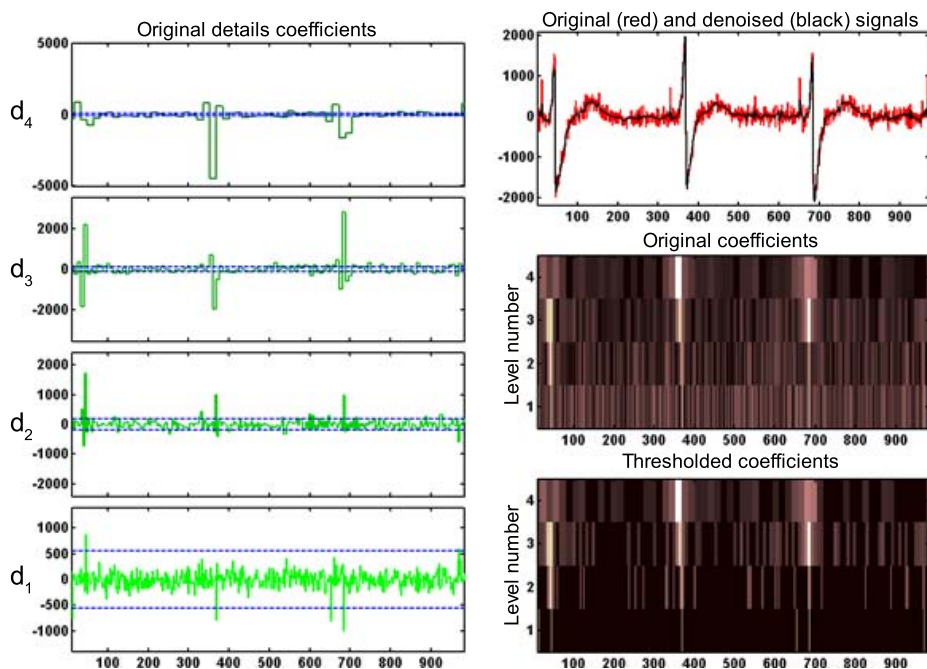
Figure 6.13: *Wavelet coefficients thresholding (heursure). Symmlet4 wavelets with 4 levels of decompositions (d_1 to d_4). On the left hand side are shown the decomposition coefficient (green) and the thresholds (blue) at each of the 4 levels. On the right hand side are shown the noisy (red) and denoised (black) signals (top), the original coefficients (middle) and the soft-thresholded coefficients (bottom). In this representation, large values of the coefficients are bright. Note the shrinkage of the coefficients present between the threshold values.*

and a soft thresholding strategy.

6.3   Ventricular activity cancellation

As introduced above, the major problem in the analysis of atrial EGM is the presence of VA. This section details VA cancellation using median template subtraction (MTS), principal component analysis based on atrial beats (PCA_1) and on both atrial and ventricular beats (PCA_2).

6.3.1   Median template subtraction

This section introduces the principle of median template subtraction, during AV block and normal AV conduction. An average template of VA can be obtained by extracting several observations of VA from the EGM and computing the mean or the median of it. The median is selected, being more robust than the mean. The location of the ventricular activity is detected from the ECG, where it is clearly visible.

In the AV block case, the resulting median template represents well VA, as long as the latter does not express large variability. A median template of VA is created at each PCL and assumes small variations in VA. The AA is obtained by subtracting the VA template from the original EGM. Figure 6.14 illustrates the extraction of VA, the obtained median template and the resulting subtraction (black) superimposed to the original signal (red dotted). The median template is not computed for

PCLs 300 and 250 ms, since the ventricular rate (40 bpm) is a multiple of those PCLs. The median template from PCLs 290 and 260 ms are preferred.
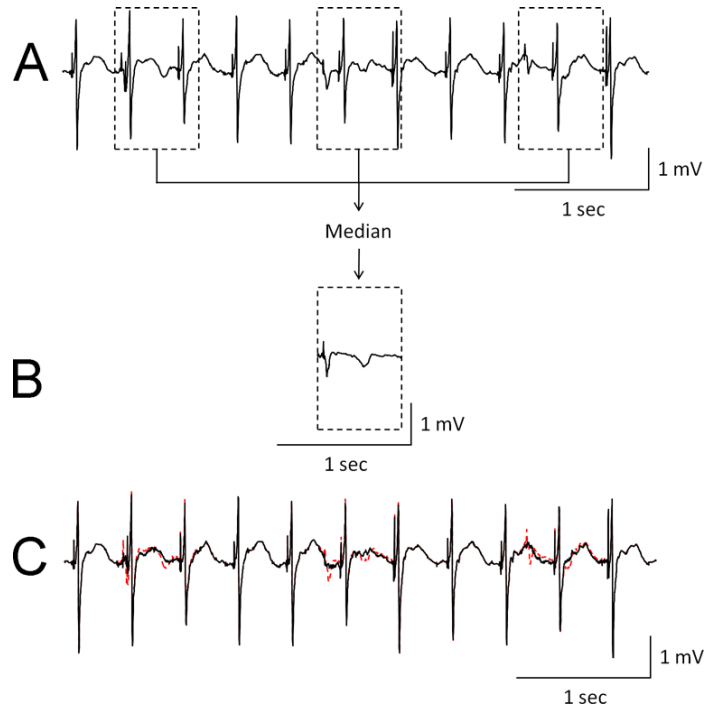
Figure 6.14: *Ventricular cancellation using template subtraction. (A) Experimental EGM with VA shown by black dotted rectangles. (B) Median template of VA. (C) Estimated AA obtained by subtracting (B) to (A).*

During normal AV conduction, building a median template of VA is not efficient. Because each observation of a ventricular beat contains the same segments of atrial beats, the median template represents both activities. The subtraction of such a template creates more distortion on AA than it removes. Another approach is needed and the next section introduces PCA and its ability to cancel VA.

6.3.2 Principal component analysis

Principal component analysis (PCA) is a well known statistical technique aiming at projecting a set of large-dimensional correlated vectors onto a smaller dimension space, while minimizing the resulting distortion. This is achieved by linearly mapping the vector components to the so-called *principal components*. Principal components are uncorrelated and can be ordered such that the first components account for most of the variability[146].

In signal processing, PCA is performed on the set of vectors built from one-dimensional signal samples. When the signals are recurrent in nature, like ECG or EGM signals, the analysis is based on vectors extracted from the same segment of different periods of the signal. PCA has been used in ECG analysis to deal with various issues such as data compression, beat detection and classification, noise reduction, signal separation and feature extraction [131].

Signal separation during AF is another recent application of PCA, in which the atrial activity is extracted so that the characteristics of the arrhythmia can be studied without interference from ven-

tricular activity. Such separation is based on the fact that the two activities originate from different bioelectrical sources. Separation may exploit temporal redundancy among successive heartbeats.

PCA on EGM starts from the sample vector of a segment located in a suitable part of the heartbeat. A fiducial point must be determined (R_a, section 6.1.3) to extract the appropriate segment within the signal. Accurate time alignment of the segment is an important point in PCA.

The signal segment of an atrial beat is represented by the column vector:

$$\mathbf{x} = \begin{bmatrix} x(1) \\ x(2) \\ \vdots \\ x(N) \end{bmatrix} \tag{6.9}$$

where N is the number of samples of the segment. Segments are extracted from successive beats, resulting in an ensemble of M beats. The entire ensemble is compactly represented by the $N \times M$ data matrix:

$$\mathbf{X} = [\mathbf{x}_1 \ \mathbf{x}_2 \ \cdots \ \mathbf{x}_M]. \tag{6.10}$$

The beats $\mathbf{x}_1, \cdots, \mathbf{x}_M$ can be viewed as M observations of a random process $\mathbf{x}$.

The derivation of principal components is based on the assumption that the signal $\mathbf{x}$ is a zero-mean random process characterized by a correlation matrix $\mathbf{R}_x = E\left[\mathbf{x}\mathbf{x}^T\right]$. The principal components of $\mathbf{x}$ result from applying an orthonormal linear transformation $\mathbf{\Psi} = [\boldsymbol{\psi}_1 \ \boldsymbol{\psi}_2 \ \cdots \ \boldsymbol{\psi}_N]$ to $\mathbf{x}$,

$$\mathbf{w} = \mathbf{\Psi}^T \mathbf{x} \tag{6.11}$$

so that the elements of the principal component vector $\mathbf{w} = [w_1 \ w_2 \ \cdots \ w_N]^T$ become mutually uncorrelated. The first principal component is obtained as a scalar product $w_1 = \boldsymbol{\psi}_1^T \mathbf{x}$, where the vector $\boldsymbol{\psi}_1$ is chosen so that the variance of w_1

$$E\left[w_1^2\right] = E\left[\boldsymbol{\psi}_1^T \mathbf{x}\mathbf{x}^T \boldsymbol{\psi}_1\right] = \boldsymbol{\psi}_1^T \mathbf{R}_x \boldsymbol{\psi}_1 \tag{6.12}$$

is maximized subject to the constraint that $\boldsymbol{\psi}_1^T \boldsymbol{\psi}_1 = 1$. The maximal variance is obtained when $\boldsymbol{\psi}_1$ is chosen as the normalized eigenvector corresponding to the largest eigenvalue of $\mathbf{R}_x$, denoted λ_1. The resulting variance is

$$E\left[w_1^2\right] = \boldsymbol{\psi}_1^T \mathbf{R}_x \boldsymbol{\psi}_1 = \lambda_1 \boldsymbol{\psi}_1^T \boldsymbol{\psi}_1 = \lambda_1. \tag{6.13}$$

Subject to the constraint that w_1 and the second principal component w_2 should be uncorrelated, w_2 is obtained by choosing $\boldsymbol{\psi}_2$ as the eigenvector corresponding to the second largest eigenvalue of $\mathbf{R}_x$, and so on until the variance of $\mathbf{x}$ is completely represented by $\mathbf{w}$. To obtain the whole set of N different principal components, the eigenvector equation for $\mathbf{R}_x$ needs to be solved

$$\mathbf{R}_x \mathbf{\Psi} = \mathbf{\Psi} \mathbf{\Lambda} \tag{6.14}$$

where $\mathbf{\Lambda}$ denotes a diagonal matrix composed of the eigenvalues $\lambda_1, \cdots, \lambda_N$ and $\mathbf{\Psi}$ denotes the eigenvector matrix. Since $\mathbf{R}_x$ is not exactly known in practice, the $N \times N$ sample correlation matrix, defined by

$$\hat{\mathbf{R}}_x = \frac{1}{M} \mathbf{X} \mathbf{X}^T \tag{6.15}$$

replaces $\mathbf{R}_x$ when the eigenvectors are calculated in 6.14.

(a) *ECG and EGM - AV block*

(b) *PCA₁, reconstruction using the first PC (K = 1)*
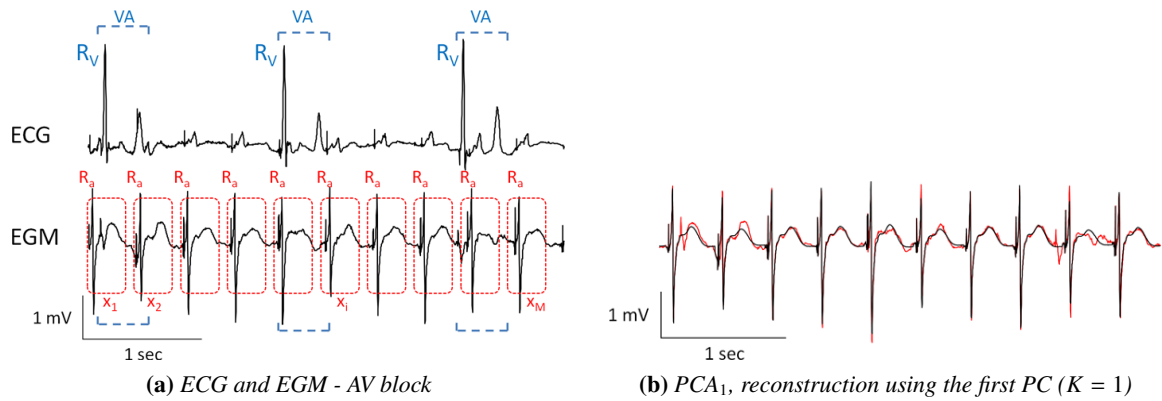
Figure 6.15: *Experimental EGM and reconstruction using the first principal component. Panel (a) shows an ECG (top) and an EGM (bottom) in a sheep with AV block. The atrial and ventricular activities (blue brackets) are dissociated. Red dotted boxes show the atrial segments (x_i) used to build the matrix **X**. Panel (b) shows the reconstruction using the first principal component (black) and the original signal (red dotted).*

The morphological beat-to-beat variability of an ensemble of beats **X** is reflected in the eigenvalues. A first principal component (PC) much larger than the other ones (i.e. $\lambda_1 >>> \lambda_i, i = 2, \cdots, N$) indicates that the ensemble exhibits a low morphological variability, while a slow fall-off indicates a large variability. The goal of PCA is to concentrate the information of **x** into a subset of components $w_1, \cdots, w_K$, where $K < \min(N, M)$. In practice, K is chosen so that the performance is clinically acceptable and that no vital signal information is lost.

Castells et al. applied PCA to reconstruct AA during AF from ECG signals [131]. They showed that the most significant component was related to the main QRST morphology, the next few to the dynamic of QRST waveform, the subsequent to AA and the remaining components to noise. The matrix **Ψ** was partitioned into three sub-matrices (**Ψ** = [**Ψ**$_{VA}$ **Ψ**$_{AA}$ **Ψ**$_N$]) and used to reconstruct the atrial, ventricular and noise activities. This partitioning is possible since VA and AA are uncorrelated and VA is of much larger amplitude than AA.

With AV block, the ventricular rate is programmed by the pacemaker at 40 bpm (1500 ms). The period of the ventricular activity is dissociated from that of the atrial contraction as shown in figure 6.15a; VA and AA can be considered as independent. The idea is to extract consecutive atrial beats, based on the R_a location and apply the PCA to exploit the atrial beats redundancy and remove VA. This approach is named PCA₁.

The signal shown in figure 6.15a has been converted into a data matrix **X** so that each of its columns contains one atrial beat, beginning before the R$_a$ wave. Based on the correlation matrix detailed in equation 6.15, the original signal (red) has been reconstructed using only the first PC ($K = 1$), as illustrated in figure 6.15b. Reconstructing AA from the first PC indeed removes VA, but cancels also any beat-to-beat alternans, as Re-ALT (fig. 6.18). Using more principal components (i.e. increasing K) permits to reconstruct the morphological differences between the beats but not to cancel VA.

We propose here an alternative algorithm, named PCA$_2$, to cancel VA and to preserve morphological changes between atrial beats. The proposed method consists in investigating the *residue* of the PCA based on atrial beats ($\mathbf{X}$) instead of the reconstructed signal. The residue is devoid of the main morphology of AA. A second PCA is then applied to the ventricular activity ($\mathbf{Y}$) present in the residue and an estimate of VA is constructed ($\widehat{VA}$). The locations of ventricular contractions are detected on the ECG. $\widehat{VA}$ is finally subtracted from the original EGM to obtain the AA. Figure 6.16 obtained from an experimental EGM (AV block, 400 ms PCL), illustrates the following steps:

1. Build $\mathbf{X}$ from the EGM signal, based on R$_a$

2. Perform PCA on the correlation matrix of $\mathbf{X}$

3. Remove rough estimate of AA ($K_{AA} = 1$), keep residual

4. Build $\mathbf{Y}$ from the residual, based on R$_V$

5. Perform PCA on the correlation matrix of $\mathbf{Y}$

6. Reconstruct an estimate of VA using K_{VA} principal components ($\widehat{VA}$)

7. Subtract $\widehat{VA}$ from the original EGM to obtain AA

The level of reconstruction in step 6 can be adapted in case of large variability in the VA morphology. However, on simulated data with ±20% variation in VA parameters, $K_{AA} = 1$ and $K_{VA} = 1$ give the lowest MSE, as shown in figure 6.17.

Figure 6.18 shows the result of both algorithms (PCA$_1$ and PCA$_2$) on an experimental EGM with AV block displaying Re-ALT. The top row shows the ECG signal while the middle and bottom rows show the original signal in red and the result of PCA$_1$ and PCA$_2$, respectively. PCA$_1$ does not preserve atrial beat-to-beat variations. PCA$_2$ focuses on VA and permits to conserve beat-to-beat variations of AA.
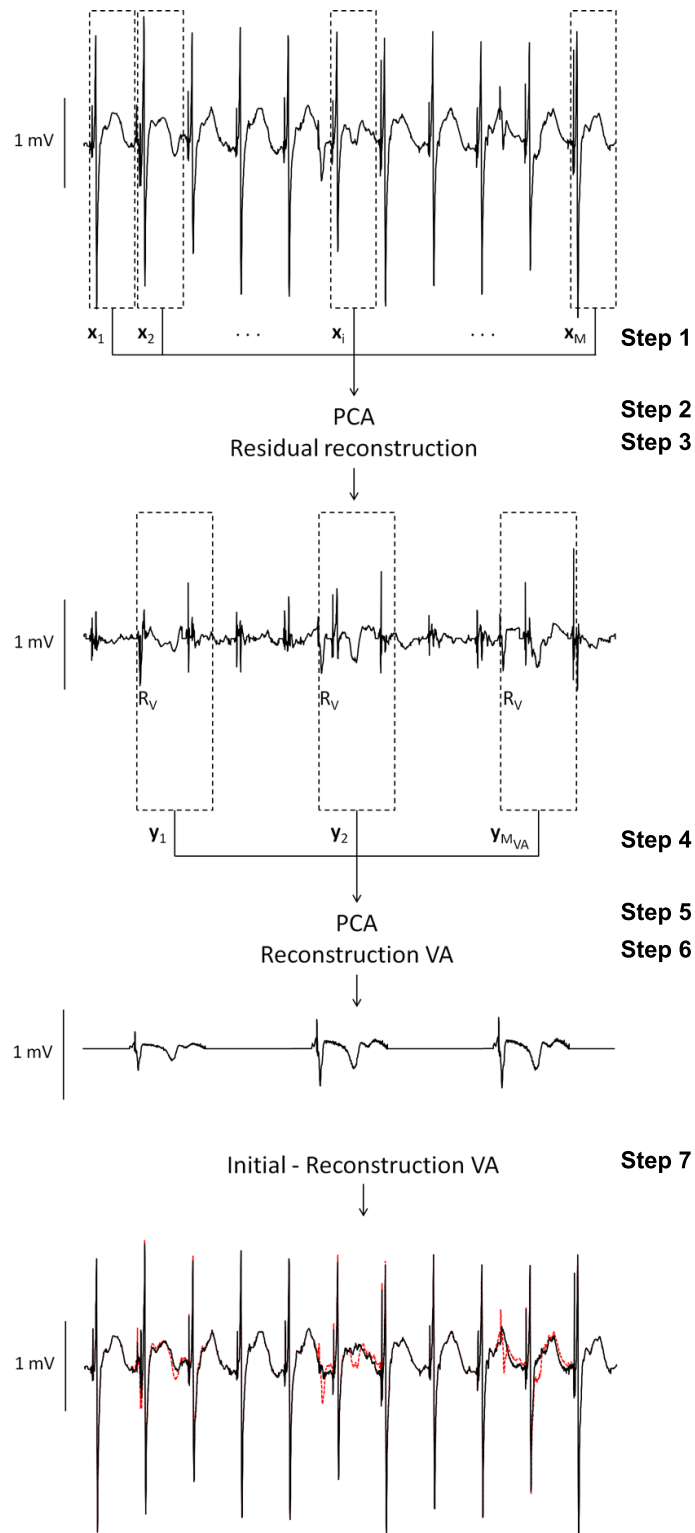
Figure 6.16: *Schematic of VA cancellation using two PCAs (PCA$_2$). Step 1: Build a matrix* **X** *aligned on atrial beats. Step 2: Perform PCA on* $\hat{\mathbf{R}}_x$*. Step 3: Reconstruct the signal without the first PC (residue). Step 4: Build a matrix* **Y** *aligned on ventricular beats. Step 5: Perform PCA on* $\hat{\mathbf{R}}_y$*. Step 6: Reconstruct the signal using the first PC, corresponding to* $\widehat{VA}$*. Step 7: Subtract* $\widehat{VA}$ *from the original EGM. The bottom trace shows the initial EGM (red dotted) and the result of the VA cancellation (black) using PCA$_2$.*
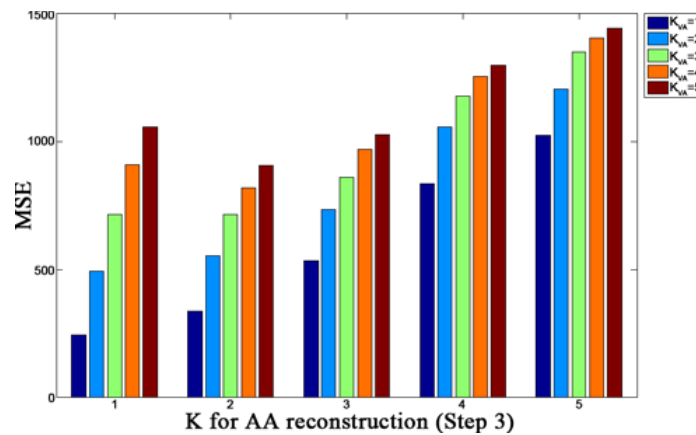
Figure 6.17: *Ventricular cancellation using PCA$_2$. The x-axis corresponds to increasing values of K_{AA}, defining the number of principal components used in step 3. The colors of the bars are associated with the value of K_{VA}, defining the number of principal components used to estimate $\widehat{VA}$ in step 6. The MSE is computed between the initial AA and the reconstructed AA from step 7.*
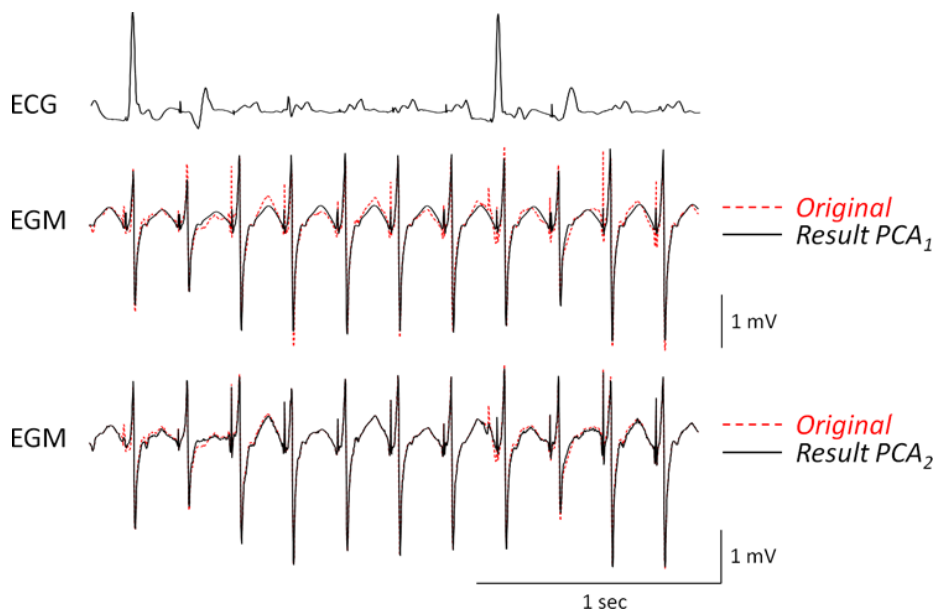
Figure 6.18: *Re-ALT and PCA. The top row shows an ECG where the ventricular contractions can easily be seen. The middle row shows the original EGM (red dotted) and the result of the cancellation (black) using PCA with $K = 1$ (PCA$_1$). Note that Re-ALT is flattened using this method. The bottom row shows the same EGM (red dotted) and the result of the cancellation (black) using two-step PCA (PCA$_2$). Note that Re-ALT is still present.*

6.3.3   Results on simulated data

Simulated data were used to evaluate the performance of the ventricular cancellation methods presented: the median template subtraction (MTS), the single PCA (PCA_1) and the two-step PCA (PCA_2). The simulated data contained both AA and VA ($s = s_{AA} + s_{VA}$). The signal s_{AA} was composed of 400 atrial beats with variations in the parameters (sec. 6.2). s_{VA} was generated in order to simulate normal AV conduction (2:1 and 3:1 AV conduction) and AV block with fixed ventricular rate (40 bpm), as shown in figure 6.9. Variations of up to 20% in the amplitude parameter of the depolarization and repolarization waves of VA were included.

The performance of the AA estimation in simulated recordings was computed by comparing the estimated and original AA ($\hat{s}_{AA}$ and s_{AA}, respectively) in terms of Pearson correlation index ρ:

$$\rho = \frac{E\left[s_{AA}\hat{s}_{AA}\right]}{\sigma_{AA}\hat{\sigma}_{AA}} \tag{6.16}$$

with E the expectation operator, and σ_{AA} and $\hat{\sigma}_{AA}$ the standard deviations of original and estimated AA.

Figure 6.19 shows the initial correlation between s and s_{AA} (dark blue bars) and compares it to the result of the cancellation methods in different cases of AV conduction. The simple MTS algorithm (brown bars) performs well only in the AV block case, and degrades the signal during 2:1 and 3:1 AV conduction, since the median template still contains AA. It can be seen that even if PCA_1 (light blue bars) removes VA, the distortion induced to AA results in a poorer correlation index in the three AV conduction schemes. To conclude, PCA_2 (yellow bars) improves the signals in the three cases, while keeping the morphological changes in AA (as seen before in figure 6.18).
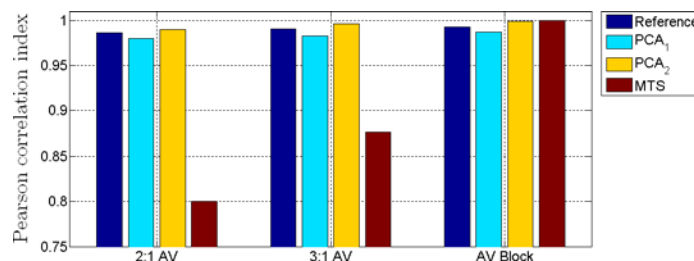
Figure 6.19: *Results of the cancellation algorithms in terms of correlation. The cancellation is performed on AA exhibiting Re-ALT. VA segments were added on a 2:1 and 3:1 basis and at a fixed rate as in AV block (40 bpm).*

6.4   Conclusions

In this chapter, initial preprocessing and denoising steps applied to ECGs and EGMs have been presented. A modeling of AA and VA using BGFs has been proposed to create synthetic EGMs mimicking different AV conductions and reproducing Re-ALT sequences. An AR model of the noise has been described and added to modeled EGM in order to select the best parameters for WD.

Three algorithms (MTS, PCA_1 and PCA_2) have been proposed to cancel VA in a single-lead EGM, during different AV conductions. Based on the synthetic EGMs, the limitations of the MTS algorithm have been rapidly shown in normal AV conduction. This approach has only been useful

in case of AV block and when VA displays small morphological variations. PCA_1 offered an alternative for removing VA but presented a major drawback, the beat-to-beat morphological differences in AA were attenuated. Finally, PCA_2 canceled VA while keeping beat-to-beat information in AA. The performance of each algorithm turned out to be optimal with AV block.

Analysis of atrial repolarization

7

This chapter reviews the existing methods developed to analyze ventricular T wave alternans (TWA) in sec. 7.1. Then, the algorithm used to detect atrial repolarization alternans is explained in sec. 7.2, tested on simulated EGM and illustrated with experimental signals. The detection of periodic behavior of Re-ALT sequences onset during S1S1 protocols is detailed in sec. 7.2.4. Using a computer model of the atria, the different measurement techniques of APD and ARI in unipolar EGM are presented in sec. 7.3.

7.1 Overview of existing methods

Energy spectral method (ESM). The first study which quantitatively related TWA to VF susceptibility was published by Adam et al. [53]. They observed beat-to-beat T wave morphology fluctuations and quantified it in terms of a T wave alternans index (TWAI). The TWAI is measured as the periodogram evaluated at 0.5 cycles-per-beat (cpb) of the normalized T wave energy series minus an estimate of the spectral background noise.

Spectral method (SM). The SM was proposed in 1988 by Smith [47] as an improved version of the ESM. The ECG beats (typically 128 beats) are aligned and periodogram-based power spectral estimates are computed for each sample in a segment of interest. The value in the aggregate power spectrum corresponding to alternans (0.5 cpb) is compared with an estimate of the noise in an adjacent spectral band to decide if TWA is present.

Complex demodulation method (CD). CD was presented in 1991 by Nearing et al. [147, 148] as an alternative to SM. CD provides a relative tolerance to non-stationary data, independence to phase shift perturbations and requires less data (i.e. < 30 s). The ECG beats are aligned, and TWA is modeled as a sinusoidal signal of frequency $f = 0.5$ cpb of variable amplitude and phase. TWA amplitude in each beat-to-beat series is estimated by demodulation of the 0.5-cpb component.

Correlation method (CM). This time-domain approach was proposed by Burattini et al. in 1997 [149–151]. Successive T waves are jointly analyzed and the information is reduced to a single cross-correlation coefficient, named alternans correlation index (ACI). A T wave is classified as alternating when it belongs to a string of a least seven T waves, the ACI of which are alternating.

Karhunen-Loève transform (KLT). In the work of Laguna et al. [152], each T wave is reduced to the first four coefficients of the KLT. Then each beat-to-beat series of coefficients is spectrally analyzed by means of the periodogram.

Poincarré mapping method (PM). The Poincarré maps are used to analyze dynamical systems displaying periodicity. Strumillo et al. applied it to TWA analysis in 2000 [153]. For each sample of the T wave, a Poincarré map is obtained by representing pairs of consecutive beat-to-beat differences (odd and even beats) in the phase space. Alternans is considered present when two clusters of points are present in the map, and is measured in terms of distance between the centroids of odd and even points.

Periodicity transform method (PT). An approach based on the periodicity transform from Sethares [154] was presented in 2002 by Srikanth et al. [155]. T wave amplitude, area and variance around a median T wave are extracted into beat-to-beat time series. The energy of the orthogonal projection of each time series on the subspace of sequences with 2-beat periodicity is used to detect alternans.

Modified moving average method (MMA). Nearing et al. proposed in 2002 the MMA as a more robust approach compared to their CD method [156]. A recursive running average of odd and even beats is continuously computed and a limiting nonlinearity is applied to the update terms of every new beat to avoid negative effects of impulsive artifacts. TWA is measured as the maximum difference between the odd and even averages over a 15-second interval.

ESM, SM and CM underestimate TWA amplitude, since they assume TWA being distributed along the entire length of the T wave. SM is not adequate for detecting non-stationary TWA; an accurate estimation of the power spectrum requires a relatively large number of beats (64 to 128) during which stationarity is assumed [149]. Spectral methods (ESM, SM, KLT) require long alternating sequences (64 to 1024 beats) to provide accurate results. The MMA method is robust to impulsive artifacts in the ECG but at the cost of underestimating transient alternans. The MMA method also needs at least the complete measurement window length (15-second interval) to adapt to phase reversal of the alternans patterns [156].

7.2   Detection of repolarization alternans

In the present study, we aimed at detecting transient Re-ALT of short duration, which prevented the use of conventional spectral methods [47, 147], as well as the MMA time-domain method [156], both of which requiring long Re-ALT sequences.

We thus developed a simple short interval time-domain algorithm based on a local feature, the apex of the T waves (T_a), and a Student t-test to detect transient Re-ALT. The T waves are smoothed by a Savitzky-Golay filter of order three to remove any residual artifact following the wavelet denoising and VA cancellation. The local maximum of each T wave segment is defined as T_a. Time series of T_a are used to determine Re-ALT sequences, which were considered significant

when the two following conditions were fulfilled:

1. T_a were alternating for more than four consecutive beats
2. odd and even T_a distributions were statistically different based on a Student t-test ($p < alpha$, one sided).

The Student t-test yields a significance threshold to decide whether the differences observed between the T_a of the odd and even beats are significant. For an alternating sequence of length N_{seq}, composed of N_{odd} and N_{even} beats, the time series of T_a can be represented as:

$$T_{odd} = \{T_a(1),\ T_a(3),\ \ldots,\ T_a(N_{odd})\} \tag{7.1}$$

$$T_{even} = \{T_a(2),\ T_a(4),\ \ldots,\ T_a(N_{even})\} \tag{7.2}$$

with $N_{seq} = N_{odd} + N_{even} \geq 5$.

The actual value of the t-statistic is calculated as:

$$t = \frac{\overline{T_{odd}} - \overline{T_{even}}}{\sigma_{seq} \sqrt{\frac{1}{N_{odd}} + \frac{1}{N_{even}}}} \tag{7.3}$$

where $\overline{T_{odd}}$ and $\overline{T_{even}}$ are the sample mean of odd and even T_a, and σ_{seq} is the pooled sample standard deviation, defined by the odd (σ_{odd}) and even(σ_{even}) standard deviations:

$$\sigma_{seq} = \sqrt{\frac{(N_{odd} - 1)\,\sigma_{odd}^2 + (N_{even} - 1)\,\sigma_{even}^2}{N_{odd} + N_{even} - 2}} \tag{7.4}$$

Given the t-statistic and the numbers of degrees of freedom ($N_{odd} + N_{even} - 2$), a one-tailed p-value is computed. When $p > \alpha$, the Re-ALT sequence is not considered significant and smaller sub-sequences of length ($N_{seq} - \delta$) are tested iteratively, starting with $\delta = 1$. At each step, there are ($\delta + 1$) possible sub-sequences of ($N_{seq} - \delta$) consecutive T_a. The iterative testing stops when alternans is considered significant in a sub-sequence ($p < \alpha$) or when $N_{seq} - \delta < 5$.

7.2.1   Noise and repolarization alternans

In order to quantify the effect of noise on the amplitude of the T wave apexes, AR noise was added to synthetic EGM (400 beats) with constant T waves morphology and amplitude. The apexes were extracted from the fitted curves of T waves and sequences of more than five alternating beats were detected. The detection of Re-ALT sequences was performed on the noisy signal without and with wavelet denoising. Table 7.1 reports the proportion of alternating sequences and the mean amplitude of the alternans over 1000 noise realizations, with and without wavelet denoising and when the t-test was applied ($\alpha = 5\%$). The t-test removes partially false detection of Re-ALT sequences.

7.2.2   VA activity and repolarization alternans

This section evaluates the effect of VA on Re-ALT analysis. Synthetic EGM of 400 beats contained AA, VA and additive AR noise. AA and VA were generated in order to simulate AV

	No preprocessing	WD	WD & t-test
% Re-ALT sequences	30.0 ± 5.8 %	26.4 ± 5.6 %	9.2 ± 5.7 %
Amplitude Re-ALT	$13.9 \pm 8.0 \mu$V	$14.0 \pm 8.5 \mu$V	$18.0 \pm 7.3 \mu$V

Table 7.1: *Percentage of Re-ALT sequences induced by additive AR noise and their corresponding amplitude (mean±SD) in modeled EGM. WD refers to wavelet denoising.*

block, 3:1 and 2:1 AV conduction. Wavelet denoising was applied, VA was canceled using PCA_2 and detection of Re-ALT was performed. As in experimental EGM, VA can impinge on different segment of AA, the time from atrial to ventricular depolarization varied from 150 ms to 250 ms, with steps of 10 ms. In addition, three behaviors of atrial repolarization patterns were simulated: without Re-ALT (tab. 7.2), with Re-ALT (tab. 7.3) and mixed (i.e. transient Re-ALT, tab. 7.4). The alternans in the amplitude of Re-ALT was set to 50 μV.

The results are reported in terms of false and true positive ratios, with detection performed on EGM with constant T wave and constant Re-ALT, respectively. Performance of detection with transient Re-ALT is reported in terms of specificity (eq. 7.5) and sensitivity (eq. 7.6).

- True positive (TP): alternating beat correctly identified as alternating
- False positive (FP): non alternating beat incorrectly identified as alternating
- True negative (TN): non alternating beat correctly identified as non alternating
- False negative (FN): alternating beat incorrectly identified as non alternating

Specificity

$$\text{Specificity} = \frac{\text{TN}}{\text{TN} + \text{FP}} \tag{7.5}$$

A specificity of 100% means that the test recognizes all actual negatives.

Sensitivity

$$\text{Sensitivity} = \frac{\text{TP}}{\text{TP} + \text{FN}} \tag{7.6}$$

A sensitivity of 100% means that the test recognizes all actual positives.

Table 7.2 reports the non-alternating sequences detected as alternating (false positive), induced by VA. Satisfactory results are obtained in the case of AV block and 3:1 conduction, both because VA cancellation performed better for these types of AV conduction and VA did not induce a 2:1 pattern. During 2:1 AV conduction simulation, a worst case has been set: the ventricular T wave flattened the atrial repolarization on a 2:1 basis. VA cancellation was only able to correct it partially as shown in figure 7.1.

Table 7.3 reports the results of the detection during stable Re-ALT (50 μV). The best results were obtained, quite logically, in the case of AV block. In the case of 3:1 AV conduction, the standard deviation of the alternans amplitude increases, indicating residual distortion induced by VA. During 2:1 AV conduction, VA can flatten or amplify the alternans, depending on the initial

	AV block	3:1 AV conduction	2:1 AV conduction
% Re-ALT sequences (false positive)	21.3 ± 11.7 %	14.3 ± 7.5 %	74.4 ± 36.0 %
Re-ALT amplitude	3.1 ± 3.1 μV	18.2 ± 11.5 μV	54.3 ± 11.7 μV

Table 7.2: *Percentage of false Re-ALT sequences induced by VA and their corresponding amplitude (mean±SD) in modeled EGM.*
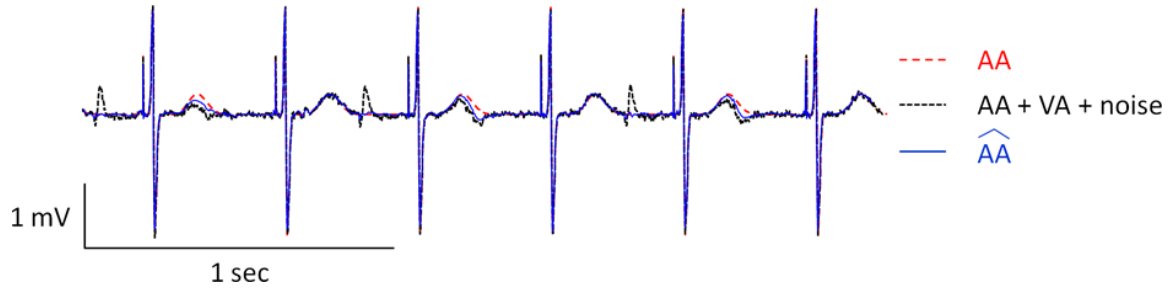
Figure 7.1: *2:1 AV conduction inducing Re-ALT. The ventricular far-field T wave flattens the atrial T wave every two beats. Initial AA: dashed red line. AA, VA and noise: dotted black line. $\widehat{AA}$: estimated AA.*

alternans pattern (high-low-high or low-high-low). The results presented in the table correspond to the case where VA flattened alternans.

Detection of transient Re-ALT is reported in table 7.4. During AV block, the algorithm was able to correctly cancel VA and track transient Re-ALT with measured Re-ALT close to simulated Re-ALT values and small standard deviation. During 3:1 AV conduction, residual VA resulted in a higher standard deviation of the detected Re-ALT and a lower sensitivity and specificity. During 2:1 AV conduction, VA induced false Re-ALT sequences (low specificity), which resulted in an overestimated amplitude of Re-ALT sequences.

	AV block	3:1 AV conduction	2:1 AV conduction
% Re-ALT sequences (true positive)	96.4 ± 2.9 %	91.4 ± 8.2 %	72.3 ± 22.4 %
Re-ALT amplitude	49.0 ± 8.5 μV	52.8 ± 22.3 μV	44.9 ± 20.8 μV

Table 7.3: *Percentage of Re-ALT sequences detected (true positive) and their corresponding amplitude (mean±SD) in modeled EGM with constant Re-ALT of 50 μV.*

	AV block	3:1 AV conduction	2:1 AV conduction
Specificity	92.5 ± 3.2 %	89.0 ± 4.9 %	31.2 ± 15.2 %
Sensitivity	94.9 ± 3.4 %	81.9 ± 17.6 %	86.7 ± 14.2 %
Detected Re-ALT amplitude	46.5 ± 7.7 μV	53.4 ± 23.8 μV	95.6 ± 50.2 μV

Table 7.4: *Specificity and sensitivity of the detection algorithm during transient Re-ALT (50 μV) and amplitude of the detected Re-ALT sequences (mean±SD).*

7.2.3   Comparison with the spectral method

This section describes the most commonly used method: the spectral method (SM). The details as well as the potential benefits and drawbacks of this method are described.

SM follows the description of Narayan and Smith [157]. The spectral method uses fast Fourier transform (FFT) to quantify alternation in a segment from beat-to-beat. An analysis window of N_B consecutive beats is chosen (from 64 to 1028). The alternans series are composed of amplitude values at points within the T wave segment in every beat from the analysis window. The alternans series are detrended by removal of the best-fit linear trend before periodogram estimation. The alternans series periodogram is obtained by taking the squared modulus values of the FFT. The periodograms obtained for every offset in the T wave segment are then summed over the whole segment to provide a *summary statistic*, as shown in figure 7.2. The spectral magnitude at 0.5 cycle per beat ($P_{0.5}$) indicates repolarization alternans.
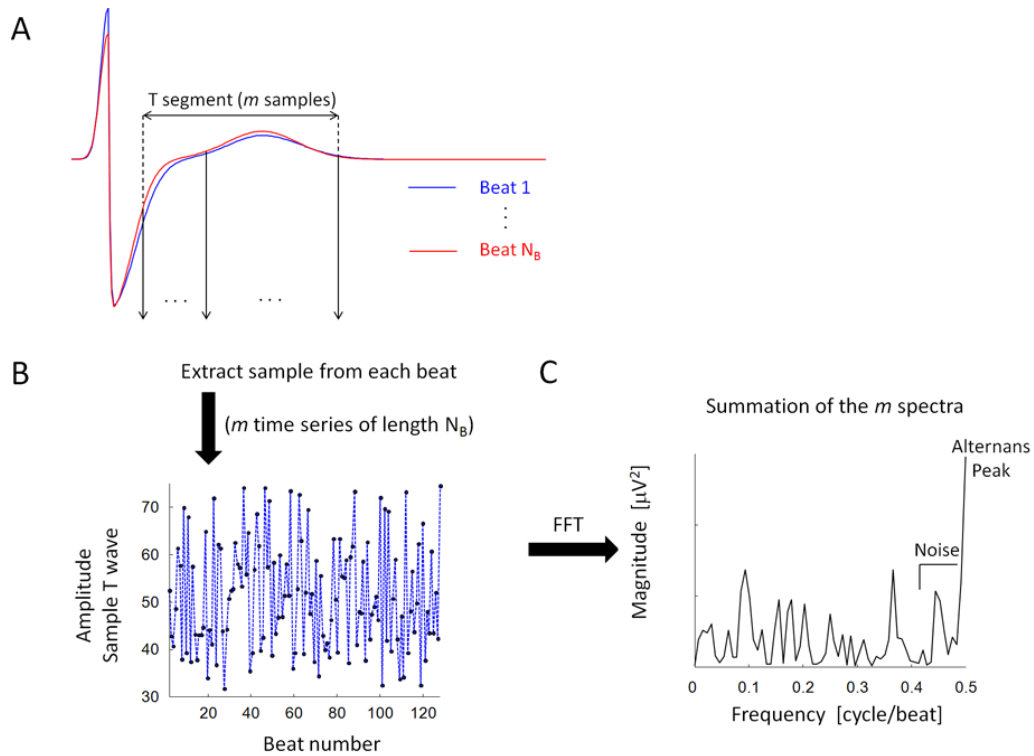
Figure 7.2: *Spectral method. (A) The N_B beats are aligned by QRS complexes. (B) Beat-to-beat oscillations reflect alternans at each time point of the segment (arrows in A). (C) Spectral analysis applies a FFT to yield a power spectrum in which alternans is the peak at 0.5 cycle/beat.*

The mean and standard deviation of the noise level (μ_{noise} and σ_{noise}) are computed from ~ 8 points in a band adjacent to the alternans one, such as 0.34-0.44 cpb or 0.39-0.49 cpb [158]. The voltage of alternans (V_{alt} measured in μV) and the ratio of alternans (κ score) are defined as:

$$V_{\text{alt}} = 2 * \sqrt{\frac{P_{0.5} - \mu_{\text{noise}}}{m}} \tag{7.7}$$

$$\kappa = (P_{0.5} - \mu_{\text{noise}}) / \sigma_{\text{noise}} \tag{7.8}$$
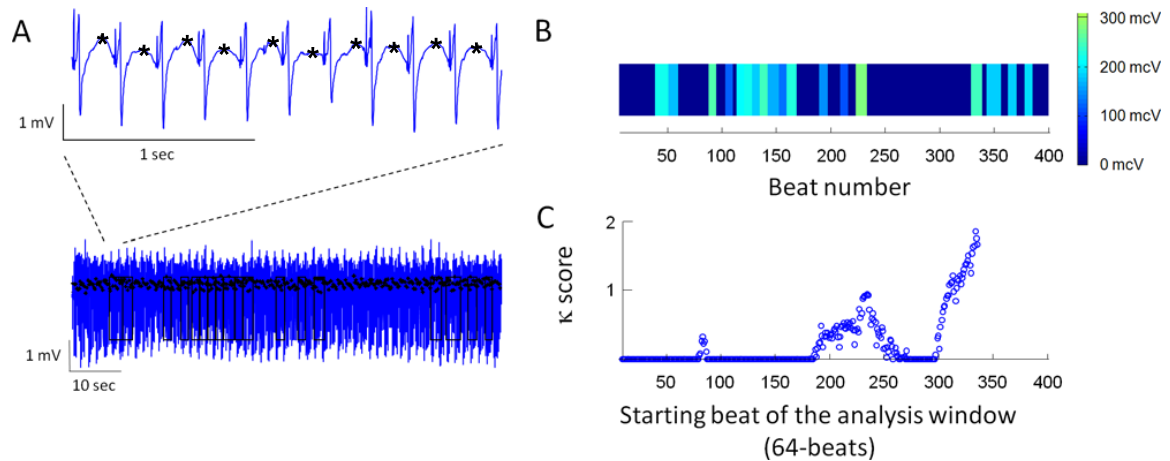
Figure 7.3: *Re-ALT detection base on time-domain and spectral method. Panel A shows Re-ALT sequence detected based on the time-domain approach (upper row) and the 400 beats of an S1S1 at 220 ms (bottom row). Panel B shows the mean peak-to-peak amplitude for each detected sequence. Panel C shows the κ score obtained with the spectral method on sliding windows of 64 beats.*

where m is the length of the T wave segment. The κ score is a measure of the signal-to-noise ratio of the measurement. In clinical applications, the analysis is performed on windows of 64 or 128 beats and a positive TWA is defined as a TWA sustained for ≥ 1 min and a κ score > 3 on several ECG leads [158].

Analysis of Re-ALT using the spectral method leads to robust results on noisy data, the long beat windows assuring a good signal-to-noise ratio. The drawback is however the averaging of Re-ALT over these periods, which reduces the ability to detect Re-ALT for shorter periods that may be relevant.

Figure 7.3 shows an example of the time-domain approach based on T_a and the κ score obtained with the SM using a sliding window of 64 beats applied to a sheep atrial EGM paced at 220 ms (sheep with AV block, not remodeled). The T waves have been extracted at a fixed interval from the R peak ([30-180] ms) and the noise band has been computed on the interval 0.39-0.49 cpb. V_{alt} obtained from the spectral method is not reported since it computes the alternans over the complete T wave while the analysis based on T_a reports a peak-to-peak alternans. Note that Re-ALT sequences of short duration with phase reversal of the alternans pattern (beats 34 to 54 and 106 to 170) are not detected by SM (panel C). Re-ALT sequences of short duration but with constant alternans pattern (beats 191 to 243 and 340 to 385) result in a higher κ score.

Figure 7.4 compares the same two algorithms, on a sheep right atrial EGM paced at PCL 180 ms. In the absence of phase reversal, the SM method yields a large κ score (note the difference in the range of κ score). This example also shows the large differences in κ score values depending on the choice of the 64-beats window.

7.2.4 Identifying periodicity in Re-ALT sequences onset

In experimental EGM, sequences of transient Re-ALT were observed. A method to identify hidden periodicities in the onset of Re-ALT sequences during a protocol is detailed in this section.
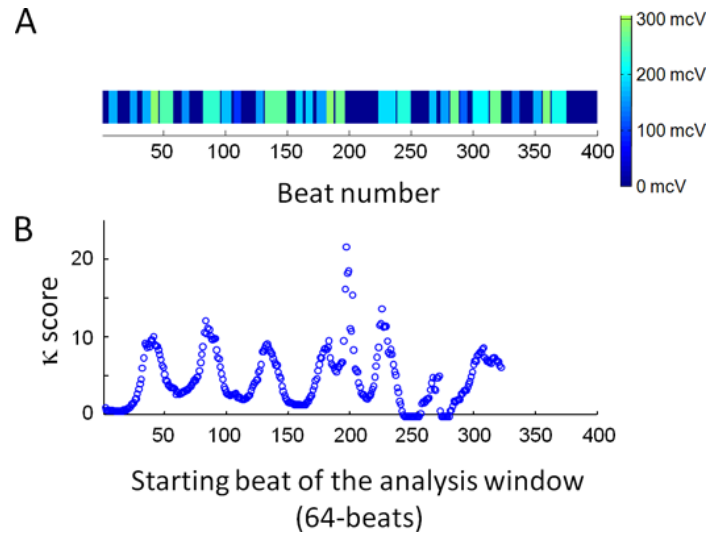
Figure 7.4: *Re-ALT detection base on time-domain and spectral method at PCL 180 ms. Panel A shows the mean peak-to-peak amplitude for each detected sequence using the time-domain approach. Panel C shows the κ score obtained with the spectral method on sliding windows of 64 beats.*

Periodic phenomena are widespread in biology, including, among others, membrane potential oscillations, cardiac rhythms or calcium oscillations. The task of finding periodicity in time series measured from a biological system can be viewed as a decision problem based on spectral analysis together with hypothesis testing. A formal statistical testing procedure for the detection of periodic expression profiles was introduced by Wichert et al. [159]. It relies on the use of a so-called *g*-statistic for which the exact null-distribution can be derived under a Gaussian noise assumption [160, 161].

The method proposed by Wichert et al. [159] is based on the periodogram spectral estimator, defined as:

$$I(\omega) = \frac{1}{N} \left| \sum_{n=1}^{N} y(n) e^{-j\omega n} \right|^2, \quad \omega \in [0, \pi] \tag{7.9}$$

where N is the time series length. The periodogram is further evaluated at discrete normalized frequencies:

$$\omega_l = \frac{2\pi l}{N}, \quad l = 0, 1, \dots, a \tag{7.10}$$

where $a = [(N-1)/2]$ and $[x]$ denotes the integer part of x. To test for the periodicity formally, some kind of test statistic must be chosen. The so-called *g*-statistic for one time series is given by:

$$g = \frac{\max_{1 \le l \le a} I(\omega_l)}{\sum_{l=1}^{a} I(\omega_l)} \tag{7.11}$$

In plain words, the *g*-statistic is the maximum periodogram ordinate divided by the sum of all periodogram ordinates for $l = 1, \dots, a$. A large value of g indicates a strong periodic component and leads to the rejection of the null hypothesis of a purely random process.

Wichert et al. [159] resort to a result by Fisher which, under the Gaussian noise assumption, gives the exact distribution of the g-statistic under the null hypothesis. The exact p-value for a realization of the g-statistic is:

$$P(g > x) = \sum_{k=1}^{b} (-1)^{k-1} \frac{a!}{k!\,(a-k)!} \, (1 - kx)^{a-1} \tag{7.12}$$

where b is the largest integer less than $1/x$ and x is the observed value of the g-statistic. Equation 7.12 yields a p-value that allows to test whether a given time series behaves like a random sequence or not.

To illustrate the presence of hidden periodicities, a simple model for simulated data is used:

$$y(n) = A \cos\left(2\pi n/T + \phi\right) + \epsilon(n) \tag{7.13}$$

where T is the period, A is the amplitude of the sinusoid, $\phi \in [-\pi, \pi]$ is the phase, $n = 1, \ldots, N$, and $\epsilon(n)$ is a sequence of uncorrelated random variables with mean 0 and variance σ_ϵ^2. Since the periodogram is invariant to the phase, ϕ can be set to zero for the simulated signals.

This method is applied to identify any periodic behavior of Re-ALT sequences onset at a given CL, with a significance level. Figure 7.6 illustrates the process. The detection of Re-ALT sequences is performed on the T_a time series (panel A). Then, the beats belonging to an Re-ALT sequence are assigned to one, the others to zero (panel B). The periodogram is computed and the significance of the period tested (panel C).

An exhaustive search of an unknown period in the time domain is possible, but is sensitive to any change in the period. This method allows variations in the length of the alternating sequences, which may be induced by false detection and therefore yields to a better solution to periodicity detection than an exhaustive search.
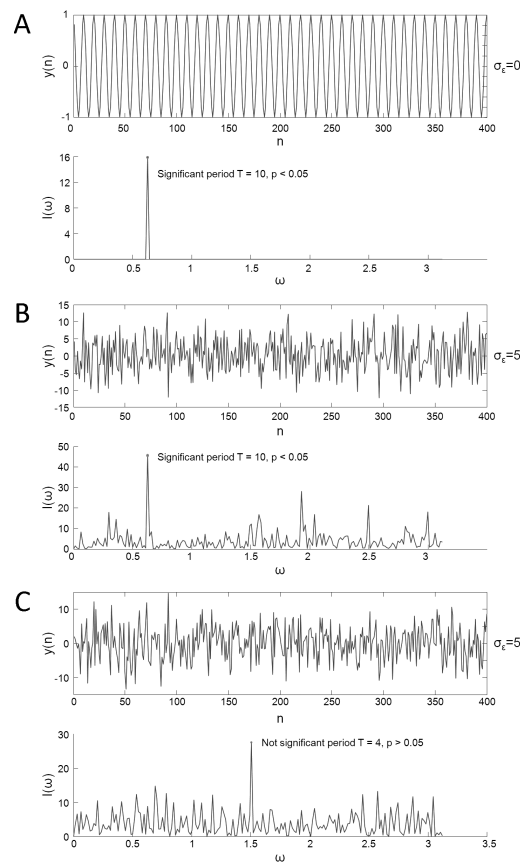
Figure 7.5: *Simulated sinusoids and their periodograms. Panel A shows the series $y_1, \ldots, y_{400}$ from equation 7.13, with period $T = 10$ and $\sigma_\epsilon = 0$. Panel B shows the same series with $\sigma_\epsilon = 5$. The correct period ($T = 10$) is detected in the periodogram and its p-value < 5%. Panel C shows a series with $\sigma_\epsilon = 5$ where a wrong period is identified ($T = 4$) but discarded due to its high p-value.*
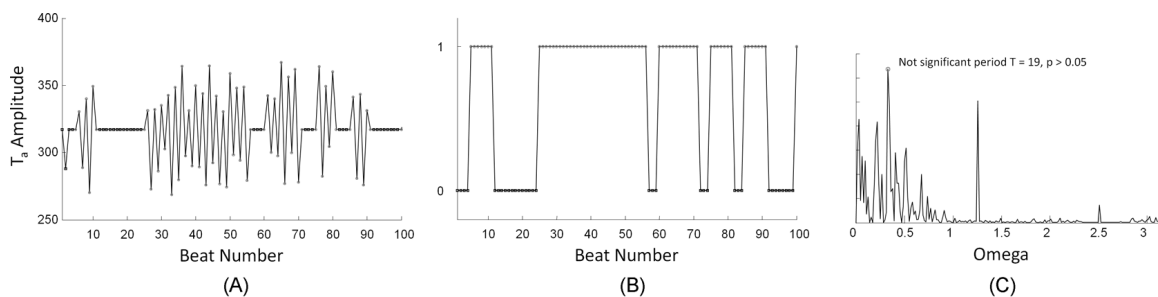
Figure 7.6: *Simulated T_a time series and its periodogram. Panel A shows a time series of T_a where the beats belonging to a Re-ALT sequence are denoted by red circles. Panel B shows the corresponding time series of alternating (1) and non alternating (0) sequences. Panel C show the resulting periodogram.*

7.3   Correlation between APD and atrial activation recovery interval

Determining activation and repolarization times on the cardiac surface is an important challenge of experimental and clinical cardiac electrophysiology. The assessment of local repolarization is related to time indexes associated to the downstroke of the transmembrane or monophasic action potential [162]. Since transmembrane or monophasic action potentials measurements can not be performed extensively in *in vivo* protocols, electrograms offer a practicable alternative to study excitation and repolarization.

The correlation between *in vivo* transmembrane APD and activation recovery interval (ARI) from ventricular EGMs has been investigated in theoretical [163, 164] and experimental studies [163, 165–167], but the application of the same methods to atrial signals has not been performed in details.

Using a computer model of the atria, we investigated different methods for the measurement of APD and ARI in atrial EGMs. The atrial biophysical model of the atria is based on human magnetic resonance images. The resulting atrial geometry is shown in figure 7.7a, with the major anatomical obstacles labeled. The surface was discretized using a 400-μm spatial resolution resulting in 100'000 nodes (fig. 7.7b) [16, 168].

The electrical propagation of the cardiac impulse was simulated using a reaction-diffusion system (monodomain formulation) based on a detailed ionic model of the cell membrane kinetics, formulated by Courtemanche, Ramirez and Nattel (CRN) [15, 169]. A finite volume approach was used to solve the monodomain propagation equations. This approach interprets the atrial tissue as a network of resistors (fig. 7.7b) [170].
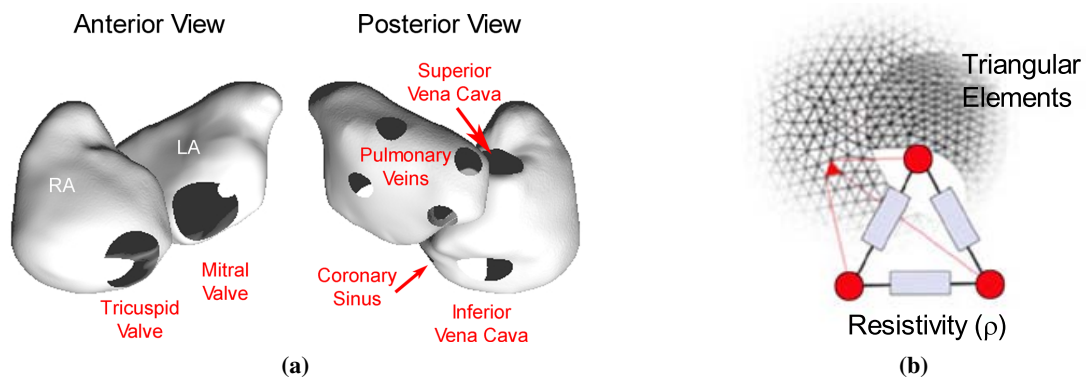
Figure 7.7: *The biophysical model of the atria. (a) Atrial geometry. (b) Atrial tissue: resistivity ρ sets CV values. Figure from Uldry et al. [16]*

The stimulation protocols were performed at three different PCL: 400, 350 and 300 ms. Two tissue conditions were used simulating baseline and remodeled states. In the baseline condition, ρ was set to 100 Ω cm resulting in a CV of 98 cm/s, while in remodeled condition ρ was set to 300 Ω cm resulting in a slower CV of 50 cm/s. In order to approximate our experimental setup, the pacing site was set in the right lateral wall and the recording site in the right atrial appendage at 1 mm of the surface (fig. 7.8).
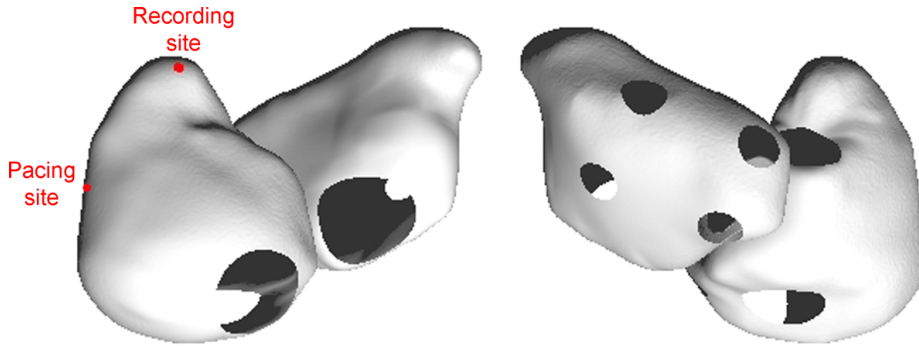
Figure 7.8: *Pacing and recording sites on the biophysical model.*
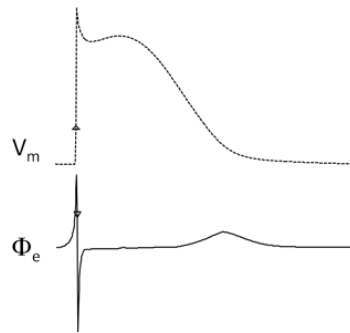
Figure 7.9: *Example of transmembrane (V_m, dashed) and extracellular (Φ_e, continuous) potentials.*

Transmembrane potentials are directly available from the model and EGMs are generated from monodomain simulations by the following equation [168]:

$$\Phi_e\left(\mathbf{r}, t\right) = \frac{1}{4\pi\sigma_e} \int \frac{I_m\left(\mathbf{r}', t\right)}{|\mathbf{r} - \mathbf{r}'|} dr' \tag{7.14}$$

where ϕ_e is the extracellular potential (i.e. EGM), $\mathbf{r}$ is the electrode location, $\mathbf{r}'$ is the source location, I_m is the transmembrane current and σ_e is the extracellular conductivity. Figure 7.9 shows a representative example of a transmembrane potential (top) and an extracellular potential (bottom) at the recording site.

Since AP exhibits a wide repolarization range, APD varies significantly depending on the method used for its measurement. APD represents the time interval from the maximum derivative during the phase 0 to the end of phase 3. The definition of the APD end point can be divided into three groups: percentage of repolarization ($APD_{90\%}$, $APD_{80\%}$, $APD_{70\%}$ and $APD_{60\%}$), return to a fixed threshold (APD_{-70mV} and APD_{-65mV}) and time of minimum repolarization derivative (APD_{MD}).

Ventricular ARI is measured as the interval between the maximum negative slope of the QRS complex and the maximum positive slope of the T wave in the unipolar EGM ($ARI_{R_{MD}T_{MD}}$)[163, 166, 171]. In the present study, we also evaluated ARIs as the time interval from the R peak to the T wave apex (ARI_{RT_a}).

A large correlation was found between ARI_{RT_a} and $APD_{90\%}$ (fig. 7.11) and between ARI_{RT_a} and APD_{-70mV}. Table 7.5 reports the average absolute difference between APD and ARI, the associated
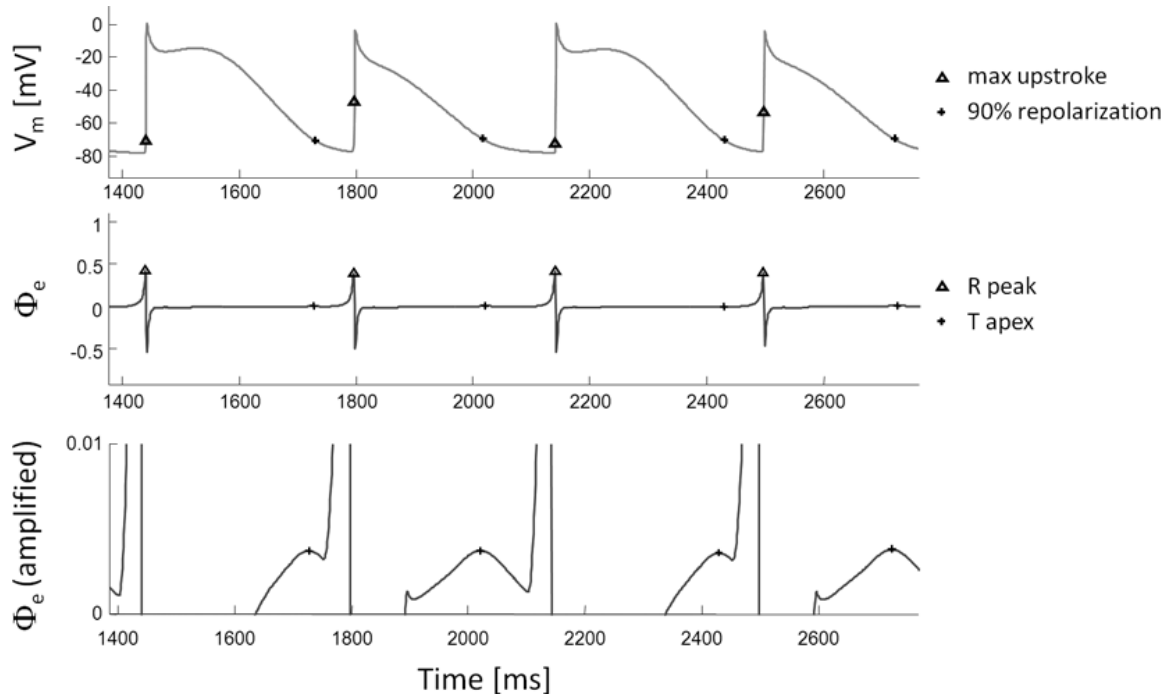
Figure 7.10: *Example of transmembrane (V_m) and extracellular (Φ_e) potentials at PCL 350 ms.*
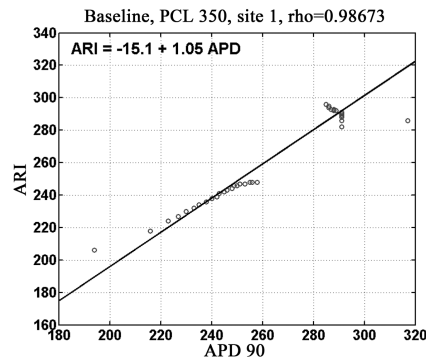
Figure 7.11: *Correlation ARI_{RT_a} - $APD_{90\%}$ at PCL 350 ms, $\rho = 100\ \Omega\ cm$.*

standard devitation, the correlation coefficient and the robust linear fit equation for a PCL of 400 ms. Choosing the R peak instead of the maximum depolarization downstroke on the EGM did not affect significantly the measure of ARI as the interval was of one or two samples. Table 7.6 reports the average absolute difference between $APD_{90\%}$ - ARI_{RT_a} and APD_{-70mV} - ARI_{RT_a} for the different PCLs and resistivities ρ.

In summary, a strong correlation between APD_{90} and ARI_{RT_a} has been found and these results using a computer model of the atria show the interest of ARI to track changes in APD in the atria.

APD	ARI	Absolute mean difference [ms]	Standard deviation [ms]	Linear regression	Correlation coefficient
$APD_{90\%}$	$ARI_{R_{MD}T_{MD}}$	50.6	7.9	ARI = -45.8 + 0.65 APD	0.993
	ARI_{RT_a}	**7.3**	**3.7**	**ARI = 8.9 + 0.94 APD**	**0.988**
$APD_{60\%}$	$ARI_{R_{MD}T_{MD}}$	27.4	9.2	ARI = 23.2 + 0.75 APD	0.827
	ARI_{RT_a}	72.4	7.6	ARI = 122 + 0.75 APD	0.992
APD_{-70mV}	$ARI_{R_{MD}T_{MD}}$	47.7	6.6	ARI = 40 + 0.68 APD	0.995
	ARI_{RT_a}	**4.4**	**1.5**	**ARI = -4.0 + 0.97 APD**	**0.998**
APD_{MD}	$ARI_{R_{MD}T_{MD}}$	22.2	5.8	ARI = -78.7 + 1.49 APD	0.975
	ARI_{RT_a}	65.5	11.2	ARI = -160 + 2.1 APD	0.955

Table 7.5: *Comparisons APD-ARI at PCL 400 ms, ρ = 100 Ωcm.*

		$APD_{90\%}$ - ARI_{RT_a}	APD_{-70mV} - ARI_{RT_a}
ρ = 100 Ωcm	PCL 400 ms	7.3 ± 3.7	4.4 ± 1.5
	PCL 350 ms	2.8 ± 3.7	3.6 ± 2.4
	PCL 300 ms	15.1 ± 2.3	6.3 ± 0.7
ρ = 300 Ωcm	PCL 400 ms	4.9 ± 2.5	1.2 ± 1.3
	PCL 350 ms	3.2 ± 2.7	1.1 ± 1.3
	PCL 300 ms	1.4 ± 2.7	2.7 ± 1.1

Table 7.6: *Mean absolute difference ± standard deviation [ms] in using ARI to estimate APD for different PCL and values of ρ.*

7.4   Conclusions

A short review of existing methods has been presented with a particular emphasis on the advantage and drawbacks of the SM illustrated on experimental EGMs. An algorithm measuring peak-to-peak alternans on a beat-to-beat basis has been presented in order to detect transient short duration Re-ALT sequences. The performance of the algorithm has been evaluated on noisy simulated EGM and on EGM after VA cancellation. Also, an application of periodogram estimate to recover periodicity in the onset of Re-ALT has been addressed. A comparison of measurement methods of APD and ARI has be performed using a computer model of the atria.

8

Clinical links

In this chapter, the results obtained on experimental data from the ovine model (chap. 5) are presented and linked with clinical observations of human data. The clinical observations are introduced in sec. 8.1. The kinetic of atrial Re-ALT is presented in sec. 8.2.1 and the intermittence of atrial Re-ALT in sec. 8.2.2. The kinetics of Re-ALT and AT preceding 2:1 atrial capture and AF episodes are presented in sec. 8.2.3 and 8.2.4, respectively. Finally, a discussion on our results and the clinical relevance of our analysis is addressed in sec. 8.3.

8.1 Clinical observations

We had observed, in humans, periods of intermittent atrial capture during rapid pacing preceded by Re-ALT and delayed activation suggestive of decreased excitability (fig. 8.1). We hypothesized that decreased excitability during rapid pacing plays a protective role against Re-ALT induced wavebreaks and AF. A chronic free-behaving ovine pacing model was developed to study the interplay during rapid pacing between atrial Re-ALT that may facilitate AF initiation, and the onset of decreased excitability that may cause 2:1 capture and prevent AF initiation.

Patients were recruited in a parallel study whose aim was to study APD and conduction velocity dynamics in patients with clinical AF prior to ablation [106]. Briefly, monophasic action potential (MAP) catheters were advanced to the right or left atrium, and APDs measured during pacing using validated software [106]. Pacing was applied for 74 beats at cycle lengths (PCL) of 500 ms, 450 ms, 400 ms, 350 ms, 300 ms, then in 10 ms steps to capture failure or AF. MAPs were filtered at 0.05 to 500 Hz and digitized at 1 kHz to 16-bit resolution. AT_{MAP} was measured from the pacing stimulus to the maximal upstroke of the MAP dV/dt, and monophasic action potential duration (MAPD) from the maximal upstroke to 90% repolarization (APD_{90}, fig. 8.1).

In a subset of patients (n=4 out of 25), rapid pacing failed to initiate AF but instead led to 2:1
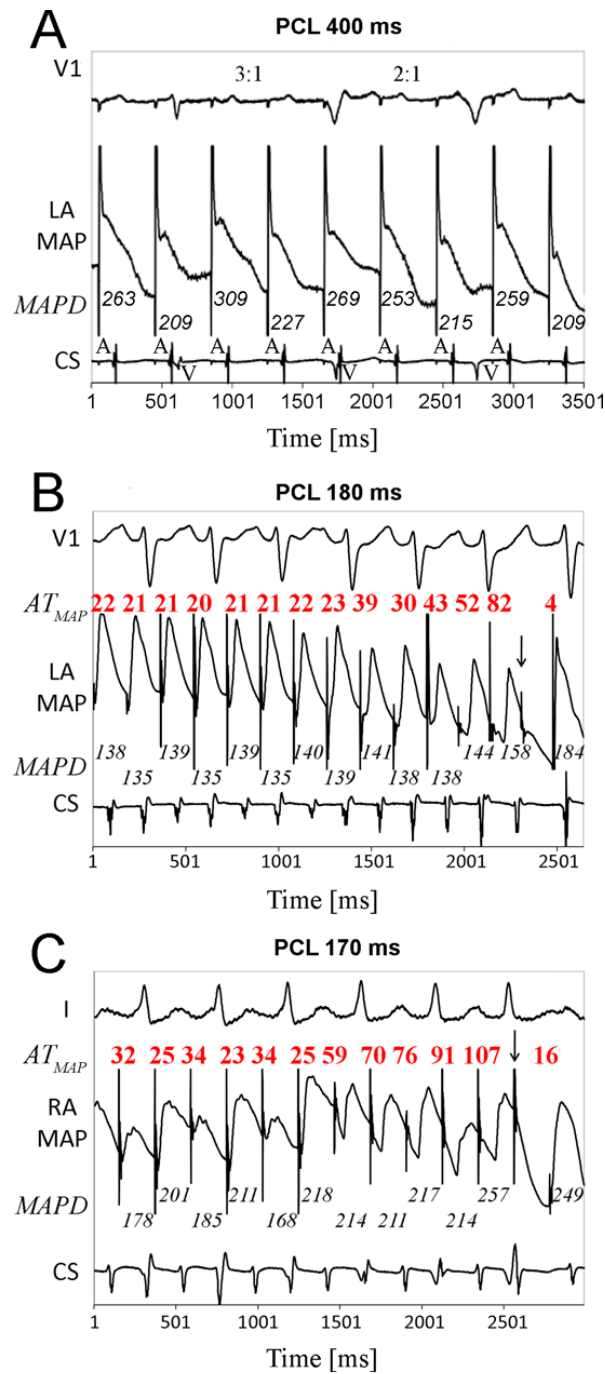
Figure 8.1: *ECG (top), MAPs (middle) and coronary sinus EGM (CS, bottom) recordings during decremental PCL. Panel A shows MAPD alternans at PCL 400 ms during 3:1 and 2:1 AV conduction. Panels B and C show left (LA, PCL 180 ms) and right (RA, PCL 170 ms) atrial MAPD alternans in two patients. Both MAPD alternans (alternating numbers) and prolongation of activation time (AT_{MAP}, red numbers) indicative of a transient reduction in excitability, gradually increased until the first beat of capture failure (arrow). Also note the presence of MAPD alternans phase reversal as shown by two consecutive long (panels A and B) and short (panels B and C) beats.*
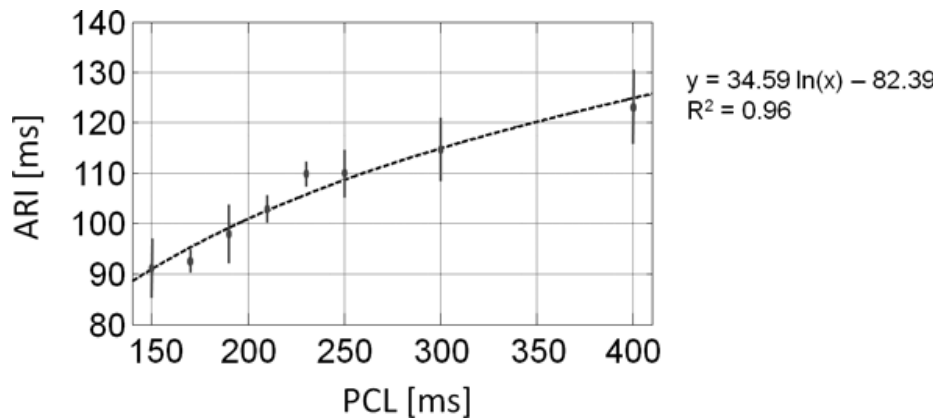
Figure 8.2: *ARI (mean±standard deviation) in function of PCL in a subset of eight sheep.*

capture failure. In the remaining 21 patients, MAPD alternans amplified to cause AF. MAPs were recorded in the left atrium in the first two patients and in the right atrium for the two others, during incremental rapid pacing to PCL 182±13 ms [106].

Figure 8.1 illustrates representative recordings of ECG (top), MAPs (middle) and coronary sinus EGM (CS, bottom) at decreasing PCLs. Panel A shows alternans of MAP in shape and duration at PCL 400 ms with variable AV conduction (2:1 and 3:1) indicating the lack of significant far-field ventricular interference on atrial repolarization in humans. Panels B and C illustrate left and right atrial MAP recordings from two patients in which MAPD alternans developed (lower numbers), but was accompanied by AT_{MAP} prolongation (upper red numbers) that progressively postponed MAP repolarization so that successive stimuli fell increasingly earlier on preceding MAPs until capture failure (arrow).

8.2 Results in animal model

Identification of the timing of pacemaker stimuli, atrial depolarization and repolarization waves (figure 8.3, panel A) were performed as introduced in sec. 6.1. The activation time (AT) were measured as the interval between the pacemaker stimuli and the atrial depolarization peak.

Activation recovery intervals (ARI) are correlated with local transmembrane APD or refractory periods [163, 165, 172, 173]. Typically, ARI are measured from the steepest downslope of QRS complex to the steepest upslope of T wave or to the peak of T wave [163, 173]. The second technique was applied to atrial unipolar EGMs (sec. 7.3). Janse et al. reported that T_a corresponds to the maximal gradient of repolarization between local action potentials (APs) [172]. The rate dependence of ARI was evaluated in a subset of eight sheep. ARI decreased as a function of PCL (fig. 8.2), supporting its relationship to atrial APDs. Figure 8.2 shows the logarithmic relationship between ARI (mean±SD) and PCL.

Panel B of figure 8.3 shows representative examples of time series of AT, ARI, T_a amplitude and its beat-to-beat differences (ΔTa) at a PCL of 210 ms. Although subtle variations were observed, they did not fulfill the criteria for beat-to-beat alternans (sec. 7.2).
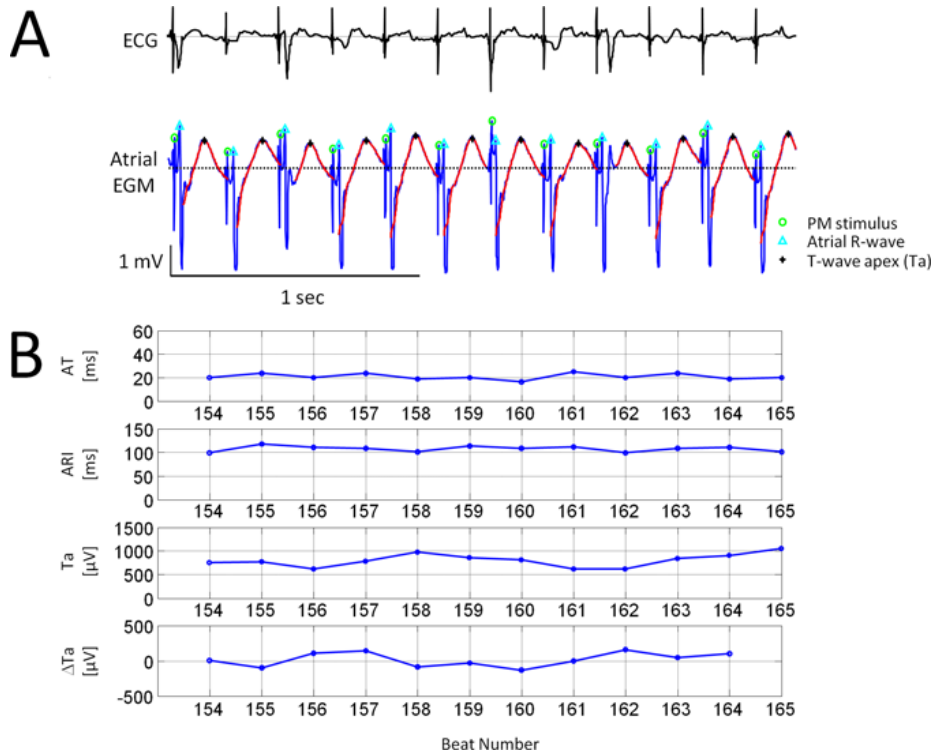
Figure 8.3: *Atrial unipolar EGM and time series. In panel A a representative example of subcutaneous bipolar ECG (top) and corresponding unipolar EGM (bottom) is shown. Green circles denote pacemaker (PM) stimuli, cyan triangles the first atrial depolarization wave (R-wave) and black stars atrial T wave apexes (T_a). Repolarization waves are highlighted by red bold curves. Panel B shows from top to bottom time series of AT, ARI, T_a and ΔT_a from the EGM shown above.*

8.2.1   Kinetics of atrial repolarization alternans in animal model

Atrial Re-ALT was detected in all sheep (with and without AV block), using the time-domain algorithm presented in sec. 7.2. At each PCL (S1S1 protocol) the occurrence and mean peak-to-peak amplitude of Re-ALT sequences were extracted. The first observation is that its amplitude increased as a function of pacing rate. Panel A of figure 8.4 illustrates representative examples of atrial unipolar EGMs at decreasing PCLs. Smoothed repolarization waves are shown in red and T_a by black stars. Re-ALT was absent at 400 ms PCL, but appeared and increased in magnitude at shorter PCLs. The decrease of PCL to 300 ms and 250 ms was associated with progressive increase in Re-ALT amplitude from a mean peak-to-peak difference (ΔT_a) of 66 μV at 300 ms to 141 μV at 250 ms.

Panel B shows a colormap of amplitude and beat locations (x-axis, from 1 to 400 beats) of Re-ALT for an entire stimulation protocol (y-axis, range 400 to 220 ms PCL) in an AV block sheep with ventricular pacing at 40 bpm (1500 ms) to dissociate far-field ventricular activity from atrial EGMs. Subtle Re-ALT was observed for long PCLs (350 to 300 ms, dark blue). For PCLs $\leq$ 290 ms, a progressive increase in duration and amplitude (light blue) of Re-ALT was noticed. Importantly, Re-ALT amplitude was much higher (red) at fast PCL (220 ms). Analysis of Re-ALT for shorter PCL ($\leq$ 210 ms to stable 2:1 capture) was not feasible in this example as the atrial depolarization waves impinged on the preceding atrial repolarization.
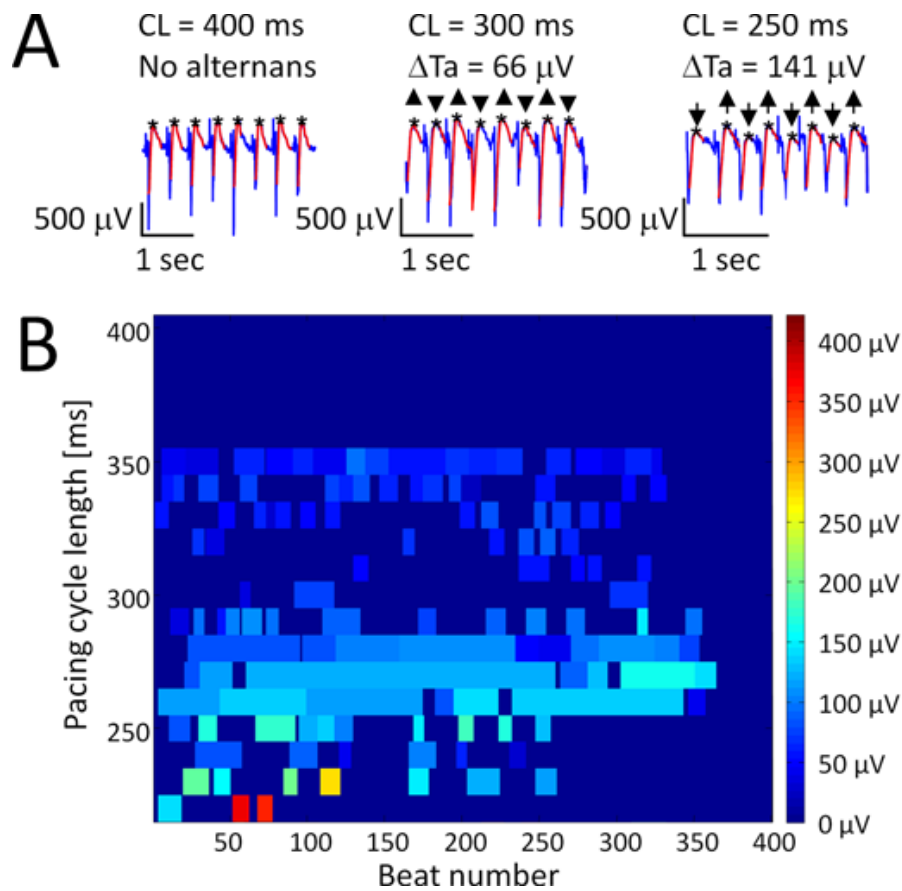
Figure 8.4: *Rate dependence of Re-ALT. Panel A shows examples of atrial EGM at decreasing PCLs. Panel B displays Re-ALT magnitude over a 400-beat pacing protocol. Significant Re-ALT sequences are displayed as rectangles of variable duration (number of beats, x-axis) and amplitude (0 to 400 μV, colorscale) at decreasing PCLs (400 to 220 ms, y-axis).*

Panels A and B of figure 8.5 show a summary of the kinetics of Re-ALT, AT-ALT and AT prolongation (mean±SD) at decremental PCLs (x-axis) in sheep (n=4) with AV block. VA was canceled and detection of Re-ALT sequences is performed as explained in sec. 7.2. Notably, Re-ALT amplitude increased linearly (R^2=0.971, p<0.001) from PCL 290 ms and became significantly larger than the background level at PCLs ≤ 230 ms (p<0.05) which we defined as the atrial Re-ALT threshold.

Panel B shows the kinetics of AT minus its mean value measured at PCL 400 ms (AT_{400}) as a function of PCL. AT remained stable until PCL 210 ms, increased exponentially, and became significantly different from baseline (400 ms PCL) at PCLs ≤ 190 ms (repeated one-way ANOVA, p<0.05) until the first instance of intermittent atrial capture (≤150 ms). Then, the potential contribution of alternans of AT to Re-ALT was evaluated. Panel A (bottom row) shows that AT-ALT was absent over the pacing protocol. In summary, both the occurrence and amplitude of atrial Re-ALT, and the kinetics of AT were rate-dependent.
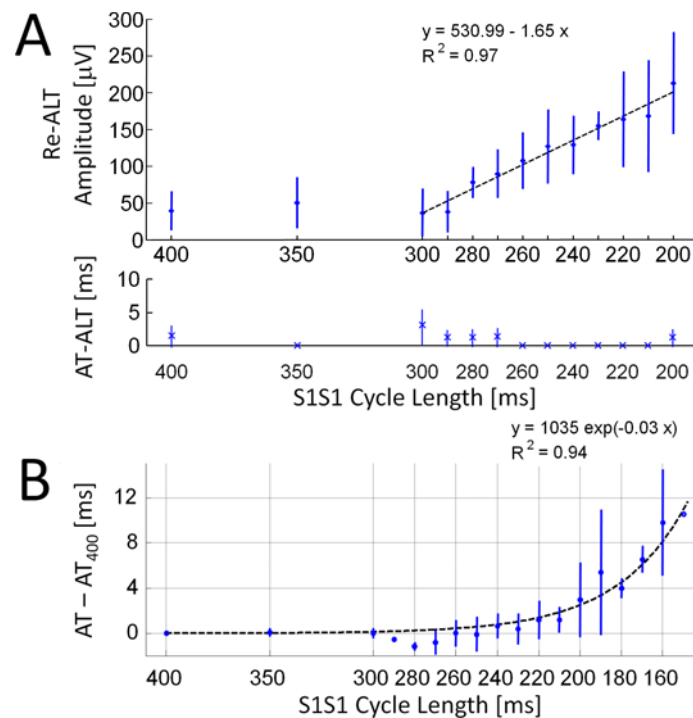
Figure 8.5: *Panel A reports mean±SD (n=4 sheep) of Re-ALT amplitude (top) and AT-ALT (bottom) as a function of PCL. Panel B reports mean±SD (n=4 sheep) of AT prolongation (defined as the difference from baseline value (AT-AT$_{400ms}$) as a function of PCL.*

8.2.2 Atrial Re-ALT was intermittent despite continued pacing

The color map (panel B) of figure 8.4 shows that once atrial Re-ALT had developed, it was not steady during the time course of the pacing protocol. Atrial Re-ALT amplitude fluctuated over time without clear periodicity. Panel A of figure 8.6 shows a representative example of atrial unipolar EGM taken between beats 74 and 135 of a 400 beat protocol at PCL 230 ms. T wave apexes are emphasized by black stars. Sequences without significant Re-ALT are highlighted by black lines of variable duration at the top of the recording.

Importantly, Re-ALT appeared intermittently and in a non-periodic pattern with rises and declines of magnitude separated by periods of no Re-ALT of variable duration as well. The periodicity in the onset of Re-ALT was tested as introduced in sec. 7.2.4.

Panel B of figure 8.6 shows corresponding time series of AT, ARI and Re-ALT (ΔT_a). Notably, depolarization wave amplitudes in panel A and AT in panel B did not show any beat-to-beat alternation, suggesting that the mechanisms underlying atrial Re-ALT at intermediate PCLs primarily involves repolarization rather than depolarization. In contrast, ΔT_a clearly exhibited periods of Re-ALT of variable magnitude and duration. At the maximum amplitude of Re-ALT (beat number 109 to 113 and 131 to 135), ARI also showed significant beat-to-beat alternation, but of shorter duration compared to ΔT_a.
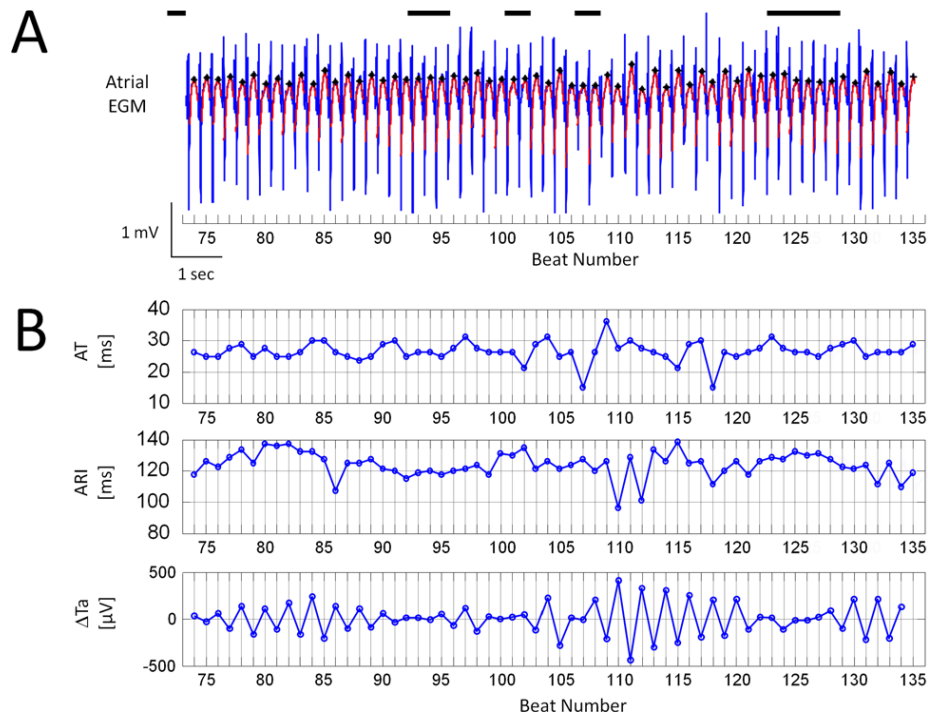
Figure 8.6: *Intermittence of Re-ALT. In panel A is shown an EGM with intermittent Re-ALT at PCL 230 ms. T_a are marked by black stars and non alternating periods by black lines. Panel B depicts the corresponding time series of AT, ARI and beat-to-beat differences in T_a (ΔT_a).*

8.2.3 Intermittent atrial capture

The 400 beat pacing protocols were pursued until stable 2:1 atrial capture which occurred at mean PCL of 128 ± 19 ms (i.e. steady state ERP). The mean PCL at which the first periods of intermittent 2:1 atrial capture intermingled with 1:1 capture was 154 ± 24 ms (i.e. 389 bpm).

Panel A of figure 8.7 illustrates an example of intermittent 1:1 and 2:1 atrial capture. No clear periodicity was observed as periods of 2:1 capture varied in duration.

Panel B shows representative recordings prior to 2:1 atrial capture exhibiting the four different patterns with their atrial unipolar EGM and corresponding AT and ΔT_a time series observed among the 186 analyzed transitions. Atrial EGMs display 1:1 atrial capture until the first non captured beat (arrow). Panel B1 shows Re-ALT with a progressive increase in ΔT_a magnitude (maximum ΔT_a 450 μV) and no AT change preceding 2:1 capture. Panel B2 shows the second pattern characterized by a similar increase in Re-ALT (maximum ΔT_a 280 μV) but associated with a gradual increase in AT (from 26 to 36 ms). Panel B3 shows the third pattern characterized by the lack of any significant Re-ALT. AT, however, markedly increased four beats prior to capture failure (from 28 to 54 ms). Panel B4 shows the last pattern characterized by the absence of any Re-ALT and AT changes preceding 2:1 capture. Table 8.1 displays the prevalence of each of the four patterns of AT and Re-ALT among the 186 episodes. 40% of the episodes were of the type as shown in panel B1 and 33% in B2. Importantly, Re-ALT was observed in 73% and AT prolongation in 49% of episodes. Only 11% of the overall episodes exhibited neither changes in AT nor Re-ALT (panel B4).
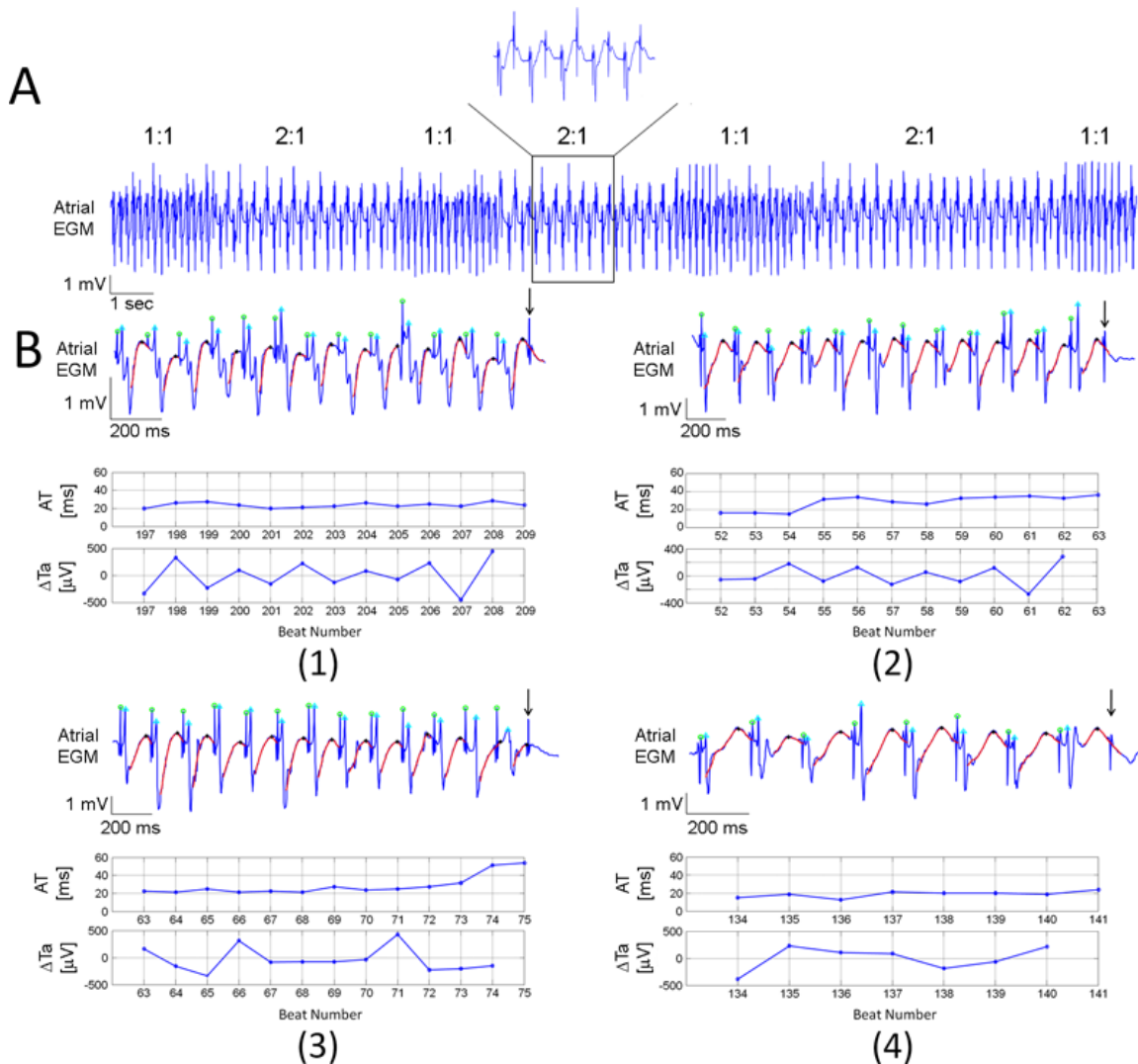
Figure 8.7: *Intermittency of atrial capture. In panel A is shown an illustrative unipolar EGM with intermittent 1:1 and 2:1 atrial capture of variable duration at PCL 160 ms. Panel B illustrates the four different patterns of EGMs and corresponding AT, ARI and ΔT_a time series until the first beat of 2:1 capture (arrow).*

Using Fisher's exact test [174] on table 8.1, no significant difference in Re-ALT prevalence (p=0.14) was observed between sequences with and without AT prolongation, supporting the lack of relationship between Re-ALT occurrence and decreased excitability exemplified by AT prolongation and capture failure and Re-ALT occurrence. The mean number of beats over which AT prolonged before capture failure was 4.9±2.5 (95% CI, 2-8).

Also, the faster the pacing rate, the longer the periods of intermittent 2:1 capture until steady state ERP. Panel A of figure 8.8 shows (top trace) the first short episodes of 2:1 capture at PCL 200 ms. The middle trace shows the same sheep at a shorter PCL (170 ms), with more frequent and longer periods of 2:1 capture. The bottom trace shows stable 2:1 atrial capture at steady state ERP (PCL 160 ms). For all pacing protocols between the first beats of capture failure and paced ERP, durations of 2:1 capture sequences were totaled, divided by the duration of the pacing protocol and expressed as the percentage of cumulative 2:1 atrial capture. Panel B of figure 8.8 shows

	Re-ALT	∅ Re-ALT	
→ AT	40% (B1)	11% (B4)	
↗ AT	33% (B2)	16% (B3)	49%
	73%		

Table 8.1: *Re-ALT and AT prolongation before capture failure. Prevalence of B1 to B4 patterns.*

summary data based on 35 recordings in 7 sheep starting at PCL 40 ms above steady state ERP and decremented by steps of 10 ms. Importantly, the cumulative percentage of intermittent atrial capture increased as the PCL was decreased. At ERP, cumulative 2:1 capture was 95% as 1:1 capture of a few beats duration was observed at initiation of the pacing protocol. In a subset of 4 sheep (20 recordings) whose ARIs were reliable enough, the last beat of 2:1 capture and the first beat of 1:1 capture were compared (panel C of figure 8.8). AT remained similar (from 34 ± 14 to 31 ± 12 ms, p=NS) but ARI decreased significantly (from 97 ± 18 to 89 ± 19 ms, p<0.05) at resumption of 1:1 capture. Also, note transient Re-ALT at resumption of 1:1 capture.
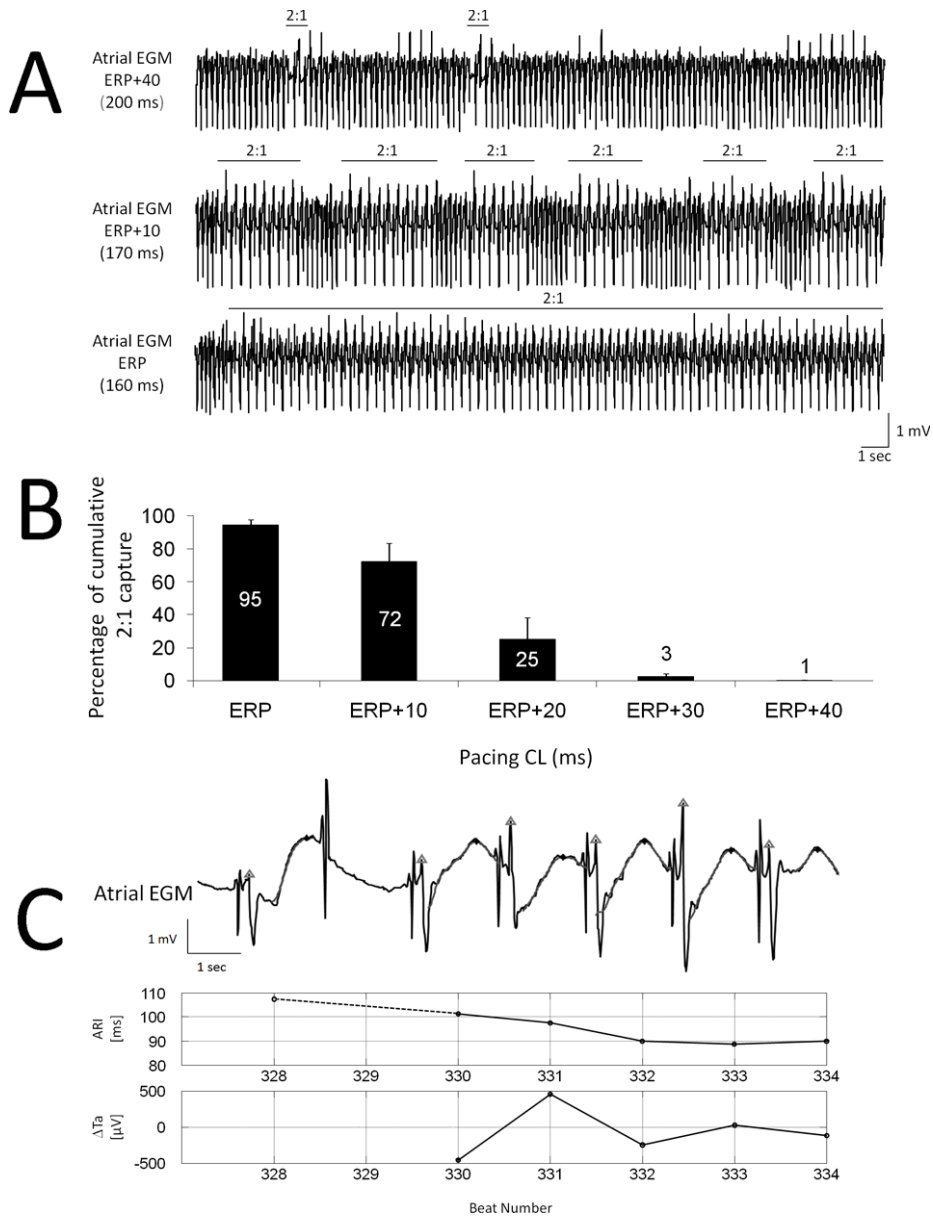
Figure 8.8: *Duration of 2:1 atrial capture is rate dependent. Panel A displays representative examples of unipolar EGM at decreasing PCLs. Rare 2:1 atrial captures of short duration are seen at PCL 40 ms above ERP (top). Middle trace illustrates the increase in 2:1 atrial capture of short duration followed by 2:1 capture. Panel B shows mean±SD of cumulative percentage of 2:1 atrial capture as a function of PCL. In panel C are shown EGM (top), ARI (middle) and Re-ALT (ΔT_a, bottom) time series ate resumption of 1:1 capture. ARI decreased before and Re-ALT emerged at resumption of 1:1 capture.*

8.2.4 Atrial fibrillation episodes

Forty-four pacing protocols were performed starting at PCL 400 ms until paced ERP, of which twelve (27%) triggered 20 episodes of non sustained AF at mean PCL 150±36ms. Re-ALT was detected in 65% of the episodes and AT prolongation in 60% and was not analyzable in 20%. Figure 8.9 shows an illustrative example at resumption of 1:1 capture where Re-ALT (ΔT_a) emerged and AT prolonged without failure to capture, leading directly to AF. Note the similar dynamics of AT prolongation and Re-ALT with episodes of 2:1 capture (figure 8.7).

In summary, both Re-ALT and AT prolongation were commonly observed before pacing-induced AF, but no specific pattern could be identified that predicted the imminence of intermittent capture rather than AF.
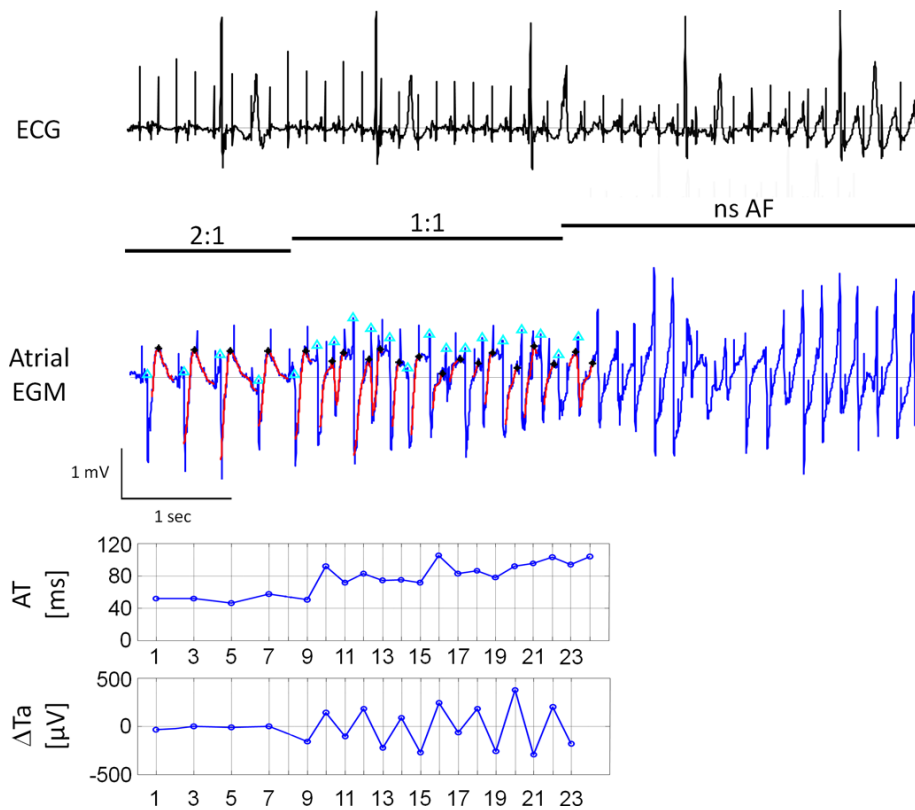
Figure 8.9: *Rapid pacing-induced AF. From top to bottom are shown ECG, atrial EGM and corresponding AT and ΔT_a time series during the transition from 2:1 to 1:1 atrial capture, followed by non sustained AF (nsAF).*

8.3 Discussion

This chapter focuses on mechanisms whereby rapid atrial pacing fails to induce AF. Based on observations in human atria that transient decrease in excitability, as exemplified by AT prolongation and capture failure during rapid pacing, may have quenched Re-ALT to cause intermittent capture and prevent AF initiation, we show in an ovine model of rapid pacing that Re-ALT and AT prolongation were present in 90% of the transitions from 1:1 to 2:1 atrial capture. Notably, 2:1 capture was imminent at PCLs <40 ms above ERP. This work also shows the feasibility of recording intra-atrial repolarization and ARI as a surrogate of APD, using available pacemaker technology. Atrial Re-ALT was reproducibly observed during rapid pacing, appeared intermittently but without periodicity and increased in amplitude as a function of pacing rate. Since rapid atrial tachycardias that promote fibrillatory conduction may also slow propagation velocity, transitions to 2:1 capture via transient decrease in excitability may protect against Re-ALT induced dispersion of repolarization and AF. A better understanding of the mechanisms causing Re-ALT and intermittent capture may allow treatments to be tailored for preventing AF induction at lower rates.

8.3.1 Kinetics of atrial repolarization alternans

Atrial Re-ALT has been recently observed using MAP [8–10, 106] and optical mapping [117]. Re-ALT increased in amplitude with rising heart rate, but none of these studies formally established the rate-dependence of atrial Re-ALT. Our study is the first to our knowledge to report the kinetics of atrial Re-ALT based on unipolar EGMs. Atrial Re-ALT was rarely observed at long PCLs, and progressively increased in duration and linearly in amplitude starting at PCL 280 ms. The PCL at which Re-ALT amplitude became significantly different from the background level (230 ms) was similar to the values (i.e. 220 to 190 ms) measured in humans prone to atrial flutter [8] and atrial fibrillation [10, 175]. Importantly, right atrial Re-ALT arose at PCLs where AT was neither prolonged nor alternating, indicating that atrial Re-ALT, as for the ventricles [50, 67], is primarily explained by beat-to-beat alternation in the repolarization time course.

8.3.2 Intermittency of atrial repolarization alternans

Selvaraj et al. reported in heart failure patients spatially out-of-phase (i.e. discordant) intermittent Re-ALT using unipolar signals [68], and Kaufmann et al. reported intermittent microvolt T wave alternans (TWA) whose oscillations decreased in magnitude in parallel to the increase in heart rate and alternans amplitude [176]. Mirinov et al. showed that intermittent Re-ALT is related to unstable nodal lines separating out-of-phase regions spanning the heart surface, which are mechanistically linked to slow APD accommodation following a change in pacing rate [105]. Based on atrial unipolar signals, we observed sequences of intermittent Re-ALT appearing in a non-periodic pattern. The rise and decline in Re-ALT amplitude preceding non alternating periods is suggestive of nodal lines spanning the right atrium, but cannot be proven as recordings were performed at a single site. Interestingly, atrial ARI displayed alternation in duration only at the maximum amplitude of the T apex alternans. ARIs are surrogates of APDs [172, 173] hence alternation of ARIs indicates APD alternans. The repolarization wave of unipolar signals is the result of repolarization gradient of surrounding excitable tissue [172]. The peak of the T wave is timed with the maximal voltage gradient between neighboring APs and the height of the T wave with the magnitude

of that maximal voltage gradient [172]. Alternation in T apex amplitude without ARI alternans suggests alternation in the steepness of the phase 2 and 3 of neighboring APs but not necessarily of APD. This hypothesis is supported by the recent clinical observation that alternans of phase 2 of MAPs better correlates with microvolt TWA than alternans of phase 3 duration [67]. In summary, ovine right atrial repolarization kinetics share common features with human and rodent ventricles including the rate-dependence and the intermittency of Re-ALT.

8.3.3   Potential mechanisms of intermittent atrial capture

Watanabe et al. showed in canine right atrium using MAPs that the ERP measured during Re-ALT after a long APD is longer than that after a short APD [9]. Hence, atrial Re-ALT combined to AT prolongation may promote the first non-captured beat by delaying the ERP to a point where the next stimulus is refractory as illustrated by figure 8.1. However, other mechanisms must be involved in the maintenance and in the rate-dependence of intermittent capture. The rate-dependence of APD has been well established with prolonged ERP at slower heart rate [9, 50, 97]. Hence, maintenance of 2:1 capture may simply be the result of the prolonged diastolic interval and ensuing ERP during intermittent capture. However, the rate-dependence of the duration of intermittent capture and the decrease in ARI preceding resumption of 1:1 capture are both suggestive of a time-dependent process. Rapid pacing of sheep atrial and ventricular tissue hyperpolarizes the cell membrane, with additional hyperpolarization at reduction of stimulation rate by way of a rise in intracellular $Na^+(Na_i,)$ [177]. The high Na_i, in turn, activates the NaKATPase pump which generates a net outward hyperpolarizing current (i.e. extrusion of 3 Na^+ for the entry of 2 K^+). As hyperpolarization is associated with longer APD [178], the reduction in ARI observed before resumption of 1:1 capture may simply be a marker of the normalization of membrane diastolic potential, of the NaKATPase activity and of Na_i. Further studies beyond the scope of our research are required to elucidate these mechanisms.

8.3.4   Clinical relevance

The present study was designed to investigate a clinical observation that transient reduction in excitability may play a physiological protective role against Re-ALT induced dispersion of repolarization and reentrant arrhythmias by promoting intermittent capture during rapid pacing. In the seminal work of Haissaguerre et al. [3], PV tachycardias triggering AF had a mean CL of 175±30 ms that fell within the ovine atrial Re-ALT window (i.e. PCL 230 ms to ERP). This finding suggest that atrial Re-ALT might be one of the mechanisms facilitating transition from focal tachycardia to AF by promoting dispersion of repolarization and wavebreaks. Our study may also explain the limited success of overdrive pacing in suppressing the AF burden [179, 180] as increasing the pacing rate may promote Re-ALT and dispersion of repolarization. AF patients and models of rapid-pacing display multiple atrial alterations including a decrease in ERP [32, 181] that may potentially shift capture failure to higher rates and Re-ALT to lower rates, both reducing the effectiveness of this potentially protective mechanism.

8.3.5   Limitation

Our study bears limitations that deserve some comments. Some uncertainties remain whether our observations apply to the stimulation site as the recording electrode was remote by 2 cm on average, and to the left atrium as the pacemaker leads were implanted into the right atrium. The catheters used in humans for MAPs allowed recording at the pacing site thanks to their original design (fig. 2.12). Figure 8.1 shows atrial Re-ALT and delayed AT preceding capture failure at the pacing site that shared all the characteristics observed in our ovine model. Figure 8.1 also shows that both atria may exhibit Re-ALT and AT prolongation before capture failure, indicating that despite electrophysiological differences [106] some similarities between atria can be expected during rapid pacing.

9

Conclusions

The work presented in this thesis aimed at a better understanding of AF initiation and at linking atrial Re-ALT to AF susceptibility. Original electrophysiological parameters extracted from unipolar EGMs, such as Re-ALT and activation time were investigated during pacing protocols.

The first step was to develop an ovine model of rapid pacing which allowed us to acquire intracardiac unipolar EGMs displaying atrial repolarization wave using standard pacemaker technology, and to design signal analysis techniques to extract the relevant information.

Then, in order to evaluate the performance of the processing techniques, a simple synthetic model of EGMs mimicking experimental ones was established. This model contained atrial and ventricular activities and was used as ground truth to evaluate the denoising procedure, the cancellation of ventricular activity and the detection of short Re-ALT sequences.

The use of these processing methods on experimental EGMs led to several electrophysiological results. We assessed the rate dependence of atrial Re-ALT in a subset of sheep and evaluated its intermittency. Moreover, the prevalence of specific patterns preceding transitions to 2:1 atrial capture was exposed. The increase in duration of 2:1 atrial capture in function of the paced ERP was shown.

This thesis also showed the feasibility of recording intracardiac repolarization and measuring activation times, repolarization alternans and activation recovery intervals, using available pacemaker technology. This study is part of a complete framework analyzing the evolution of electrographic measurements, cardiac tissues, gene and protein expressions during rapid pacing. Each of them allows a better understanding of the results obtained from EGMs.

9.1   Summary of achievements

In this thesis the major achievements can be summarized as follows:

Experimental ovine model

This model allowed us to acquire in vivo atrial unipolar EGMs. Using the ventricular port of the pacemaker led to high-pass filtered signals (0.4 Hz). The resulting EGMs displayed the slow atrial repolarization waves which is not standard in pacemaker recordings. Our recording setup was less invasive than optical or electrical mapping of the atria which alters the conditions, but provided only a single site recording remote from the pacing site. The intermittent burst pacing used to remodel the atria was close to intermittent atrial tachycardias seen in human.

Signal processing

We proposed a simple model based on an experimental EGM, which contained atrial and ventricular activities with additive AR noise. This model simulated different atrioventricular conductions and was used to determine the parameters of the wavelet denoising method and to quantify the errors of the ventricular cancellation techniques. The detection of Re-ALT with additive noise and different dynamics of Re-ALT (i.e. stable or transient) was evaluated after cancellation of ventricular activity.

Three cancellation techniques, MTS, PCA_1 and PCA_2 were developed. MTS built a simple median template of ventricular activity and assumed small morphological variability in ventricular activity. PCA_1 offered a better alternative but included a major drawback: it reconstructed the atrial activity from the first principal component yielding a reduction in atrial morphological variations. PCA_2 differed from PCA_1 by investigating a two-step approach. This new method estimated the ventricular activity more accurately while it kept important atrial morphological variations. However, the three algorithms led to optimal results in AV block, pointing out the importance of atrioventricular node ablation.

Electrophysiological results

We observed in human atria using monophasic action potential recordings transient decrease in excitability (as exemplified by activation time prolongation) and capture failure that appeared to quench repolarization alternans driven by rapid pacing. Using our ovine model of rapid pacing, human observations were successfully reproduced, which allowed us to analyze repolarization alternans and activation time kinetics until the first beat of capture failure. Prolongation of activation time, which is suggestive of decreased excitability, and repolarization alternans preceded 90% of the transitions from 1:1 to 2:1 atrial capture during rapid pacing. Notably, 2:1 capture was imminent at PCLs <40 ms above ERP.

This work also demonstrated the feasibility of recording intra-atrial repolarization and ARI as a surrogate of APD, using available pacemaker technology. Atrial Re-ALT was reproducibly observed during rapid pacing, appearing intermittently but without periodicity and increasing in amplitude as a function of pacing rate. Since rapid atrial tachycardias promoting fibrillatory conduction may also slow propagation velocity, transitions to 2:1 capture via transient decrease in excitability may protect against Re-ALT induced dispersion of repolarization and AF. A better understanding of the mechanisms causing Re-ALT and intermittent capture may allow treatments to be tailored for preventing AF induction at lower rates.

This finding suggests that atrial Re-ALT might be one of the mechanisms facilitating transition from focal tachycardia to AF by promoting dispersion of repolarization and wavebreaks.

9.2 Perspectives

The exploration of the information contained in atrial EGMs to predict AF susceptibility is at its prelude.

Using a biophysical model of atria, a measure of the ARI as a surrogate of APD has been presented. Although both realistic anatomical geometry and dedicated atrial cellular model were implemented in this computer model, it remains that several atrial properties such as tissue heterogeneities or anisotropy for conduction were not considered. As a result, it can be expected that experimental conditions may largely differ. Therefore, investigating in our ovine model the ability of ARI to track changes in APD from unipolar EGMs is necessary.

We introduced the dynamics of Re-ALT and AT preceding AF episodes. A new analysis concerning the evolution of the duration of AF episodes during rapid pacing from baseline condition until burst-pacing induced AF is currently under investigation.

Ultimately, if AF susceptibility detection can be accurately determined using implantable devices, a transfer of the proposed method to clinic and industry (i.e. pacemaker upload) can be considered. Obviously, the processing techniques will have to be adapted to pseudo real-time. Achieving this new kind of pacemaker able to detect AF susceptibility will constitute a major progress in patient care, with the potential to contain health care costs.

Appendix

Biochemistry and histology A
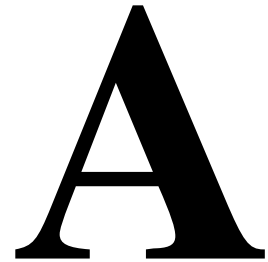
Different behaviors concerning propagation velocity were observed between sheep with and without AV block. It appears that sheep without AV block displayed a decrease in propagation velocity at baseline and a further one during the time course of pacing-induced remodeling, while sheep with AV block maintained a normal propagation velocity over the entire experiment.

A.1 Biochemistry

Samples from control and AF sheep hearts were analyzed to determine the expression of proteins involved in intracellular Ca^{2+} cycling. Ryanodine, SERCA and Phospholamban were successfully identified using human and rabbit antibodies. This has not been the case for L-type Ca^{2+} channels, which do not appear conserved between species. Below is a summary of the preliminary findings.

Tissues from both right and left ventricles and atria as well as pulmonary veins were frozen in liquid nitrogen and kept at -80°C before analysis. Cardiac samples were homogenized in Lysis Buffer. Incubation with first antibodies was done over night at 4°C. Then, secondary antibodies were added at room temperature. Analysis was performed using Odyssey Infrared Imaging System and Graphpad prism software. Within each experiment, Serca2ATPase, Phospholamban and Ryanodine receptor expression was normalized with actin level. Statistical evaluations were performed according to unpaired Student's t-tests.

Figure A.1 shows the comparison of SERCA and Phospholamban between control (n=3) and remodeled sheep (n=3) both with AV block. Interestingly, all tested cavities, included both atria, showed significantly reduced expression of the two measured proteins despite conservation of ventricular function as assessed by echocardiography. Ryanodine receptor expression, however, did not show any significant difference (data not shown). We intend to confirm these findings by normaliz-

ing protein expression levels with an intracellular protein (GAPDH) less prone to downregulation.

Discussion: Recent experimental and numerical studies [67, 82, 84, 96, 182] point towards intracellular Ca^{2+} alternans as driving APD alternans. Although the present analysis did not measure the protein expression of all sarcolemmal channels, our findings of reduced expression of SERCA and Phospholamban, but not of Ryanodine receptors, point towards the Ca^{2+} re-uptake side of the SR as the culprit for the increased susceptibility to repolarization alternans during pacing-induced atrial remodeling. Importantly, in contrast the study of Watanabe et al. [9] which showed lower APD alternans threshold following short duration of rapid atrial pacing, atrial repolarization alternans threshold did not change over time, but the CL range during which alternans was observed increased in parallel to the decrease in atrial ERP. How this relates to decreased expression of SERCA and Phospholamban remains undetermined yet.
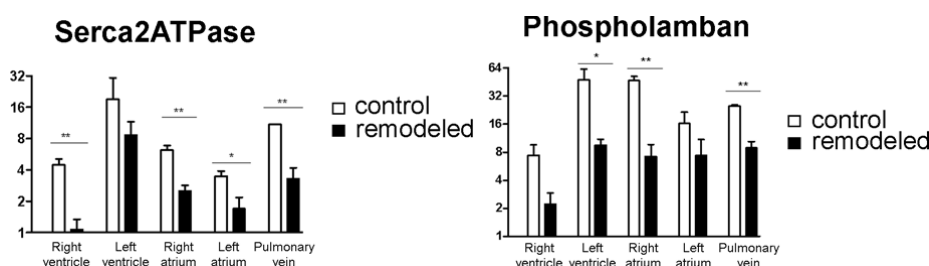
Figure A.1: *Biochemistry. Expression of SERCA and Phospholamban in control (white) and remodeled sheep (black). * P<0.05; ** P<0.01.*

A.2   Histology

Right and left atria of control with AV block (n=3) and remodeled sheep with AV block (n=3) have been collected and conserved in formalin, and sections were analysed under light microscope. Below are a short description and illustration of the preliminary findings.

Despite aggressive atrial burst pacing protocol in remodeled sheep, significant changes in atrial histology were not observed. Figure A.2a shows some nuclei hypertrophy (arrows) suggestive of slight atrial stress, but no cellular hypertrophy. Figure A.2b shows the absence of interstitial fibrosis (Masson's trichrome) in a sheep with AF. Comparison of fibrosis extent in control and remodeled sheep did not show statistically significant difference. These preliminary findings suggest that electrophysiological alterations such as decreased atrial ERP and increased range of CL during which repolarization alternans occurred, are unrelated to significant atrial tissue alterations in sheep with AV block, but involved subcellular alterations including at least important proteins involved in intracellular Ca^{2+} cycling.

An unusual finding was that sheep were prone to VF during ablation of the AV junction, and showed narrow QRS during ventricular pacing independent of the pacing site. These observations appear to be related to an unexpectedly broad His-Purkinje system. Figure A.2c shows some fast conducting fibers (arrows) located at the subendocardial level. This large network of conducting fibers may favor conduction of alternative radio-frequency current to the ventricles during AV junction ablation, promoting VF. It is also appealing to hypothesize that this large network of conduction fibers helps to synchronize ventricular pacing wherever the pacing site is.

(a) *Myocardiocytes with en-larged nuclei.*

(b) *Fibrosis (in blue).*

(c) *Fast conduction fibers in the left ventricle.*
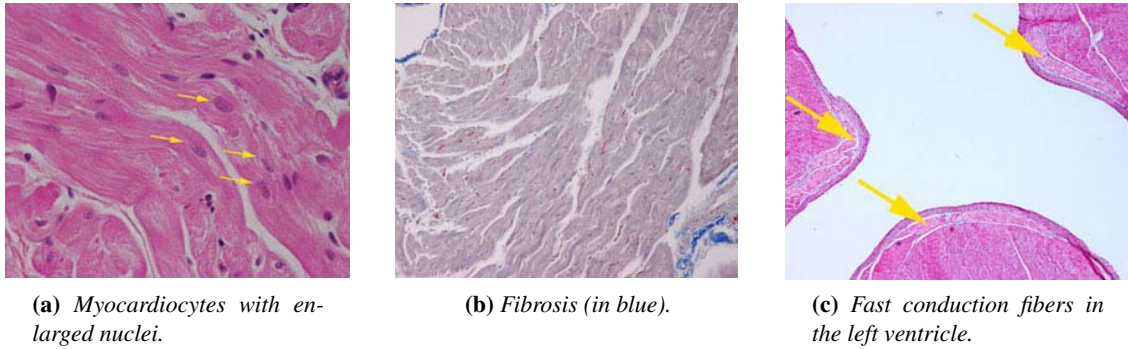
Figure A.2: *Histological analysis under light microscope.*

Additional samples from non-implanted sheep (n=7) and from sheep with intact AV junction (n=3) are under analysis (histology and biochemistry).

B

Devices

B.1 Pacemakers

B.1.1 Vitatron T70

The Vitatron T70 was used to record the atrial intracardiac signals (fig. B.1). In our study, we had to connect the atrial lead into the ventricular connector as only the ventricular port displayed the filter characteristics allowing us to record atrial repolarization wave, i.e. with a high pass filter set at 0.4 Hz. The atrial port, as for most pacemaker connectors, filters the signal using a 20-80 Hz bandpass filter preventing any recording of slow repolarization components [20].

B.1.2 Medtronic Diamond 3

The Medtronic Diamond 3 is a double chamber cardiac pacemaker used for permanent atrial and ventricular stimulation.

Figure B.1: *Vitatron® T70 pacemaker.*

	Impedance	Voltage threshold
Normal lead placement	normal	normal
Lead displacement or exit block	normal	high
Lead fracture	high	high
Lead insulation defect	low	may be moderately increased

Table B.1: *Analysis of lead problems.*

Control

Before any data acquisition, each pacemaker was check to detect any lead problem, listed in table B.1. The controls were performed by the mean of the Medtronic Carelink programmer.

Downloading

A custom software (called EP RAM-Routine) has been developed to enable the T70 pacemaker to deliver custom electrophysiological protocols.

Functionality

When the EP RAM-Routine is downloaded, it can be used in three modes:

- *OFF*   The pacemaker functions according to the programmed mode
- *Burst*   The pacemaker delivers bursts of atrial paces
- *EP*   The pacemaker gives one burst of atrial paces

This mode is chosen through the (*"PM Syndrome"*) parameter on the patient information screen, accessible from the programmer, according to the following indications:

- **"-"**   Off, normal programmed mode
- **"yes"**   Burst mode
- **"no"**   EP mode
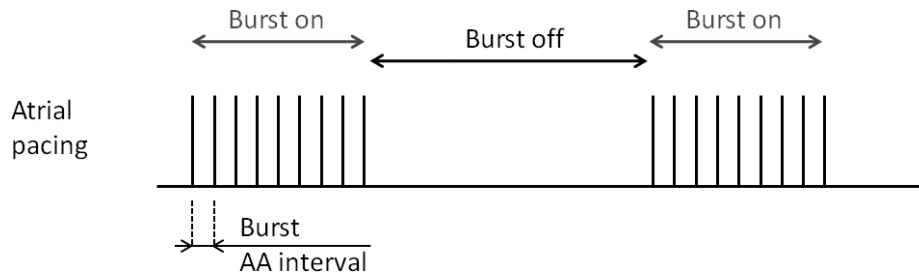
Figure B.2: *Burst pacing.*
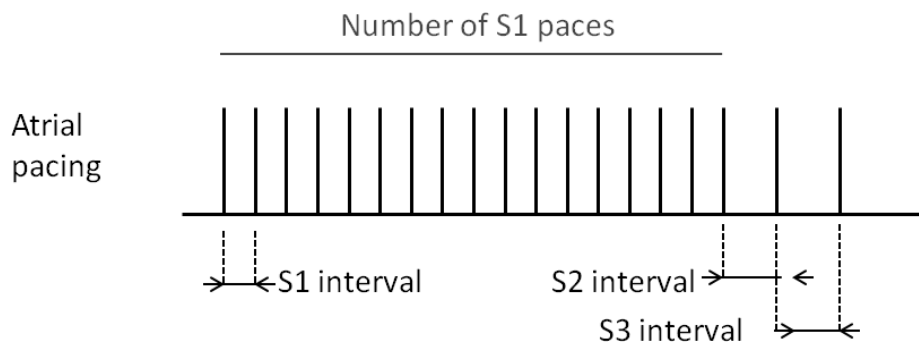
Figure B.3: *EP mode. Allowing the generation of S1S1, S1S2 and S1S2S3 protocols.*

Burst mode

In the burst mode, the pacemaker continuously generate bursts of atrial paces (fig. B.2). During a burst period, atrial and ventricular sensing is disabled. It is possible to enable ventricular backup pacing in a burst period, with a fixed VV interval.

Between two bursts, the pacemaker behaves as in the programmed mode (e.g. DDD).

The following parameters can be set:
– the duration of a burst period
– the duration of the period between two bursts
– the AA interval during a burst (i.e. the pacing cycle length)
– the VV interval during a burst, if the V backup is enable

EP mode

In the EP mode, the pacemaker generates a single burst of atrial paces. During the burst, atrial and ventricular sensing are disabled. There is no possibility to enable ventricular backup pacing during the burst. One burst consists of a series of S1 paces, followed by an S2 and an optional S3 pace (fig. B.3)

After the burst, the pacemaker returns to the programmed mode (e.g. DDD).

Burst duration. The duration of the burst is defined in the number of S1 paces. The number of S1 paces is programmed through the year of the pacemaker implantation date (*"Implant"*). Every

Programmed year (*Implant*)	00	01	02	⋯	97	98	99
Number of S1 paces	1	11	21	⋯	971	981	991

Table B.2: *Examples of settings for the number of S1 paces.*

Programmed year (*Birth*)	00	01	⋯	07	08	09	⋯	97	98	99
S1 interval [ms]	80	80	⋯	80	80	90	⋯	970	980	990

Table B.3: *Examples of settings for the S1 interval.*

year stands for approximatively 10 S1 paces while the century is ignored.

Pacing intervals. The S1-interval is programmed through the year of the patient birth date (*Birth*), and is in 10 ms units (i.e. every year stands for approximatively 10 milliseconds) ignoring the century. The smallest possible S1 interval is 80 ms, any smaller programmed value is clamped at 80 ms.

The S2-interval is programmed through the day and month of the patient birth date (*Birth*). The S3 interval is programmed through the day and month of the pacemaker implantation date (*Implant*). The days field are in 10 ms units. The month field, decreased by 1, is in 100 ms units. Examples of settings are given in table B.3

The smallest possible value for the S2 and the S3 interval is 30 ms. If the S2 interval is programmed to a smaller value, the actual value will be clamped to 30 ms. If the S3 interval is programmed to a smaller value than 30 ms, the S3 pace will be skipped and the burst will end with the S2 pace. The table B.4 shows examples of settings for the S2 and S3 intervals.

Automation. It is possible to automatically step through different S2 intervals. the auto-decrease EP mode is activated by programming *Angina* to *yes*. The first EP burst has the S2 interval as programmed and the user interface (implant month and day of the patient birth). After each EP burst, the S2 interval is decreased by 10 ms, until the minimum S2 interval of 30 ms is reached. There is a fixed interval of 2 seconds between consecutive bursts. The pacemaker returns to the programmed mode (e.g. DDD) after the EP burst at the minimum S2 interval of 30 ms has ended, or whenever EP is disabled by programming *PM Syndrome* to *yes* or -.

Programmed month / day *Birth*: S2 *Implant*: S3	01/02	01/03	01/04	01/05	02/25	03/17	04/07
S2 interval [ms]	30	30	40	50	350	370	370
S3 interval [ms]	*Off*	30	40	50	350	370	370

Table B.4: *Examples of settings for the S2 and S3 intervals.*

Battery drain

The pacemaker battery was not developed to handle the high pacing rates that are possible during the EP or the burst mode. To reduce the risk of battery exhaust, the following action can be performed:
  – increasing the pacing interval during a burst
  – decreasing the duration of a burst period
  – increasing the duration of the period between two bursts
  – decreasing the pacing amplitude

B.2   Medtronic Carelink programmer 2090

The Medtronic Carelink® programmer is a transportable system enabling the interrogation and programming of implantable devices from Medtronic and Vitatron (fig. B.4).

Figure B.4: *Medtronic Carelink® programmer.*

B.3   The Holter device

The Holter device, named Mobi system, is produced by Twente Medical Systems International (TMSi). The Mobi system is a multichannel system to measure a variety of (electro)-physiological signals in the field of human movement sciences, rehabilitation, ergonomics, sports and telemedicine.

The Mobi is designed for ambulatory measurements, but can be used stationary as well. In stationary use, the data is directly sent to a PC by BlueTooth wireless telemetry. Thus the user has optimal freedom during the measurement. And of course it is possible to store the data locally on a flash disk.

The Holter is linked to the recording pacemaker (Diamond 3) by the mean of an antenna (fig. B.5a). Four needles (fig. B.5b) were connected to the Holter for the recording of subcutaneous

(a)   (b)
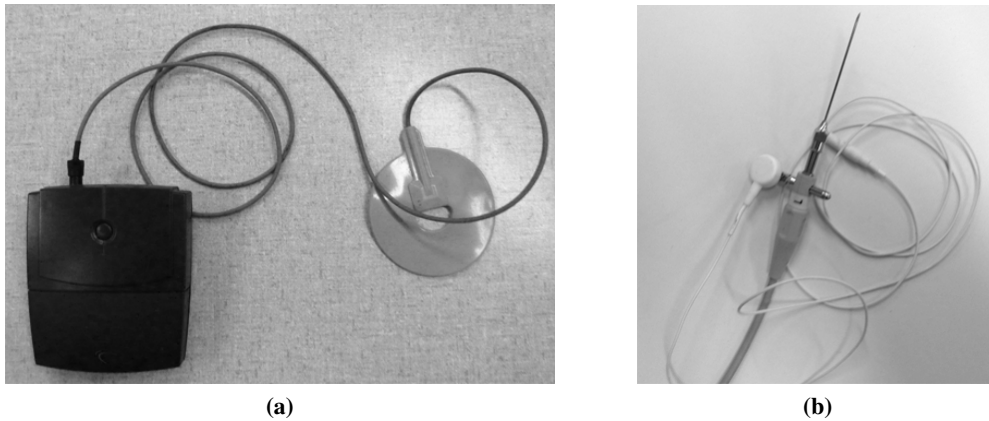
Figure B.5: *Holter device and connectors. (a) TMSi® Mobi System. (b) Needle for subcutaneous ECG.*

ECGs.

B.4   Echocardiography

The Siemens Acuson Sequoia (fig. B.6) was used to assess the structure and correct function of the heart throughout the remodeling process of the atria.

Figure B.6: *Siemens Acuson Sequoia.*

B.5   Radioscopie

The Philips Pulsera mobile C-arm (fig. B.7) was used to measure the inter-electrodes distances in order to estimate the propagation velocity or to detect any obvious atrial stretch.
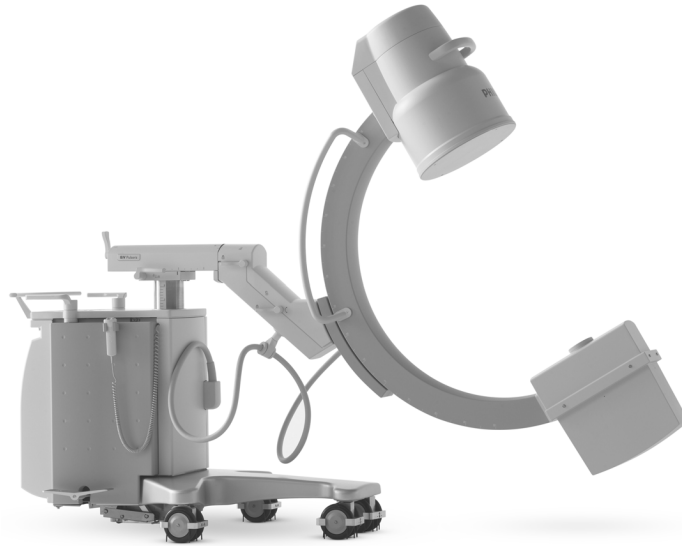
Figure B.7: *Philips Pulsera.*

Index

Bibliography

[1] Y. Miyasaka, M. E. Barnes, B. J. Gersh, S. S. Cha, K. R. Bailey, W. P. Abhayaratna, J. B. Seward, and T. S. Tsang, "Secular trends in incidence of atrial fibrillation in olmsted county, minnesota, 1980 to 2000, and implications on the projections for future prevalence," *Circulation*, vol. 114, no. 2, pp. 119–25, 2006.

[2] A. Jahangir, V. Lee, P. A. Friedman, J. M. Trusty, D. O. Hodge, S. L. Kopecky, D. L. Packer, S. C. Hammill, W. K. Shen, and B. J. Gersh, "Long-term progression and outcomes with aging in patients with lone atrial fibrillation: a 30-year follow-up study," *Circulation*, vol. 115, no. 24, pp. 3050–6, 2007.

[3] M. Haissaguerre, P. Jais, D. C. Shah, A. Takahashi, M. Hocini, G. Quiniou, S. Garrigue, A. Le Mouroux, P. Le Metayer, and J. Clementy, "Spontaneous initiation of atrial fibrillation by ectopic beats originating in the pulmonary veins," *N Engl J Med*, vol. 339, no. 10, pp. 659–66, 1998.

[4] S. A. Chen, M. H. Hsieh, C. T. Tai, C. F. Tsai, V. S. Prakash, W. C. Yu, T. L. Hsu, Y. A. Ding, and M. S. Chang, "Initiation of atrial fibrillation by ectopic beats originating from the pulmonary veins: electrophysiological characteristics, pharmacological responses, and effects of radiofrequency ablation," *Circulation*, vol. 100, no. 18, pp. 1879–86, 1999.

[5] J. Ausma, M. Wijffels, F. Thone, L. Wouters, M. Allessie, and M. Borgers, "Structural changes of atrial myocardium due to sustained atrial fibrillation in the goat," *Circulation*, vol. 96, no. 9, pp. 3157–63, 1997.

[6] D. S. Rosenbaum, L. E. Jackson, J. M. Smith, H. Garan, J. N. Ruskin, and R. J. Cohen, "Electrical alternans and vulnerability to ventricular arrhythmias," *N Engl J Med*, vol. 330, no. 4, pp. 235–241, 1994.

[7] D. M. Bloomfield, R. C. Steinman, P. B. Namerow, M. Parides, J. Davidenko, E. S. Kaufman, T. Shinn, A. Curtis, J. Fontaine, D. Holmes, A. Russo, C. Tang, and J. Bigger, J. Thomas, "Microvolt t-wave alternans distinguishes between patients likely and patients not likely to benefit from implanted cardiac defibrillator therapy: A solution to the multicenter automatic defibrillator implantation trial (madit) ii conundrum," *Circulation*, vol. 110, no. 14, pp. 1885–1889, 2004.

[8] S. M. Narayan, F. Bode, P. L. Karasik, and M. R. Franz, "Alternans of atrial action potentials during atrial flutter as a precursor to atrial fibrillation," *Circulation*, pp. 1968–1973, 2002.

[9] I. Watanabe, R. Masaki, M. Nuo, N. Oshikawa, K. Okubo, and Y. Okumura, "Effect of 60 minutes of rapid atrial pacing on atrial action potential duration in the in-situ canine heart," *Journal of Interventional Cardiac Electrophysiology*, vol. 8, pp. 165–171, 2003.

[10] B.-S. Kim, Y.-H. Kim, G.-S. Hwang, H.-N. Pak, S. C. Lee, W. J. Shim, D. J. Oh, and Y. M. Ro, "Action potential duration restitution kinetics in human atrial fibrillation," *Journal of the American College of Cardiology*, vol. 39, no. 8, pp. 1329–1336, 2002.

[11] Y. Gong, F. Xie, K. M. Stein, A. Garfinkel, C. A. Culianu, B. B. Lerman, and D. J. Christini, "Mechanism underlying initiation of paroxysmal atrial flutter/atrial fibrillation by ectopic foci: a simulation study," *Circulation*, vol. 115, no. 16, pp. 2094–102, 2007.

[12] R. E. Klabunde, *Cardiovascular Physiology Concepts*. Lippincott Williams & Wilkins, 2005.

[13] N. Sperelakis, Y. Kurachi, A. Terzic, and M. Cohen, *Heart physiology and pathophysiology*. Academic Press, 4th revised ed., 2000.

[14] C. H. Luo and Y. Rudy, "A model of the ventricular cardiac action potential. depolarization, repolarization, and their interaction," *Circ Res*, vol. 68, no. 6, pp. 1501–26, 1991.

[15] V. Jacquemet, N. Virag, and L. Kappenberger, "Wavelength and vulnerability to atrial fibrillation: Insights from a computer model of human atria," *Europace*, vol. 7 Suppl 2, pp. 83–92, 2005.

[16] L. Uldry, N. Virag, V. Jacquemet, J.-M. Vesin, and L. Kappenberger, "Optimizing local capture of atrial fibrillation by rapid pacing: Study of the influence of tissue dynamics," *Annals of Biomedical Engineering*, 2010.

[17] A. D. Waller, *Human physiology*. London: Longman, Green, 1891.

[18] W. Einthoven, "Die galvanometrische registrierung des menschlichen elektrokardiogramms, zugleich eine beurtheilung der anwendung des capillarelektrometers in der physiolgie," *Pfügers Archiv für die gesamte Physiologie des Menschen und der Tiere*, vol. 99, pp. 472–480, 1903.

[19] J. Malmivuo and R. Plonsey, *Bioelectromagnetism: Principles and Applications of Bioelectric and Biomagnetic Fields*. Oxford University Press, 1995.

[20] S. S. Barold, R. X. Stroobandt, and A. F. Sinnaeve, *Cardiac pacemakers step by step: an illustrated guide*. Wiley-Blackwell, 2004.

[21] A. Chicos and A. Kadish, "Intracardiac electrograms," in *Practical signal and image processing in clinical cardiology*, pp. 319–346, 2010.

[22] H. J. Moore and M. R. Franz, "Monophasic action potential recordings in humans," *Journal of Cardiovascular Electrophysiology*, vol. 18, no. 7, pp. 787–790, 2007.

[23] M. Kondo, V. Nesterenko, and C. Antzelevitch, "Cellular basis for the monophasic action potential. which electrode is the recording electrode?," *Cardiovascular Research*, vol. 63, no. 4, pp. 635–644, 2004.

[24] M. L. Koller, M. L. Riccio, and J. Gilmour, R. F., "Dynamic restitution of action potential duration during electrical alternans and ventricular fibrillation," *Am J Physiol*, vol. 275, no. 5 Pt 2, pp. H1635–42, 1998.

[25] S. Nattel, "New ideas about atrial fibrillation 50 years on," *Nature*, vol. 415, no. 6868, pp. 219–226, 2002.

[26] M. A. Allessie, P. A. Boyden, A. J. Camm, A. G. Kleber, M. J. Lab, M. J. Legato, M. R. Rosen, P. J. Schwartz, P. M. Spooner, D. R. Van Wagoner, and A. L. Waldo, "Pathophysiology and prevention of atrial fibrillation," *Circulation*, vol. 103, no. 5, pp. 769–777, 2001.

[27] T. L. Brunton and J. Fayrer, "Note on independent pulsation of the pulmonary veins and vena cava," *Proceedings of the Royal Society of London*, vol. 25, pp. 174–176, 1876.

[28] D. P. Zipes and J. Jalife, *Cardiac Electrophysiology: From Cell to Bedside*. Saunder, 4th ed., 2004.

[29] M. A. Allessie, "Atrial electrophysiologic remodeling: Another vicious circle?," *Journal of Cardiovascular Electrophysiology*, vol. 9, no. 12, pp. 1378–1393, 1998.

[30] M. Allessie, J. Ausma, and U. Schotten, "Electrical, contractile and structural remodeling during atrial fibrillation," *Cardiovasc Res*, vol. 54, no. 2, pp. 230–46, 2002.

[31] C. A. Morillo, G. J. Klein, D. L. Jones, and C. M. Guiraudon, "Chronic rapid atrial pacing : Structural, functional, and electrophysiological characteristics of a new model of sustained atrial fibrillation," *Circulation*, vol. 91, no. 5, pp. 1588–1595, 1995.

[32] M. C. Wijffels, C. J. Kirchhof, R. Dorland, and M. A. Allessie, "Atrial fibrillation begets atrial fibrillation: A study in awake chronically instrumented goats," *Circulation*, vol. 92, no. 7, pp. 1954–1968, 1995.

[33] L. Yue, J. Feng, R. Gaspo, G. R. Li, Z. Wang, and S. Nattel, "Ionic remodeling underlying action potential changes in a canine model of atrial fibrillation," *Circ Res*, vol. 81, no. 4, pp. 512–25, 1997.

[34] D. R. Van Wagoner, A. L. Pond, M. Lamorgese, S. S. Rossie, P. M. McCarthy, and J. M. Nerbonne, "Atrial l-type ca2+ currents and human atrial fibrillation," *Circ Res*, vol. 85, no. 5, pp. 428–36, 1999.

[35] R. F. Bosch, X. Zeng, J. B. Grammer, K. Popovic, C. Mewis, and V. Kuhlkamp, "Ionic mechanisms of electrical remodeling in human atrial fibrillation," *Cardiovasc Res*, vol. 44, no. 1, pp. 121–31, 1999.

[36] E. G. Daoud, F. Bogun, R. Goyal, M. Harvey, K. C. Man, S. A. Strickberger, and F. Morady, "Effect of atrial fibrillation on atrial refractoriness in humans," *Circulation*, vol. 94, no. 7, pp. 1600–1606, 1996.

[37] A. Elvan, X. D. Huang, M. L. Pressler, and D. P. Zipes, "Radiofrequency catheter ablation of the atria eliminates pacing-induced sustained atrial fibrillation and reduces connexin 43 in dogs," *Circulation*, vol. 96, no. 5, pp. 1675–85, 1997.

[38] H. M. van der Velden, M. J. van Kempen, M. C. Wijffels, M. van Zijverden, W. A. Groe-
     newegen, M. A. Allessie, and H. J. Jongsma, "Altered pattern of connexin40 distribution in
     persistent atrial fibrillation in the goat," *J Cardiovasc Electrophysiol*, vol. 9, no. 6, pp. 596–
     607, 1998.

[39] G. D. Dispersyn, J. Ausma, F. Thone, W. Flameng, J. L. Vanoverschelde, M. A. Allessie, F. C.
     Ramaekers, and M. Borgers, "Cardiomyocyte remodelling during myocardial hibernation
     and atrial fibrillation: prelude to apoptosis," *Cardiovasc Res*, vol. 43, no. 4, pp. 947–57,
     1999.

[40] J. Ausma, G. D. Dispersyn, H. Duimel, F. ThonÃ©, L. Ver Donck, M. A. Allessie, and
     M. Borgers, "Changes in ultrastructural calcium distribution in goat atria during atrial fibril-
     lation," *Journal of Molecular and Cellular Cardiology*, vol. 32, no. 3, pp. 355–364, 2000.

[41] T. H. t. Everett, H. Li, J. M. Mangrum, I. D. McRury, M. A. Mitchell, J. A. Redick, and D. E.
     Haines, "Electrical, morphological, and ultrastructural remodeling and reverse remodeling
     in a canine model of chronic atrial fibrillation," *Circulation*, vol. 102, no. 12, pp. 1454–60,
     2000.

[42] D. Lloyd-Jones, R. Adams, M. Carnethon, G. De Simone, T. B. Ferguson, K. Flegal, E. Ford,
     K. Furie, A. Go, K. Greenlund, N. Haase, S. Hailpern, M. Ho, V. Howard, B. Kissela,
     S. Kittner, D. Lackland, L. Lisabeth, A. Marelli, M. McDermott, J. Meigs, D. Mozaffar-
     ian, G. Nichol, C. O'Donnell, V. Roger, W. Rosamond, R. Sacco, P. Sorlie, R. Stafford,
     J. Steinberger, T. Thom, S. Wasserthiel-Smoller, N. Wong, J. Wylie-Rosett, Y. Hong, f. t. A.
     H. A. S. Committee, and S. S. Subcommittee, "Heart disease and stroke statistics–2009 up-
     date: A report from the american heart association statistics committee and stroke statistics
     subcommittee," *Circulation*, vol. 119, no. 3, pp. e21–181, 2009.

[43] G. D. Clifford, F. Azuaje, and P. McSharrz, *Advanced Methods And Tools for ECG Data
     Analysis*. Artech House Publishers, 2006.

[44] H. Herring, "Experimentelle studien an saugetieren Ã¼ber das elektrokardiogramm.," *Z Ex-
     per Med*, no. 7, p. 363, 1909.

[45] M. Puletti, M. Curione, G. Righetti, and G. Jacobellis, "Alternans of the st segment and t
     wave in acute myocardial infarction," *J Electrocardiol*, vol. 13, no. 3, pp. 297–300, 1980.

[46] S. B. Platt, J. M. Vijgen, P. Albrecht, G. F. Van Hare, M. D. Carlson, and D. S. Rosenbaum,
     "Occult t wave alternans in long qt syndrome," *J Cardiovasc Electrophysiol*, vol. 7, no. 2,
     pp. 144–8, 1996.

[47] J. M. Smith, E. A. Clancy, C. R. Valeri, J. N. Ruskin, and R. J. Cohen, "Electrical alternans
     and cardiac electrical instability," *Circulation*, vol. 77, no. 1, pp. 110–121, 1988.

[48] M. Kleinfeld and J. Rozanski, "Alternans of the st segment in prinzmetal's angina," *Circula-
     tion*, vol. 55, no. 4, pp. 574–577, 1977.

[49] M. R. Gold, D. M. Bloomfield, K. P. Anderson, N. E. El-Sherif, D. J. Wilber, W. J. Groh,
     N. A. M. Estes, E. S. Kaufman, M. L. Greenberg, and D. S. Rosenbaum, "A comparison of t-
     wave alternans, signal averaged electrocardiography and programmed ventricular stimulation
     for arrhythmia risk stratification," *Journal of the American College of Cardiology*, vol. 36,
     no. 7, pp. 2247–2253, 2000.

[50] J. M. Pastore, S. D. Girouard, K. R. Laurita, F. G. Akar, and D. S. Rosenbaum, "Mechanism linking t-wave alternans to the genesis of cardiac fibrillation," *Circulation*, vol. 99, no. 10, pp. 1385–1394, 1999.

[51] J. M. Pastore and D. S. Rosenbaum, "Role of structural barriers in the mechanism of alternans-induced reentry," *Circulation Research*, vol. 87, no. 12, pp. 1157–1163, 2000.

[52] S. M. Narayan, "The pathophysiology guided assessment of t wave alternans," in *Advanced Methods And Tools for ECG Data Analysis*, pp. 197–214, Artech House Publishers, 2006.

[53] D. R. Adam, J. M. Smith, S. Akselrod, S. Nyberg, A. O. Powell, and R. J. Cohen, "Fluctuations in t-wave morphology and susceptibility to ventricular fibrillation," *J Electrocardiol*, vol. 17, no. 3, pp. 209–18, 1984.

[54] S. H. Hohnloser, T. Klingenheben, Y.-G. Li, M. Zabel, J. O. Y. Peetermans, and R. J. Cohen, "T wave alternans as a predictor of recurrent ventricular tachyarrhythmias in icd recipients: Prospective comparison with conventional risk markers," *J Cardiovasc Electrophysiol*, vol. 9, no. 12, pp. 1258–1268, 1998.

[55] H. Kitamura, Y. Ohnishi, K. Okajima, A. Ishida, E. Galeano, K. Adachi, and M. Yokoyama, "Onset heart rate of microvolt-level t-wave alternans provides clinical and prognostic value in nonischemic dilated cardiomyopathy," *J Am Coll Cardiol*, vol. 39, no. 2, pp. 295–300, 2002.

[56] E. J. Rashba, A. F. Osman, K. MacMurdy, M. M. Kirk, S. Sarang, R. W. Peters, S. R. Shorofsky, and M. R. Gold, "Exercise is superior to pacing for t wave alternans measurement in subjects with chronic coronary artery disease and left ventricular dysfunction," *J Cardiovasc Electrophysiol*, vol. 13, no. 9, pp. 845–50, 2002.

[57] E. J. Rashba, A. F. Osman, K. MacMurdy, M. M. Kirk, S. Sarang, R. W. Peters, S. R. Shorofsky, and M. R. Gold, "Influence of qrs duration on the prognostic value of t wave alternans," *J Cardiovasc Electrophysiol*, vol. 13, no. 8, pp. 770–5, 2002.

[58] N. A. Estes, G. Michaud, D. P. Zipes, N. El-Sherif, F. J. Venditti, D. S. Rosenbaum, P. Albrecht, P. J. Wang, and R. J. Cohen, "Electrical alternans during rest and exercise as predictors of vulnerability to ventricular arrhythmias," *Am J Cardiol*, vol. 80, no. 10, pp. 1314–8, 1997.

[59] S. M. Narayan and J. M. Smith, "Differing rate dependence and temporal distribution of repolarization alternans in patients with and without ventricular tachycardia," *Journal of Cardiovascular Electrophysiology*, vol. 10, no. 1, pp. 61–71, 1999.

[60] T. Klingenheben, M. Zabel, R. B. D'Agostino, R. J. Cohen, and S. H. Hohnloser, "Predictive value of t-wave alternans for arrhythmic events in patients with congestive heart failure," *Lancet*, vol. 356, no. 9230, pp. 651–2, 2000.

[61] T. Ikeda, T. Sakata, M. Takami, N. Kondo, N. Tezuka, T. Nakae, M. Noro, Y. Enjoji, R. Abe, K. Sugi, and T. Yamaguchi, "Combined assessment of t-wave alternans and late potentials used to predict arrhythmic events after myocardial infarction. a prospective study," *J Am Coll Cardiol*, vol. 35, no. 3, pp. 722–30, 2000.

[62] T. Ikeda, H. Saito, K. Tanno, H. Shimizu, J. Watanabe, Y. Ohnishi, Y. Kasamaki, and Y. Ozawa, "T-wave alternans as a predictor for sudden cardiac death after myocardial infarction," *Am J Cardiol*, vol. 89, no. 1, pp. 79–82, 2002.

[63] K. Adachi, Y. Ohnishi, and M. Yokoyama, "Risk stratification for sudden cardiac death in dilated cardiomyopathy using microvolt-level t-wave alternans," *Jpn Circ J*, vol. 65, no. 2, pp. 76–80, 2001.

[64] T. Klingenheben, G. Gronefeld, Y. G. Li, and S. H. Hohnloser, "Effect of metoprolol and d,l-sotalol on microvolt-level t-wave alternans. results of a prospective, double-blind, randomized study," *J Am Coll Cardiol*, vol. 38, no. 7, pp. 2013–9, 2001.

[65] M. L. Koller, S. K. Maier, A. R. Gelzer, W. R. Bauer, M. Meesmann, and J. Gilmour, Robert F., "Altered dynamics of action potential restitution and alternans in humans with structural heart disease," *Circulation*, vol. 112, no. 11, pp. 1542–1548, 2005.

[66] S. M. Narayan, M. R. Franz, G. Lalani, J. Kim, and A. Sastry, "T-wave alternans, restitution of human action potential duration, and outcome," *Journal of the American College of Cardiology*, vol. 50, no. 25, pp. 2385–2392, 2007.

[67] S. M. Narayan, J. D. Bayer, G. Lalani, and N. A. Trayanova, "Action potential dynamics explain arrhythmic vulnerability in human heart failure: A clinical and modeling study implicating abnormal calcium handling," *Journal of the American College of Cardiology*, vol. 52, no. 22, pp. 1782–1792, 2008.

[68] P. Selvaraj, Raja J Picton, K. Nanthakumar, S. Mak, and V. S. Chauhan, "Endocardial and epicardial repolarization alternans in human cardiomyopathy: Evidence for spatiotemporal heterogeneity and correlation with body surace t-wave alternans," *Journal of the American College of Cardiology*, vol. 49, no. 3, pp. 338–347, 2007.

[69] H. Saitoh, J. C. Bailey, and B. Surawicz, "Alternans of action potential duration after abrupt shortening of cycle length: differences between dog purkinje and ventricular muscle fibers," *Circ Res*, vol. 62, no. 5, pp. 1027–40, 1988.

[70] J. Huser, Y. G. Wang, K. A. Sheehan, F. Cifuentes, S. L. Lipsius, and L. A. Blatter, "Functional coupling between glycolysis and excitation-contraction coupling underlies alternans in cat heart cells," *J Physiol*, vol. 524 Pt 3, pp. 795–806, 2000.

[71] Z. Qu, A. Garfinkel, P.-S. Chen, and J. N. Weiss, "Mechanisms of discordant alternans and induction of reentry in simulated cardiac tissue," *Circulation*, vol. 102, no. 14, pp. 1664–1670, 2000.

[72] J. J. Fox, M. L. Riccio, F. Hua, E. Bodenschatz, and J. Gilmour, R. F., "Spatiotemporal transition to conduction block in canine ventricle," *Circ Res*, vol. 90, no. 3, pp. 289–96, 2002.

[73] I. Banville and R. A. Gray, "Effect of action potential duration and conduction velocity restitution and their spatial dispersion on alternans and the stability of arrhythmias," *J Cardiovasc Electrophysiol*, vol. 13, no. 11, pp. 1141–9, 2002.

[74] O. Hauswirth, D. Noble, and R. W. Tsien, "Separation of the pace-maker and plateau components of delayed rectification in cardiac purkinje fibres," *J Physiol*, vol. 225, no. 1, pp. 211–35, 1972.

[75] M. L. Riccio, M. L. Koller, and J. Gilmour, R. F., "Electrical restitution and spatiotemporal organization during ventricular fibrillation," *Circ Res*, vol. 84, no. 8, pp. 955–63, 1999.

[76] A. Garfinkel, Y.-H. Kim, O. Voroshilovsky, Z. Qu, J. R. Kil, M.-H. Lee, H. S. Karagueuzian, J. N. Weiss, and P.-S. Chen, "Preventing ventricular fibrillation by flattening cardiac restitution," *Proceedings of the National Academy of Sciences of the United States of America*, vol. 97, no. 11, pp. 6061–6066, 2000.

[77] M. A. Watanabe, F. Fenton, S. J. Evans, H. M. Hastings, and A. Karma, "Mechanisms for discordant alternans," *J Cardiovasc Electrophysiol*, vol. 12, no. 2, pp. 196–206, 2001.

[78] J. J. Fox, J. L. McHarg, and J. Gilmour, R. F., "Ionic mechanism of electrical alternans," *Am J Physiol Heart Circ Physiol*, vol. 282, no. 2, pp. H516–30, 2002.

[79] L. A. Blatter, J. Kockskamper, K. A. Sheehan, A. V. Zima, J. Huser, and S. L. Lipsius, "Local calcium gradients during excitation-contraction coupling and alternans in atrial myocytes," *J Physiol*, vol. 546, no. Pt 1, pp. 19–31, 2003.

[80] E. Pruvot, R. P. Katra, D. S. Rosenbaum, and K. R. Laurita, "Weaker calcium-induced calcium-release as a mechanism of regional heterogeneity of repolarization alternans in the intact guinea pig heart.," 2003.

[81] E. Pruvot, R. P. Katra, X. Wan, D. S. Rosenbaum, and K. R. Laurita, "Weaker sr calcium uptake as a mechanism for regional development of repolarization alternans in the intact heart," *Circulation*, vol. 108[17], no. IV-8, 2003.

[82] E. J. Pruvot, R. P. Katra, D. S. Rosenbaum, and K. R. Laurita, "Role of calcium cycling versus restitution in the mechanism of repolarization alternans," *Circ Res*, vol. 94, no. 8, pp. 1083–90, 2004.

[83] X. Wan, K. R. Laurita, E. J. Pruvot, and D. S. Rosenbaum, "Molecular correlates of repolarization alternans in cardiac myocytes," *Journal of Molecular and Cellular Cardiology*, vol. 39, no. 3, pp. 419–428, 2005.

[84] J. I. Goldhaber, L.-H. Xie, T. Duong, C. Motter, K. Khuu, and J. N. Weiss, "Action potential duration restitution and alternans in rabbit ventricular myocytes: The key role of intracellular calcium cycling," *Circ Res*, vol. 96, no. 4, pp. 459–466, 2005.

[85] E. Chudin, J. Goldhaber, A. Garfinkel, J. Weiss, and B. Kogan, "Intracellular ca(2+) dynamics and the stability of ventricular tachycardia," *Biophys J*, vol. 77, no. 6, pp. 2930–41, 1999.

[86] C. H. Orchard, E. McCall, M. S. Kirby, and M. R. Boyett, "Mechanical alternans during acidosis in ferret heart muscle," *Circ Res*, vol. 68, no. 1, pp. 69–76, 1991.

[87] J. F. Spear and E. N. Moore, "A comparison of alternation in myocardial action potentials and contractility," *Am J Physiol*, vol. 220, no. 6, pp. 1708–16, 1971.

[88] Y. Hirayama, H. Saitoh, H. Atarashi, and H. Hayakawa, "Electrical and mechanical alternans in canine myocardium in vivo. dependence on intracellular calcium cycling," *Circulation*, vol. 88, no. 6, pp. 2894–902, 1993.

[89] B. R. Choi and G. Salama, "Simultaneous maps of optical action potentials and calcium transients in guinea-pig hearts: mechanisms underlying concordant alternans," *J Physiol*, vol. 529 Pt 1, pp. 171–88, 2000.

[90] M. L. Walker, X. Wan, G. E. Kirsch, and D. S. Rosenbaum, "Hysteresis effect implicates calcium cycling as a mechanism of repolarization alternans," *Circulation*, vol. 108, no. 21, pp. 2704–9, 2003.

[91] S. M. Narayan and J. M. Smith, "Exploiting rate-related hysteresis in repolarization alternans to improve risk stratification for ventricular tachycardia," *J Am Coll Cardiol*, vol. 35, no. 6, pp. 1485–92, 2000.

[92] P. Narayan, S. A. McCune, P. M. Robitaille, C. M. Hohl, and R. A. Altschuld, "Mechanical alternans and the force-frequency relationship in failing rat hearts," *J Mol Cell Cardiol*, vol. 27, no. 1, pp. 523–30, 1995.

[93] D. S. Rubenstein and S. L. Lipsius, "Premature beats elicit a phase reversal of mechanoelectrical alternans in cat ventricular myocytes. a possible mechanism for reentrant arrhythmias," *Circulation*, vol. 91, no. 1, pp. 201–14, 1995.

[94] S. G. Dilly and M. J. Lab, "Electrophysiological alternans and restitution during acute regional ischaemia in myocardium of anaesthetized pig," *J Physiol*, vol. 402, pp. 315–33, 1988.

[95] C. Steenbergen, E. Murphy, J. A. Watts, and R. E. London, "Correlation between cytosolic free calcium, contracture, atp, and irreversible ischemic injury in perfused rat heart," *Circ Res*, vol. 66, no. 1, pp. 135–46, 1990.

[96] L. M. Livshitz and Y. Rudy, "Regulation of ca2+ and electrical alternans in cardiac myocytes: role of camkii and repolarizing currents," *Am J Physiol Heart Circ Physiol*, vol. 292, no. 6, pp. H2854–66, 2007.

[97] J. N. Weiss, A. Karma, Y. Shiferaw, P.-S. Chen, A. Garfinkel, and Z. Qu, "From pulsus to pulseless: The saga of cardiac alternans," *Circ Res*, vol. 98, no. 10, pp. 1244–1253, 2006.

[98] C. S. Kuo, K. Munakata, C. P. Reddy, and B. Surawicz, "Characteristics and possible mechanism of ventricular arrhythmia dependent on the dispersion of action potential durations," *Circulation*, vol. 67, no. 6, pp. 1356–67, 1983.

[99] J. M. Pastore, K. R. Laurita, and D. S. Rosenbaum, "Importance of spatiotemporal heterogeneity of cellular restitution in mechanism of arrhythmogenic discordant alternans," *Heart rhythm*, vol. 3, no. 6, pp. 711–9, 2006.

[100] M. Chinushi, D. Kozhevnikov, E. B. Caref, M. Restivo, and N. El-Sherif, "Mechanism of discordant t wave alternans in the in vivo heart," *J Cardiovasc Electrophysiol*, vol. 14, no. 6, pp. 632–8, 2003.

[101] H. Hayashi, Y. Shiferaw, D. Sato, M. Nihei, S.-F. Lin, P.-S. Chen, A. Garfinkel, J. N. Weiss, and Z. Qu, "Dynamic origin of spatially discordant alternans in cardiac tissue," *Biophysical Journal*, vol. 92, no. 2, pp. 448–460, 2007.

[102] F. H. Fenton, E. M. Cherry, H. M. Hastings, and S. J. Evans, "Multiple mechanisms of spiral wave breakup in a model of cardiac electrical activity," *Chaos*, vol. 12, no. 3, pp. 852–892, 2002.

[103] M. R. Franz, "The electrical restitution curve revisited: steep or flat slope: which is better?," *J Cardiovasc Electrophysiol*, vol. 14, no. 10 Suppl, pp. S140–7, 2003.

[104] P. Taggart, P. Sutton, Z. Chalabi, M. R. Boyett, R. Simon, D. Elliott, and J. S. Gill, "Effect of adrenergic stimulation on action potential duration restitution in humans," *Circulation*, vol. 107, no. 2, pp. 285–9, 2003.

[105] S. Mironov, J. Jalife, and E. G. Tolkacheva, "Role of conduction velocity restitution and short-term memory in the development of action potential duration alternans in isolated rabbit hearts," *Circulation*, vol. 118, no. 1, pp. 17–25, 2008.

[106] S. M. Narayan, D. Kazi, D. E. Krummen, and W.-J. Rappel, "Repolarization and activation restitution near human pulmonary veins and atrial fibrillation initiation: A mechanism for the initiation of atrial fibrillation by premature beats," *Journal of the American College of Cardiology*, vol. 52, no. 15, pp. 1222–1230, 2008.

[107] M. Haissaguerre, M. Wright, M. Hocini, and P. Jais, "The substrate maintaining persistent atrial fibrillation," *Circ Arrhythmia Electrophysiol*, vol. 1, no. 1, pp. 2–5, 2008.

[108] S. H. Hohnloser, T. Klingenheben, M. Zabel, Y. G. Li, P. Albrecht, and R. J. Cohen, "T wave alternans during exercise and atrial pacing in humans," *J Cardiovasc Electrophysiol*, vol. 8, no. 9, pp. 987–93, 1997.

[109] D. P. Zipes, M. J. Mihalick, and G. T. Robbins, "Effects of selective vagal and stellate ganglion stimulation of atrial refractoriness," *Cardiovasc Res*, vol. 8, no. 5, pp. 647–55, 1974.

[110] L. Liu and S. Nattel, "Differing sympathetic and vagal effects on atrial fibrillation in dogs: role of refractoriness heterogeneity," *Am J Physiol*, vol. 273, no. 2 Pt 2, pp. H805–16, 1997.

[111] C. W. Chiou, J. N. Eble, and D. P. Zipes, "Efferent vagal innervation of the canine atria and sinus and atrioventricular nodes. the third fat pad," *Circulation*, vol. 95, no. 11, pp. 2573–84, 1997.

[112] P. Schauerte, B. J. Scherlag, E. Patterson, M. A. Scherlag, K. Matsudaria, H. Nakagawa, R. Lazzara, and W. M. Jackman, "Focal atrial fibrillation: experimental evidence for a pathophysiologic role of the autonomic nervous system," *J Cardiovasc Electrophysiol*, vol. 12, no. 5, pp. 592–9, 2001.

[113] P. Schauerte, B. J. Scherlag, J. Pitha, M. A. Scherlag, D. Reynolds, R. Lazzara, and W. M. Jackman, "Catheter ablation of cardiac autonomic nerves for prevention of vagal atrial fibrillation," *Circulation*, vol. 102, no. 22, pp. 2774–80, 2000.

[114] P. Coumel, P. Attuel, J. Lavallee, D. Flammang, J. F. Leclercq, and R. Slama, "[the atrial arrhythmia syndrome of vagal origin]," *Arch Mal Coeur Vaiss*, vol. 71, no. 6, pp. 645–56, 1978.

[115] P. Coumel, P. Attuel, J. F. Leclercq, and P. Friocourt, "[atrial arrhythmias of vagal or catecholaminergic origin: comparative effects of beta-blocker treatment and the escape phenomenon]," *Arch Mal Coeur Vaiss*, vol. 75, no. 4, pp. 373–87, 1982.

[116] J. V. Jayachandran, H. J. Sih, W. Winkle, D. P. Zipes, G. D. Hutchins, and J. E. Olgin, "Atrial fibrillation produced by prolonged rapid atrial pacing is associated with heterogeneous changes in atrial sympathetic innervation," *Circulation*, vol. 101, no. 10, pp. 1185–1191, 2000.

[117] Y. Miyauchi, S. Zhou, Y. Okuyama, M. Miyauchi, H. Hayashi, A. Hamabe, M. C. Fishbein, W. J. Mandel, L. S. Chen, P. S. Chen, and H. S. Karagueuzian, "Altered atrial electrical restitution and heterogeneous sympathetic hyperinnervation in hearts with chronic left ventricular myocardial infarction: implications for atrial fibrillation," *Circulation*, vol. 108, no. 3, pp. 360–6, 2003.

[118] A. R. Misier, T. Opthof, N. M. van Hemel, J. J. Defauw, J. M. de Bakker, M. J. Janse, and F. J. van Capelle, "Increased dispersion of "refractoriness" in patients with idiopathic paroxysmal atrial fibrillation," *J Am Coll Cardiol*, vol. 19, no. 7, pp. 1531–5, 1992.

[119] F. G. Cosio, J. Palacios, J. M. Vidal, E. G. Cocina, M. A. Gomez-Sanchez, and L. Tamargo, "Electrophysiologic studies in atrial fibrillation. slow conduction of premature impulses: a possible manifestation of the background for reentry," *Am J Cardiol*, vol. 51, no. 1, pp. 122–30, 1983.

[120] M. R. Gold, J. H. Ip, O. Costantini, J. E. Poole, S. McNulty, D. B. Mark, K. L. Lee, and G. H. Bardy, "Role of microvolt t-wave alternans in assessment of arrhythmia vulnerability among patients with heart failure and systolic dysfunction: Primary results from the t-wave alternans sudden cardiac death in heart failure trial substudy," *Circulation*, vol. 118, no. 20, pp. 2022–2028, 2008.

[121] D. S. Rosenbaum, "T-wave alternans in the sudden cardiac death in heart failure trial population: Signal or noise?," *Circulation*, vol. 118, no. 20, pp. 2015–2018, 2008.

[122] Z. Issa, J. M. Miller, and D. P. Zipes, *Clinical Arrhythmology and Electrophysiology: A Companion to Braunwald's Heart Disease*. Saunders, 2008.

[123] K. Nademanee, J. McKenzie, E. Kosar, M. Schwab, B. Sunsaneewitayakul, T. Vasavakul, C. Khunnawat, and T. Ngarmukos, "A new approach for catheter ablation of atrial fibrillation: mapping of the electrophysiologic substrate," *J Am Coll Cardiol*, vol. 43, no. 11, pp. 2044–53, 2004.

[124] Z. Shan, P. H. Van Der Voort, Y. Blaauw, M. Duytschaever, and M. A. Allessie, "Fractionation of electrograms and linking of activation during pharmacologic cardioversion of persistent atrial fibrillation in the goat," *J Cardiovasc Electrophysiol*, vol. 15, no. 5, pp. 572–80, 2004.

[125] D. J. Dosdall and R. E. Ideker, "Intracardiac atrial defibrillation," *Heart rhythm*, vol. 4, no. 3 Suppl, pp. S51–6, 2007.

[126] M. Stridh and L. Sornmo, "Spatiotemporal qrst cancellation techniques for analysis of atrial fibrillation," *Biomedical Engineering, IEEE Transactions on*, vol. 48, no. 1, pp. 105–111, 2001.

[127] J. J. Rieta, F. Castells, C. Sanchez, V. Zarzoso, and J. Millet, "Atrial activity extraction for atrial fibrillation analysis using blind source separation," *Biomedical Engineering, IEEE Transactions on*, vol. 51, no. 7, pp. 1176–1186, 2004.

[128] M. Lemay, J.-M. Vesin, A. Van Oosterom, V. Jacquemet, and L. Kappenberger, "Cancellation of ventricular activity in the ecg: Evaluation of novel and existing methods," *IEEE Trans Biomed Eng*, vol. 54, no. 3, pp. 542–546, 2007.

[129] M. Lemay, *Data Processing Techniques for the Characterization of Atrial Fibrillation*. PhD thesis, Ecole Polytechnique Fédérale de Lausanne (EPFL), 2007.

[130] J. J. Rieta and F. Hornero, "Comparative study of methods for ventricular activity cancellation in atrial electrograms of atrial fibrillation," *Physiol Meas*, vol. 28, no. 8, pp. 925–36, 2007.

[131] F. Castells, P. Laguna, L. Sörnmo, A. Bollmann, and J. Millet, "Principal component analysis in ecg signal processing," *EURASIP Journal on Advances in Signal Processing*, vol. 2007, no. 14, 2007.

[132] A. Bollmann, K. Sonne, H.-D. Esperer, I. Toepffer, J. J. Langberg, and H. U. Klein, "Non-invasive assessment of fibrillatory activity in patients with paroxysmal and persistent atrial fibrillation using the holter ecg," *Cardiovascular Research*, vol. 44, no. 1, pp. 60–66, 1999.

[133] L. Sornmo and P. Laguna, *Bioelectrical Signal Processing in Cardiac and Neurological Application*. Elsevier Academi Press, 2005.

[134] P. S. Addison, *The illustrated wavelet transform handbook*. Taylor & Francis, 2002.

[135] S. G. Mallat, "A theory for multiresolution signal decomposition: the wavelet representation," *IEEE Transactions on Pattern Analysis and Machine Intelligence*, vol. 11, pp. 674–693, 1989.

[136] D. L. Donoho, "De-noising by soft-thresholding," *Information Theory, IEEE Transactions on*, vol. 41, no. 3, pp. 613–627, 1995.

[137] M. Misiti, Y. Misiti, G. Oppenheim, and J.-M. Poggi, *Matlab Wavelet Toolbox User's Guide*. 4.6 ed., 2010.

[138] D. L. Donoho and I. N. Johnstone, "Minimax estimation via wavelet shrinkage," *Annals of statistics*, vol. 26, no. 3, pp. 879–921, 1998.

[139] C. M. Stein, "Estimation of the mean of a multivariate normal distribution," *The annals of Statistics*, vol. 9, no. 6, pp. 1135–1151, 1981.

[140] J. F. Kaiser, "Some useful properties of teager's energy operators," in *Acoustics, Speech, and Signal Processing, 1993. ICASSP-93., 1993 IEEE International Conference on*, vol. 3, pp. 149–152 vol.3, 1993.

[141] S. J. Orfanidis, *Introduction to Signal Processing*. Prentice Hall, 1996.

[142] R. Dubois, P. Maison-Blanche, B. Quenet, and G. Dreyfus, "Automatic ecg wave extraction in long-term recordings using gaussian mesa function models and nonlinear probability estimators," *Computer Methods and Programs in Biomedicine*, vol. 88, no. 3, pp. 217–233, 2007.

[143] G. Ljung and G. Box, "On a measure of lack of fit in time series models," *Biometrika*, vol. 65, no. 2, pp. 297–303, 1978.

[144] M. H. Hayes, *Statistical digital signal processing and modeling*. Wiley, 1996.

[145] P. D. Grunwald, *The Minimum Description Length Principle*. The MIT Press, 2007.

[146] I. T. Jolliffe, *Principal component analysis*. Springer, 2nd edition ed., 2002.

[147] B. D. Nearing, A. H. Huang, and R. L. Verrier, "Dynamic tracking of cardiac vulnerability by complex demodulation of the t wave," *Science*, vol. 252, no. 5004, pp. 437–40, 1991.

[148] B. D. Nearing and R. L. Verrier, "Personal computer system for tracking cardiac vulnerability by complex demodulation of the t wave," *J Appl Physiol*, vol. 74, no. 5, pp. 2606–2612, 1993.

[149] L. Burattini, W. Zareba, J. P. Couderc, E. L. Titlebaum, and A. J. Moss, "Computer detection of non-stationary t wave alternans using a new correlation method," in *Computers in Cardiology 1997*, pp. 657–660, 1997.

[150] L. Burattini, W. Zareba, J. P. Couderc, J. A. Konecki, and A. J. Moss, "Optimizing ecg signal sampling frequency for t-wave alternans detection," in *Computers in Cardiology 1998*, pp. 721–724, 1998.

[151] L. Burattini, W. Zareba, and A. J. Moss, "Correlation method for detection of transient t-wave alternans in digital holter ecg recordings," *Annals of Noninvasive Electrocardiology*, vol. 4, no. 4, pp. 416–424, 1999.

[152] P. Laguna, M. Ruiz, G. B. Moody, and R. G. Mark, "Repolarization alternans detection using the kl transform and the beatquency spectrum," in *Computers in Cardiology 1996*, pp. 673–676, 1996.

[153] P. Strumillo and J. Ruta, "Poincare mapping for detecting abnormal dynamics of cardiac repolarization," *Engineering in Medicine and Biology Magazine, IEEE*, vol. 21, no. 1, pp. 62–65, 2002.

[154] W. A. Sethares and T. W. Staley, "Periodicity transforms," *Signal Processing, IEEE Transactions on [see also Acoustics, Speech, and Signal Processing, IEEE Transactions on]*, vol. 47, no. 11, pp. 2953–2964, 1999.

[155] T. Srikanth, D. Lin, N. Kanaan, and H. Gu, "Estimation of low level alternans using periodicity transform - simulation and european st/t database results," in *[Engineering in Medicine and Biology, 2002. 24th Annual Conference and the Annual Fall Meeting of the Biomedical Engineering Society] EMBS/BMES Conference, 2002. Proceedings of the Second Joint*, vol. 2, pp. 1407–1408 vol.2, 2002.

[156] B. D. Nearing and R. L. Verrier, "Modified moving average analysis of t-wave alternans to predict ventricular fibrillation with high accuracy," *J Appl Physiol*, vol. 92, no. 2, pp. 541–549, 2002.

[157] S. M. Narayan and J. M. Smith, "The pathophysiology guided assessment of t-wave alternans," in *Advanced methods and tools for ECG data analysis* (G. Clifford, F. Azuaje, and P. E. McSharry, eds.), pp. 197–214, Artech House, 2006.

[158] A. Sastry and S. M. Narayan, "Advanced signal processing applications of the ecg: T wave alternans, heart rate variability, and the signal averaged ecg," in *Practical signal and image processing* (J. J. Goldberger and J. Ng, eds.), pp. 347–378, 2010.

[159] S. Wichert, K. Fokianos, and K. Strimmer, "Identifying periodically expressed transcripts in microarray time series data," *Bioinformatics*, vol. 20, no. 1, pp. 5–20, 2004.

[160] R. A. Fisher, "Test of significance in harmonic analysis," *Proceedings of the Royal Society of London. Series A, Containing Papers of a Mathematical and Physical Character*, vol. 125, no. 796, pp. 54–59, 1929.

[161] P. J. Brockwell and R. A. Davis, *Time Series: Theory and Methods*. Springer Series in Statistics, Springer, 1998.

[162] M. R. Franz, *Monophasic action potentials: Bridging cells to bedside*. Futura publishing company, armonk ny ed., 2000.

[163] C. W. Haws and R. L. Lux, "Correlation between in vivo transmembrane action potential durations and activation-recovery intervals from electrograms. effects of interventions that alter repolarization time," *Circulation*, vol. 81, no. 1, pp. 281–8, 1990.

[164] P. Colli Franzone, L. F. Pavarino, S. Scacchi, and B. Taccardi, "Monophasic action potentials generated by bidomain modeling as a tool for detecting cardiac repolarization times," *Am J Physiol Heart Circ Physiol*, vol. 293, no. 5, pp. H2771–2785, 2007.

[165] C. K. Millar, F. A. Kralios, and R. L. Lux, "Correlation between refractory periods and activation-recovery intervals from electrograms: effects of rate and adrenergic interventions," *Circulation*, vol. 72, no. 6, pp. 1372–9, 1985.

[166] R. Wyatt, "Comparison of estimates of activation and recovery times from bipolar and unipolar electrograms to in vivo transmembrane action potential durations," in *Proc.IEEE/Eng. Med. Biol. Soc. 2nd Ann. Conf.*, (Washington, DC), pp. 22–25, 1980.

[167] P. Chen, K. Moser, W. Dembitsky, W. Auger, P. Daily, C. Calisi, S. Jamieson, and G. Feld, "Epicardial activation and repolarization patterns in patients with right ventricular hypertrophy," *Circulation*, vol. 83, no. 1, pp. 104–118, 1991.

[168] V. Jacquemet, N. Virag, Z. Ihara, L. Dang, O. Blanc, S. Zozor, J. M. Vesin, L. Kappenberger, and C. Henriquez, "Study of unipolar electrogram morphology in a computer model of atrial fibrillation," *J Cardiovasc Electrophysiol*, vol. 14, no. 10 Suppl, pp. S172–9, 2003.

[169] M. Courtemanche, R. J. Ramirez, and S. Nattel, "Ionic mechanisms underlying human atrial action potential properties: insights from a mathematical model," *Am J Physiol*, vol. 275, no. 1 Pt 2, pp. H301–21, 1998.

[170] S. Zozor, O. Blanc, V. Jacquemet, N. Virag, J. M. Vesin, E. Pruvot, L. Kappenberger, and C. Henriquez, "A numerical scheme for modeling wavefront propagation on a monolayer of arbitrary geometry," *Biomedical Engineering, IEEE Transactions on*, vol. 50, no. 4, pp. 412–420, 2003.

[171] B. Steinhaus, "Estimating cardiac transmembrane activation and recovery times from unipolar and bipolar extracellular electrograms: a simulation study," *Circ Res*, vol. 64, no. 3, pp. 449–462, 1989.

[172] M. J. Janse, E. A. Sosunov, R. Coronel, T. Opthof, E. P. Anyukhovsky, J. M. T. de Bakker, A. N. Plotnikov, I. N. Shlapakova, J. Danilo, Peter, J. G. P. Tijssen, and M. R. Rosen, "Repolarization gradients in the canine left ventricle before and after induction of short-term cardiac memory," *Circulation*, vol. 112, no. 12, pp. 1711–1718, 2005.

[173] E. P. Anyukhovsky, E. A. Sosunov, S. J. Feinmark, and M. R. Rosen, "Effects of quinidine on repolarization in canine epicardium, midmyocardium, and endocardium: Ii. in vivo study," *Circulation*, vol. 96, no. 11, pp. 4019–26, 1997.

[174] D. E. Matthews and V. T. Farewell, *Using and Understanding Medical Statistics*. 4th ed., 2007.

[175] K. Hiromoto, H. Shimizu, Y. Furukawa, T. Kanemori, T. Mine, T. Masuyama, and M. Ohyanagi, "Discordant repolarization alternans-induced atrial fibrillation is suppressed by verapamil," *Circ J*, vol. 69, no. 11, pp. 1368–73, 2005.

[176] E. S. Kaufman, J. A. Mackall, B. Julka, C. Drabek, and D. S. Rosenbaum, "Influence of heart rate and sympathetic stimulation on arrhythmogenic t wave alternans," *Am J Physiol Heart Circ Physiol*, vol. 279, no. 3, pp. H1248–1255, 2000.

[177] C. Cohen, H. Fozzard, and S. Sheu, "Increase in intracellular sodium ion activity during stimulation in mammalian cardiac muscle," *Circ Res*, vol. 50, no. 5, pp. 651–662, 1982.

[178] J. J. Van der Walt and E. Carmeliet, "Hyperpolarization and duration of the cardiac action potential," *Arch Int Physiol Biochim*, vol. 79, no. 1, pp. 149–63, 1971.

[179] M. D. Carlson, J. Ip, J. Messenger, S. Beau, S. Kalbfleisch, P. Gervais, D. A. Cameron, A. Duran, J. Val-Mejias, J. Mackall, and M. Gold, "A new pacemaker algorithm for the treatment of atrial fibrillation: results of the atrial dynamic overdrive pacing trial (adopt)," *J Am Coll Cardiol*, vol. 42, no. 4, pp. 627–33, 2003.

[180] A. J. Camm, N. Sulke, N. Edvardsson, P. Ritter, B. A. Albers, J. H. Ruiter, T. Lewalter, P. A. Capucci, and E. Hoffmann, "Conventional and dedicated atrial overdrive pacing for the prevention of paroxysmal atrial fibrillation: the aftherapy study," *Europace*, vol. 9, no. 12, pp. 1110–8, 2007.

[181] W. Anne, R. Willems, P. Holemans, F. Beckers, T. Roskams, I. Lenaerts, H. Ector, and H. Heidbüchel, "Self-terminating af depends on electrical remodeling while persistent af depends on additional structural changes in a rapid atrially paced sheep model," *J Mol Cell Cardiol*, vol. 43, no. 2, pp. 148–158, 2007.

[182] M. E. Diaz, D. A. Eisner, and S. C. O'Neill, "Depressed ryanodine receptor activity increases variability and duration of the systolic ca2+ transient in rat ventricular myocytes," *Circ Res*, vol. 91, no. 7, pp. 585–93, 2002.

Florian JOUSSET

Rue des Alpes 8b
1020 Renens - CH
Phone: +41 79 504 60 47
Email: florian@jousset.ch

Date of birth: March 23, 1981
(29 year old)
Nationality: Swiss
Marital status: Single

Education

2006 − 2011	École Polytechnique Fédérale de Lausanne, Switzerland Ph.D. in Biomedical Signal Processing *Characterization of atrial repolarization alternans and activation time kinetics based on intracardiac electrograms*
2000 − 2006	École Polytechnique Fédérale de Lausanne, Switzerland M.Sc. in Communication Systems
1996 − 2000	Collège St-Michel, Fribourg, Switzerland Scientific Baccalauréat

Academic Experience

2008 − 2010	École Polytechnique Fédérale de Lausanne Teaching assistant for lab sessions in the courses *Analyse informatique de données* and *Biomedical signal processing*
2006 − 2008	École Polytechnique Fédérale de Lausanne Teaching assistant for exercises and lab sessions in the courses *Traitement d'images* and *Advanced image processing*

Work Experience

2006 (6 months)	Philips Research, Information system and security, Eindhoven, Netherlands Master project entitled *Biometric identification using electrocardiograms*

Language

French:	mother tongue
English:	fluent
German:	college level

Computer Skills

· Good knowledge of Java programming language, as well as Web languages such as PHP, XML, CSS and JavaScript
· Basic knowledge of C/C++
· Experience with Matlab, Maple and Labview
· Good working knowledge of Microsoft Windows XP/Vista/7 and Office as well as Linux

Interests and Activities

· Squash, Tennis

References

Available upon request

Publications

Journal papers

E. Pruvot, F. Jousset, P. Ruchat, J.-M. Vesin, Y. Prudat, T. Zerm, M. Fromer. *Propagation velocity kinetics and repolarization alternans in a free-behaving sheep model of pacing-induced atrial fibrillation*, Europace, 9(S6), vi83-vi88, 2007.

F. Jousset, J.-M. Vesin, J. Tenkorang, P. Pascale, P. Ruchat, S.C. Schaefer, M. Fromer, S. Narayan, E. Pruvot. *Decreased Excitability As A Protective Mechanism Against Pacing-Induced Repolarization Alternans and Atrial Fibrillation*, European Heart Journal, *submitted*.

Conference papers

M. Lemay, V. Jacquemet, F. Jousset, J.-M. Vesin, A. van Oosterom. *The Mean Firing Rate of Atrial Fibrillation as Estimated from the ECG Evaluation Using a Biophysical Model*, In Proc Comput Cardiol 2007, CinC 2007, Durham, USA, October 2007.

F. Jousset, M. Lemay, J.-M. Vesin. *Computers in Cardiology/Physonet Challenge 2009: Prediction acute hypotensive episodes*, In Proc Comput Cardiol 2009, CinC 2009, Park City, USA, September 2009.

F. Jousset, J.-M. Vesin, P. Pascale, P. Ruchat, S.C. Schaefer, M. Fromer, E. Pruvot. *In vivo measurements of atrial repolarization alternans based on standard pacemaker technology*, In Proc Comput Cardiol 2009, CinC 2009, Park City, USA, September 2009.

Abstracts

E. Pruvot, F. Jousset, P. Ruchat, J.-M. Vesin, T. Zerm, M. Fromer. *Atrial repolarization alternans in a chronic sheep model of pacing-induced atrial fibrillation*, presented at: SUK Project "Heart Remodeling in Health and Disease", Bern, April 2008.

E. Pruvot, F. Jousset, P. Ruchat, J.-M. Vesin, M. Fromer. *Atrial repolarization alternans in a chronic sheep model of pacing-induced atrial fibrillation*, presented at: Swiss Society of Cardiology Congress, Bern, May 28-30, 2008.

E. Pruvot, F. Jousset, P. Ruchat, J.-M. Vesin, T. Zerm, M. Fromer. *Atrial repolarization alternans and conduction velocity kinetics in a sheep model of pacing-induced atrial fibrillation.*, presented at: Cardiostim, Nice, June 2008.

F. Jousset, P. Ruchat, J.-M. Vesin, P. Pascale, M. Fromer, E. Pruvot. *Atrial repolarization alternans in a chronic sheep model of pacing-induced atrial fibrillation* presented at: Changins Meeting, Changins, November 13, 2008.

F. Jousset, P. Ruchat, P. Pascale, M. Fromer, J.-M. Vesin, E. Pruvot. *Atrial repolarization alternans in a chronic sheep model of pacing-induced atrial fibrillation*, presented at: CHUV Research Day, Lausanne, January 29, 2009.

F. Jousset, P. Ruchat, P. Pascale, M. Fromer, J.-M. Vesin, E. Pruvot. *In-Vivo Measurements of Atrial Repolarization Alternans Based on Standard Pacemaker Technology*, presented at: Swiss Society of Cardiology Congress, Lausanne, June 10-12, 2009.

F. Jousset, P. Ruchat, P. Pascale, M. Fromer, J.-M. Vesin, E. Pruvot. *Atrial Repolarization Alternans in a Chronic Sheep Model of Pacing-Induced Atrial Fibrillation*, presented at: European Society of Cardiology Congress, Barcelona, August 29 - September 2, 2009.

F. Jousset, P. Ruchat, P. Pascale, J. Tenkorang, S.C. Schaefer, M. Fromer, J.-M. Vesin, E. Pruvot. *Atrial Repolarization Alternans in a Chronic Sheep Model of Pacing-Induced Atrial Fibrillation*, presented at: Changins Meeging, Changins, November 12, 2009.

F. Jousset, J. Tenkorang, P. Ruchat, J.-M. Vesin, P. Pascale, M. Fromer, S.C. Schaefer, S.M. Narayan, E. Pruvot. *Decreased Excitability as a Protective Mechanism Against Repolarization Alternans-Induced Atrial Reentry*, presented at: Swiss Society of Cardiology Congress, St-Gallen, June 9-11, 2010.
Received the best poster award.

J. Tenkorang, F. Jousset, P. Ruchat, J.-M. Vesin, P. Pascale, M. Fromer, S.C. Schaefer, S.M. Narayan, E. Pruvot. *Rate-dependence of 2:1 atrial capture as a protective mechanism against atrial tachycardia-induced atrial fibrillation*, presented at: Cardiostim, Nice, France, June 13-16, 2010.

J. Tenkorang, F. Jousset, P. Ruchat, J.-M. Vesin, P. Pascale, M. Fromer, S.C. Schaefer, S.M. Narayan, E. Pruvot. *Long-term intermittent atrial tachycardia decreases activation recovery interval, flattens its kinetics and blunts its rate dependence before sustained atrial fibrillation*, presented at: European Society of Cardiology Congress, Stockholm, Sweden, August 28 - September 1, 2010.

J. Tenkorang, F. Jousset, P. Ruchat, J.-M. Vesin, P. Pascale, M. Fromer, S.C. Schaefer, S.M. Narayan, E. Pruvot. *Long-term intermittent atrial tachycardia decreases activation recovery interval, flattens its kinetics and blunts its rate dependence before sustained atrial fibrillation*, presented at: Heart Rhythm Congress, Birmingham, UK, October 3 - 6, 2010.